Lehrstuhl für Theoretische Chemie
der Technischen Universität München

Vibronic Coupling by the Spin-Orbit Operator in Linear Molecules

Sabyashachi Mishra

Vollständiger Abdruck der von der Fakultät für Chemie der Technischen Universität München zur Erlangung des akademischen Grades eines

Doktors der Naturwissenschaften

genehmigten Dissertation.

Vorsitzender: Univ.-Prof. Dr. Rainer Niewa
Prüfer der Dissertation:
1. Univ.-Prof. Dr. Wolfgang Domcke
2. Univ.-Prof. Dr. Hans Jürgen Neusser

Die Dissertation wurde am 17.10.2006 bei der Technischen Universität München eingereicht und durch die Fakultät für Chemie am 24.10.2006 angenommen.

It is a great pleasure for me to do my Ph.D. at the chair of Theoretical Chemistry of the Technical University of Munich. I express my sincere gratitude to all the visitors, group leaders, postdocs, and graduate students who happened to work at the chair during my stay at Garching for giving me an opportunity to come in contact with them and for providing a nice working atmosphere.

I am highly indebted to Prof. Wolfgang Domcke for giving me the present project. His continuous support and guidance has played a pivotal role for my Ph.D. thesis. His scientific knowledge and human skills are somethings which I will cherish forever.

I am thankful to Prof. Leonid V. Poluyanov and Dr. Valérie Vallet whose contributions are clearly visible in my Ph.D. thesis. While the former guided me with his vast knowledge in mathematics, the latter shared her expertise in quantum chemistry with me.

I thank Frau Ruth Mösch for her help in all semi-academic matters, especially for her help in translating German letters to English!

I would like to thank Prof. T. P. Radhakrishnan and Dr. Susanta Mahapatra of University of Hyderabad for their prompt help and valuable suggestions.

I am highly thankful to my Indian friends in Munich as well as in other parts of Germany for giving a great friendly environment in a foreign land. Sanjay *da* and Kiran *da* need a special mention for their help in the early days of my Ph.D.

I am grateful to Swarna for her invaluable support.

Finally, I wish to thank my parents and extended family for their love, care, and support without which life would have appeared pale.

Contents

List of Abbreviations

$\mathbf{1}_n$	n-dimensional unit matrix
aug-cc-pVnZ	augmented correlation consistent polarized valence n zeta
B3LYP	Becke's 3-parameter LYP (DFT functional)
CASSCF	complete active space self consistent field
CC	coupled cluster
CCSD(T)	CC singles, doubles, and perturbative triples
CI	configuration interaction
CPP	core polarization potential
DFT	density functional theory
DHF	Dirac Hartree Fock
ECP	effective core potential
FWHM	full width at half maximum
IP	ionization potential
JT	Jahn Teller
LRVC	linear relativistic vibronic coupling
MRCI	multi reference CI
OVGF	outer valence Green's function
PE	potential energy
PJT	pseudo Jahn Teller
RECP	relativistic effective core potential
RT	Renner Teller
SO	spin orbit
TR	time reversal
VC	vibronic coupling

Chapter 1

Introduction

According to the Born-Oppenheimer adiabatic approximation, the calculation of dynamical processes in molecules can be divided into two steps. While the first step involves solution of the electronic problem by keeping the atomic nuclei fixed in space, the nuclear dynamics on a predetermined electronic potential-energy (PE) surface is treated in the second step [1, 2, 3]. This approximation is based on the fact that the spacing of electronic eigenvalues is generally large compared to typical spacings associated with nuclear motion. Clearly, this approximation breaks down when electronic states are close in energy.

The most striking deviations from the adiabatic approximation are the orbitally degenerate electronic states. In 1937, Jahn and Teller formulated the idea of instability and spontaneous distortion of the nuclear configuration of a nonlinear molecule in an orbitally degenerate electronic state [4, 5]. This vibronic coupling (VC) is known as the Jahn-Teller (JT) effect. In the presence of the JT effect, the electrons do not adiabatically follow the motions of the nuclei and the nuclear states are determined not only by the averaged field of the electron, but also by the details of the electronic structure and their changes with nuclear displacements. Öpik and Pryce in 1957 [6] first noted that effects similar to the JT effect may be inherent in systems with near (quasi-degenerate or pseudo-degenerate) electronic states. This is known as pseudo-Jahn-Teller (PJT) effect.

The JT effect as well as the PJT effect have been studied extensively over the past decades, see [7, 8, 9, 10, 11, 12, 13, 14] and references therein. Although the majority of the applications of the JT effect has been in the field of spectroscopy, stereochemistry, and structural phase transformations, the JT effect has played the role of "guiding idea" [15] in one of the most important (Nobel prize winning) discoveries of modern physics: high-temperature superconductivity. The JT effect is also found instrumental in understanding

the mechanisms of chemical reactions, the properties of fullerenes, and the recent discovery of the colossal magnetoresistance [14].

Linear molecules are exceptions from the JT theorem but they too are subject to similar instabilities in their degenerate or pseudo-degenerate states when quadratic terms of VC are considered [16, 14]. This VC in linear molecules is known as the Renner-Teller (RT) effect, following the original paper of Renner in 1934 [17] that describes the vibronic interactions in degenerate Π electronic states of linear triatomic molecules. Experimental observations of Renner's predictions in the spectrum of the NH_2 radical [18, 19] stimulated early methodological developments for the treatment of the RT effect [20, 21, 22]. These early theoretical descriptions, which were based on perturbation theory, were later supplemented by variational methods for the calculation of RT spectra [23, 24, 16]. In the course of time, the RT effect has been extended to consider tetra-atomic linear molecules [25], treatment of Δ states [26], inclusion of magnetic-coupling effects [27], inclusion of anharmonic coupling and Fermi Resonances [28], inclusion of molecular rotation [22], etc. Several interesting applications of the RT effect, including processes like protonation, charge transfer, photodissociation, etc. suggest the importance of the RT effect in chemical and molecular physics. For a detailed survey of the RT effect, see the review by Rosmus and Chambaud [29].

The inclusion of the spin of the unpaired electron in the analysis of vibronic spectra of linear molecules was first considered by Pople [30]. He treated the spin-orbit (SO) coupling as a perturbation of the RT Hamiltonian of a $^2\Pi$ state and obtained the spin-vibronic energy corrections up to second order. Since then, numerous studies on the interplay of RT and SO-coupling effects have been performed, see Refs. [16, 20, 22, 23, 24, 31, 32, 33, 34] for reviews and representative examples. The majority of the existing RT-SO treatments, however, have been based on the simplified phenomenological form of the SO operator introduced by Pople [30]

$$H_{\mathrm{SO}} = AL_zS_z, \tag{1.1}$$

rather than on the microscopic form of SO coupling given by the Breit-Pauli Hamiltonian [35, 36]. Here L_z and S_z are the projections of the electronic orbital and spin angular momenta on the molecular axis, respectively, and A is a phenomenological constant. The simplification was argued to be justified since the x and y components of the orbital angular momentum should be effectively quenched for linear molecules [30]. The simplified operator (1.1) separately conserves the z-axis projections of orbital and spin angular momentum, while the true SO operator only conserves the z-axis projection of the total (orbital+spin) angular momentum.

In Chapter 3, a microscopically founded description of SO-coupling effects in RT systems is presented and the limitations of the L_zS_z approximation are explored. The RT-SO problem of an isolated $^2\Pi$ state is described by a 4×4 vibronic matrix instead of a 2×2 matrix (as in the nonrelativistic or in the L_zS_z approximation). An expansion of the matrix elements of the Breit-Pauli SO operator for an isolated $^2\Pi$ electronic state in a quasi-linear molecule yields, in addition to the well-known quadratic nonrelativistic RT coupling, a linear (that is, of first order in the bending coordinates) VC term of SO origin. This term is absent when the simplified phenomenological form (1.1) of the SO operator is employed. The generic effect of this linear-relativistic VC (LRVC) mechanism on the vibronic energy levels and spectral intensity distribution is studied by variational calculations, i.e., numerical diagonalization of large secular matrices, for the so-called resonant case, where the SO splitting of the $^2\Pi$ state and the bending vibrational frequency are approximately equal. In such resonant cases, the LRVC term is shown to have substantial effects on the vibronic spectra.

The relevance of the LRVC term in the $^2\Pi$ ground state of a series of radicals and radical cations with 15 valence electrons (BS_2, CS_2^+, OCS^+, OBS) is briefly discussed in Chapter 3.4.1. The VC parameters have been obtained by employing accurate *ab initio* electronic-structure methods. The $\tilde{X}\ ^2\Pi$ vibronic spectra of this series of molecules involving one second-row element: sulfur, illustrate the interplay of nonrelativistic and relativistic VC mechanisms in RT systems.

In another application of the present RT-SO model, we address certain perturbations of the usual pattern of RT-SO vibronic energy levels, which have been observed in $^2\Pi$ electronic states of several triatomic systems, in particular NCO, NCS, and GeCH [37, 38, 39]. These perturbations have been termed "Sears resonances" [39]. An explanation of these perturbations has been given in terms of a perturbative analysis of RT and SO coupling effects of the $^2\Pi$ state, invoking (nonrelativistic) VC effects within the $^2\Pi$ state with a distant $^2\Sigma^+$ state [37, 39]. In Chapter 3.4.2, we show that these perturbations can quantitatively be described by the LRVC term within the $^2\Pi$ state. Both *ab initio* electronic-structure calculations as well as the fitting of the measured energy level spectrum within the RT-SO vibronic model reveal the existence of a significant LRVC term in the $\tilde{X}^2\Pi$ state of GeCH.

In another application of the present model, the RT-SO analysis of the $\tilde{X}\ ^2\Pi$ state of XCN^+, (X= F, Cl, and Br) is combined with the treatment of the stretching modes within the so-called linear-VC model [40, 41] to provide an improved *ab initio* based simulation of the vibronic band shape of the photoelectron spectra by assuming the $\tilde{X}\ ^2\Pi$ state to be an isolated electronic state. The XCN^+ cations have been extensively studied

by different types of spectroscopic methods such as absorption [42], emission [43, 44, 45], laser excitation [46], infrared and microwave [47] as well as photoelectron [48, 49, 50, 51, 52]. The photoelectron spectra of these cations consist of three bands in the outer-valence region. Although the photoelectron spectra of BrCN and ICN have been recorded with high resolution [51, 52, 53], the photoelectron spectra available for FCN and ClCN are not highly resolved [48, 49, 50]. There are, however, a limited number of theoretical studies on these systems. The neutral species FCN and ClCN have been studied by Lee et al. and the molecular structures, vibrational frequencies, and quartic force fields have been determined [54, 55]. Similar studies have been performed by Wang et al. [56] for the $\tilde{X}\ ^2\Pi$ and $\tilde{A}\ ^2\Sigma^+$ states of FCN^+ and $ClCN^+$. They have estimated the molecular structures and vibrational frequencies as well as the adiabatic ionization energies employing various *ab initio* methods. The vibrational structure of the photoelectron spectra has been simulated via the calculation of Franck-Condon factors [56]. This analysis has been restricted to the two totally symmetric stretching modes; neither the RT coupling of degenerate bending mode with degenerate electronic state nor the SO coupling of the unpaired electron in the ground state of the cation has been taken into account. In the present work, the geometric as well as the spin-vibronic parameters are determined by employing accurate *ab initio* electronic-structure methods. The $\tilde{X}\ ^2\Pi$ state of the $ClCN^+$ is found to be of particular interest: here the resonance condition for linear relativistic RT coupling is approximately fulfilled. This coupling mechanism leads to a significant intensity transfer to vibronic levels with odd quanta of the bending mode. The calculated spectrum indicates that this novel relativistic VC effect should be observable in high-resolution (electron energy resolution of the order of a few meV) photoelectron spectra of ClCN.

The spectra of isolated $^2\Pi$ electronic states in many triatomic and tetraatomic molecules have been quantitatively analyzed by both perturbative and variational methods [17, 20, 21, 22, 23, 24, 16, 25, 26, 28, 57]. Quite often, however, the interaction of a degenerate $^2\Pi$ state with other close-lying electronic states is also important. These close-lying electronic states show strong VC which leads to the breakdown of the Born-Oppenheimer approximation. Examples are the absorption spectra of NCO [58] and NCS [59] and the photoelectron spectra of HCN [60, 61, 62, 63, 64], N_2O [65], and C_2N_2 [66]. In radicals like CCH [67, 68, 69, 70], CCF [71], and CCCl [72, 73], the vibronic interaction of closely spaced $^2\Pi$ and $^2\Sigma$ states leads to very complex vibronic energy-level spectra. The CCH radical in particular, is known to possess a rather low-energy conical intersection of the PE surfaces corresponding to the $^2\Sigma$ and $^2\Pi$ states. Several experimental and theoretical studies have been

devoted to the understanding of the complicated spectroscopy of the $\tilde{A}\ ^2\Pi$-$\tilde{X}\ ^2\Sigma^+$ system of this radical [74, 75, 76, 77, 78, 79, 80, 67, 68, 69, 70, 81, 82]. Some selected effects of $\Sigma - \Pi$ VC have been calculated by perturbation theory, e.g., corrections to rotational energy levels [58, 83], modifications of Zeeman orbital g-factors [83, 84], and intensity borrowing effects [83]. A comprehensive discussion of the effects associated with the weak perturbation of a Π electronic state by a Σ electronic state has been given by Aarts [85]. A detailed analysis of strong VC of closely spaced $^2\Sigma$ and $^2\Pi$ states of a linear molecule has been given by Köppel et al. [57], using variational methods.

In Chapter 4, the analysis of SO induced VC effects is extended to vibronically coupled $^2\Pi$ and $^2\Sigma$ electronic states by employing microscopic (Breit-Pauli) SO-coupling operator in the single-electron approximation. The matrix elements of the SO operator in a diabatic electronic basis are expanded in powers of the bending coordinate up to second order. This results in a 6×6 vibronic Hamiltonian, which contains zeroth-, first-, and second-order $\Sigma - \Pi$ VC terms of SO origin. Several of these terms are absent when the usual phenomenological form of the SO operator (1.1) is used. The influence of these $\Sigma - \Pi$ SO VC mechanisms on the vibronic energy levels and spectral intensity distribution corresponding to the transition from an unperturbed initial state to the vibronically coupled $^2\Sigma$ and $^2\Pi$ states is investigated by variational calculations for selected models. The phenomena are particularly interesting when the $\Sigma - \Pi$ coupling as well as the SO coupling are strong. The interplay of strong $\Sigma - \Pi$ VC and strong SO splitting of the Π state results in unexpectedly complex vibronic spectra. These complex spectra are qualitatively interpreted by the help of the calculated adiabatic PE curves.

The 6×6 $\Sigma - \Pi$ SO VC model is combined with the treatment of the stretching modes within the linear-VC model [40, 41] to calculate the vibronic structure of the $\tilde{X}\ ^2\Sigma^+$ and $\tilde{A}\ ^2\Pi$ states in the photodetachment spectrum of $CCCl^-$ and $CCBr^-$. In these systems the $^2\Sigma$ and $^2\Pi$ states are closely spaced. While there have been limited studies on CCF [71, 86, 87, 88] and no attention has been paid to CCBr and CCI, there exists a considerable amount of theoretical research on the electronic structure of CCCl [86, 89, 90, 91, 92, 93, 72, 94]. Early *ab initio* calculations of this radical by Largo et al. [86] concluded the radical to be linear, with some ambiguities concerning the nature of the ground electronic state. While Hartree-Fock calculations with a small basis set predicted a $^2\Sigma$ ground state, calculations with improved basis sets and inclusion of electron correlation effects favored a $^2\Pi$ ground state [86]. The energy separation between the two states was found to be less than 900 cm^{-1} [89]. A decade later the same authors suggested a nonlinear structure for the radical with a $^2A'$ ground state on the basis of density functional theory (DFT) calculations [91]. There has been no

experimental information on the radical until recently, when Sumiyoshi et al. reported a detailed characterization of the CCCl radical in the $\tilde{X}\ ^2A'$ state by Fourier-transform microwave spectroscopy [73]. Their experiment and corroborating *ab initio* studies lead to the conclusion that the ground state of the nonlinear radical has $^2\Sigma^+$ symmetry in the limit of linearity [73]. They found the first excited electronic state to be only 200 cm^{-1} above the ground state, in contrast to the CCH radical, where this separation is about 3700 cm^{-1} [81, 82]. They have also recognized a $^2\Sigma^+$-$^2\Pi$ conical intersection which is only 1200 cm^{-1} higher in energy than the minimum [73]. This experimental study inspired Tarroni and Carter, to perform a calculation of the infrared absorption spectrum of the radical [72]. These authors were the first to calculate the SO splitting of the $^2\Pi$ electronic state. In the present work, the nonrelativistic and relativistic VC parameters have been obtained by accurate *ab initio* electronic-structure calculations. The calculated photodetachment spectra of both the anions have complicated vibronic structure due to strong $\Sigma - \Pi$ VC. The spectral envelopes of the calculated photodetachment spectra exhibit double-hump reminiscent of strongly coupled E×E JT systems.

Chapter 2

Theoretical background

2.1 Theory of vibronic-coupling effects

2.1.1 Adiabatic approximation and diabatic basis

We consider a molecule described by the Hamiltonian

$$H = T_e + T_{\mathrm{N}} + U(\mathbf{r}, \mathbf{Q}) \tag{2.1}$$

where T_e and T_{N} are the operators of the kinetic energy of the electrons and nuclei, respectively, and $U(\mathbf{r}, \mathbf{Q})$ is the total PE of the electrons and nuclei. The vector $\mathbf{r}$ denotes the set of electronic coordinates describing the displacements from a reference configuration. For fixed nuclei, i.e., $T_{\mathrm{N}} = 0$, the orthonormal electronic wave functions $\Phi_n(\mathbf{r}, \mathbf{Q})$ and energies $V_n(\mathbf{Q})$ defined by

$$\left[\underbrace{T_e + U(\mathbf{r}, \mathbf{Q})}_{H_e} - V_n(\mathbf{Q})\right] \Phi_n(\mathbf{r}, \mathbf{Q}) = 0 \tag{2.2}$$

depend parametrically on the nuclear geometry. They are known as the Born-Oppenheimer electronic states and PE surfaces [2]. The exact eigenstates of the system can be expanded in the Born-Oppenheimer electronic states

$$\Psi(\mathbf{r}, \mathbf{Q}) = \sum_n \chi_n(\mathbf{Q}) \Phi_n(\mathbf{r}, \mathbf{Q}). \tag{2.3}$$

Inserting this ansatz into the Schrödinger equation

$$(H - E)\Psi(\mathbf{r}, \mathbf{Q}) = 0 \tag{2.4}$$

one readily obtains [2] the following set of coupled equations for the expansion coefficients in Eq. (2.3)

$$[T_{\mathrm{N}} + V_n(\mathbf{Q}) - E]\,\chi_n(\mathbf{Q}) = \sum_m \hat{\Lambda}_{nm}\chi_m(\mathbf{Q}). \tag{2.5}$$

The operators $\hat{\Lambda}_{nm}$ are known as the nonadiabatic operators, given by [3]

$$\hat{\Lambda}_{nm} = -\int \mathrm{d}\mathbf{r}\; \Phi_n^* \left[T_{\mathrm{N}}, \Phi_m\right]. \tag{2.6}$$

Rewriting the fundamental set of equations given in Eq. (2.5) as a matrix Schrödinger equation, we have

$$\left(\underbrace{T_{\mathrm{N}}\mathbf{1} + \mathbf{V}(\mathbf{Q}) - \hat{\mathbf{\Lambda}}}_{\mathbf{H}} - E\mathbf{1} \right) \chi = 0. \tag{2.7}$$

The matrix Hamiltonian $\mathbf{H}$ describes the nuclear motion in the manifold of electronic states. χ is the column vector with elements χ_n; $\mathbf{1}$ is the unit matrix, and $\mathbf{V}(\mathbf{Q}) = V_n(\mathbf{Q})\delta_{nm}$ is the diagonal matrix of electronic energies.

The adiabatic approximation is obtained by neglecting the nonadiabatic operator $\hat{\Lambda}$ in Eq. (2.6) [2]. This approximation is based on the assumption that the kinetic-energy operator of the nuclei can be considered as a small perturbation of the electronic motion. In the adiabatic approximation the matrix Hamiltonian $\mathbf{H}$ becomes diagonal and the total wave function (2.3) becomes a product of a nuclear and electronic wave function

$$\Psi(\mathbf{r}, \mathbf{Q}) = \chi_n(\mathbf{Q})\Phi_n(\mathbf{r}, \mathbf{Q}). \tag{2.8}$$

The nuclear motion can be thought of as proceeding on the PE surface $V_n(\mathbf{Q})$ of a given electronic state characterized by the index n.

Although the adiabatic approximation is often a very useful approach, it may fail in cases where the PE surfaces of different electronic states are energetically close. In these cases the nonadiabatic operators $\hat{\Lambda}_{nm}$ cannot be neglected in the Hamiltonian $\mathbf{H}$ for those electronic indices n and m which belong to the manifold of closely lying electronic states. These electronic states are now vibronically coupled via $\hat{\Lambda}_{nm}$. The nonadiabatic operators, which reflect the fast changes of the adiabatic electronic states with the nuclear coordinates in the vicinity of avoided crossing or conical intersection of PE surfaces become very complicated and hence solution of the Schrödinger equation becomes tedious. To overcome this problem the adiabatic wave functions $\Phi_n(\mathbf{r}, \mathbf{Q})$ are replaced by smooth and slowly varying

functions $\phi_n(\mathbf{r}, \mathbf{Q})$ of the nuclear coordinates and correspond to PE surfaces that may cross at the avoided crossings of the adiabatic PE surfaces. These slow-varying functions represent the diabatic basis [95, 96, 97]. The diabatic basis is constructed by orthogonal transformation of the adiabatic functions such that the nonadiabatic operators are negligibly small in the transformed basis. The concept of diabatic basis has been found to be useful in many fields ranging from atom-atom collision to spectroscopy. There has been considerable amount of work devoted to the construction of diabatic bases [98, 99, 100, 101, 102, 103].

2.1.2 Linear-vibronic-coupling approach

For a given set of vibronically interacting electronic states the matrix Hamiltonian in the diabatic basis is given by

$$\mathbf{H} = (T_{\mathrm{N}} + V_0(\mathbf{Q}))\mathbf{1} + \mathbf{W}(\mathbf{Q}). \tag{2.9}$$

Where the quantity $V_0(\mathbf{Q})$ is the PE surface of the state from which the molecule is excited to the manifold of vibronically coupled electronic states. The matrix elements of the potential matrix $\mathbf{W}(\mathbf{Q})$ are

$$W_{nm}(\mathbf{Q}) = \int \mathrm{d}\mathbf{r}\ \phi_n^*(\mathbf{r}, \mathbf{Q}) H_e \phi_m(\mathbf{r}, \mathbf{Q}). \tag{2.10}$$

The ϕ_n are the diabatic wave functions for an electronic state of index n. For a polyatomic molecule, the accurate solution of matrix Hamiltonian (2.9) requires an extreme effort. Therefore an approximate form of the matrix Hamiltonian is often considered for which the Schrödinger equation can be accurately solved. The simplest, but elegant, approximation is to expand the PE matrix $\mathbf{W}(\mathbf{Q})$ about a reference nuclear configuration $\mathbf{Q_0}$ and retaining the terms linear in $\mathbf{Q}$ for the offdiagonal terms. This method is known as the linear-VC approach [40, 41]. The linear approximation is often sufficient since the elements of the $\mathbf{W}(\mathbf{Q})$ matrix are, by definition, slowly varying functions of $\mathbf{Q}$. Without loss of generality it is assumed that the diabatic and adiabatic states are identical at the reference geometry $\mathbf{Q_0}$.

The elements of the matrix Hamiltonian in the linear approximation are

$$\begin{aligned} H_{nn} &= T_{\mathrm{N}} + V_0(\mathbf{Q}) + W_{nn}(\mathbf{Q_0}) + \sum_s \kappa_s^{(n)} Q_s \\ H_{nm} &= \sum_s \lambda_s^{(n,m)} Q_s. \end{aligned} \tag{2.11}$$

The quantities $\kappa_s^{(n)}$ and $\lambda_s^{(n,m)}$ are known as intrastate and interstate electron-vibrational coupling constants, respectively, given by

$$\kappa_s^{(n)} = \left(\frac{\partial V_n(\mathbf{Q})}{\partial Q_s} \right)_{\mathbf{Q_0}} \tag{2.12}$$

$$\lambda_s^{(n,m)} = \left(\frac{\partial V_{nm}(\mathbf{Q})}{\partial Q_s} \right)_{\mathbf{Q_0}} . \tag{2.13}$$

The nonvanishing interstate coupling constants $\lambda_s^{(n,m)}$ are those for which the product of the irreducible representations of ϕ_n, ϕ_m, and of the nuclear coordinate Q_s contains the totally symmetric representation Γ_A, i.e.,

$$\Gamma_n \times \Gamma_{Q_s} \times \Gamma_m \supset \Gamma_A. \tag{2.14}$$

The analogous condition for the intrastate coupling constants $\kappa_s^{(n)}$ is

$$\Gamma_n \times \Gamma_{Q_s} \times \Gamma_n \supset \Gamma_A. \tag{2.15}$$

This shows that all totally symmetric modes can couple to the electronic motion.

2.1.3 Vibronic coupling involving degenerate mode and degenerate states

Degenerate electronic states are outstanding examples of the failure of the adiabatic approximation. In the case of linear molecules the VC problem is known as RT coupling; otherwise it is known as JT coupling.

(A) Jahn-Teller effect

Nearly all molecules in the C_{3v} group or higher molecular point groups possess degenerate electronic states and degenerate vibrational modes. For degenerate states in nonlinear molecules, Jahn and Teller have shown that there always exists a nontotally symmetric vibrational mode that can lift the degeneracy in first order due to VC between the electronic component states [5, 4]. Considering a two-fold degenerate (E) electronic state, the symmetry of the desired vibrational mode for VC should be such that it is contained in the decomposition of the symmetrized product $(\mathrm{E})^2$. It is then found that in all but seven molecular-point groups (with four-fold principal rotation axis, e.g., C_{4v}, C_{4h}, etc.) degenerate vibrations can be JT active, leading to the E×E JT effect [10, 7, 12, 11, 104, 105].

Let us consider a system with a doubly degenerate electronic state and three-fold principal rotation axis C_3. The doubly degenerate JT active vibrational mode in Cartesian coordinates be represented as (Q_x, Q_y). In polar coordinates (ρ, ϕ), the x and y components of the degenerate vibrational mode can be written as

$$Q_x = \rho\cos\phi \quad Q_y = \rho\sin\phi. \tag{2.16}$$

Lets define

$$Q_\pm = Q_x \pm iQ_y = \rho e^{\pm i\phi}. \tag{2.17}$$

The transformation properties of $Q_\pm$ under C_3 are

$$C_3 Q_\pm = \exp\left(\pm\frac{2\pi i}{3}\right) Q_\pm. \tag{2.18}$$

The doubly degenerate electronic states can be expressed by the diabatic wave functions in the Cartesian coordinate as (ψ_x, ψ_y), The linear combinations

$$\psi_\pm = \frac{1}{\sqrt{2}}\left(\psi_x \pm i\psi_y\right) \tag{2.19}$$

have the following transformation properties under C_3 operation

$$C_3\psi_\pm = \exp\left(\pm\frac{2\pi i}{3}\right)\psi_\pm. \tag{2.20}$$

By expanding the electronic part of the Hamiltonian (2.9) in a Taylor series up to first order in $Q_\pm$ and evaluating matrix elements with the diabatic basis states Eq. (2.19), taking into account the symmetry properties of Eqs. (2.18) and (2.20), one obtains [20, 105, 7]

$$H_{\mathrm{JT}} = (T_{\mathrm{N}} + V_0)\mathbf{1}_2 + \begin{pmatrix} 0 & f\rho e^{i\phi} \\ f\rho e^{-i\phi} & 0 \end{pmatrix} \tag{2.21}$$

where $V_0 = \frac{\omega}{2}\rho^2$ and

$$T_{\mathrm{N}} = -\frac{\omega}{2}\left(\frac{\partial^2}{\partial\rho^2} + \frac{1}{\rho}\frac{\partial}{\partial\rho} + \frac{1}{\rho^2}\frac{\partial^2}{\partial\phi^2}\right). \tag{2.22}$$

ω is the vibrational frequency associated with the degenerate mode and f is known as linear JT coupling constant.

The corresponding adiabatic potential functions obtained by diagonalizing the JT Hamiltonian at a fixed-nuclear geometry, i.e., $T_{\mathrm{N}} = 0$,

$$V_{1,2} = \frac{\omega}{2}\rho^2 \pm f\rho, \tag{2.23}$$

are the well-known "Mexican-hat potentials" [20, 105, 7].

The JT Hamiltonian (2.21) can be shown to commute with the total angular momentum operator of the following form

$$j'_z = \frac{1}{i}\frac{\partial}{\partial\phi}\begin{pmatrix} 1 & 0 \\ 0 & 1 \end{pmatrix} + \frac{1}{2}\begin{pmatrix} -1 & 0 \\ 0 & 1 \end{pmatrix}. \tag{2.24}$$

The eigenvalues of j'_z are half-integer numbers.

(B) Renner-Teller effect

The VC within degenerate states of linear molecule requires a special treatment, since the lowest order VC terms are at least quadratic [17, 22, 16]. For linear molecules, the z component of the electronic orbital angular momentum around the molecular axis takes one of the values $\Lambda = 0, \pm 1, \pm 2 \cdots$. The corresponding electronic states are called Σ, Π, $\Delta \cdots$ states. For all nonzero values of Λ, the electronic state is two-fold degenerate. Since linear molecules possess a continuous rotational symmetry, the diabatic functions associated with a given value of Λ are subject to the following transformation under the action of C_ϕ

$$C_\phi \psi_\Lambda = e^{i\Lambda\phi}\psi_\Lambda, \quad \Lambda = 0, \pm 1, \pm 2 \cdots \tag{2.25}$$

In the original work of Renner, the VC of the degenerate Π electronic state was considered. Since then, this case has received most of the attention [22, 20, 31, 23, 32, 33, 34]. According to Eq. (2.14), the bending vibrational mode of Π symmetry is RT active. The degenerate bending mode can be described by the Cartesian coordinates (Q_x, Q_y) and polar coordinates (ρ, ϕ) defined in Eqs. (2.16) and (2.17). The transformation properties of $Q_\pm$ under C_ϕ are

$$C_\phi Q_\pm = e^{\pm i\Lambda\phi} Q_\pm. \tag{2.26}$$

By performing the Taylor expansion of the electronic part of the Hamiltonian (2.9) with respect to $Q_\pm$ and using the symmetry properties Eqs. (2.25) and (2.26), the RT Hamiltonian is obtained as [57]

$$H_{\mathrm{RT}} = (T_{\mathrm{N}} + V_0)\mathbf{1}_2 + \begin{pmatrix} 0 & c\rho^2 e^{2i\phi} \\ c\rho^2 e^{-2i\phi} & 0 \end{pmatrix} \tag{2.27}$$

where c is the quadratic RT coupling constant. T_{N} and V_0 have the same form as in the JT coupling case. The RT Hamiltonian commutes with the following total vibronic angular momentum operator

$$j'_z = \frac{1}{i}\frac{\partial}{\partial\phi}\begin{pmatrix} 1 & 0 \\ 0 & 1 \end{pmatrix} + \begin{pmatrix} -1 & 0 \\ 0 & 1 \end{pmatrix}. \tag{2.28}$$

The eigenvalues of j'_z are integer numbers.

(C) $\Sigma - \Pi$ coupling

In addition to the VC of the two components of the degenerate Π electronic state, the degenerate bending vibrational mode of Π symmetry can couple a doubly degenerate Π electronic state with a nondegenerate Σ electronic state in linear molecules. This coupling is known as $\Sigma - \Pi$ coupling. This coupling mechanism becomes important when a doubly degenerate Π state lies close in energy to a Σ state [58, 59, 61, 62, 65, 68, 69]. By considering the diabatic basis states $\psi_{\pm}$ and ψ_0 for the Π and Σ states, respectively, and following the steps described above, the $\Sigma - \Pi$ Hamiltonian is obtained as [57]

$$H_{\Sigma-\Pi} = (T_{\mathrm{N}} + V_0)\mathbf{1}_3 + \begin{pmatrix} -\Delta/2 & \lambda\rho e^{i\phi} & c\rho^2 e^{2i\phi} \\ \lambda\rho e^{-i\phi} & \Delta/2 & \lambda\rho e^{i\phi} \\ c\rho^2 e^{-2i\phi} & \lambda\rho e^{-i\phi} & -\Delta/2 \end{pmatrix}. \tag{2.29}$$

λ is known as the $\Sigma - \Pi$ coupling constant and Δ is the energy difference between the Σ and the Π state at linear configuration.

The $\Sigma - \Pi$ Hamiltonian commutes with the following form of the total vibronic angular momentum operator

$$j'_z = \frac{1}{i}\frac{\partial}{\partial\phi}\begin{pmatrix} 1 & 0 & 0 \\ 0 & 1 & 0 \\ 0 & 0 & 1 \end{pmatrix} + \begin{pmatrix} -1 & 0 & 0 \\ 0 & 0 & 0 \\ 0 & 0 & 1 \end{pmatrix}. \tag{2.30}$$

The eigenvalues of j'_z are integer numbers.

2.1.4 Inclusion of totally symmetric modes

From Eq. (2.11) it is clear that the totally symmetric modes modulate the relative separation between the electronic states whereas the nontotally symmetric modes satisfying Eq. (2.14) describe the coupling between two electronic states. Therefore the totally symmetric modes are also called as "tuning modes" and the nontotally symmetric modes as "coupling modes". In the linear-VC approach, the tuning modes contribute only to the diagonal elements of the electronic Hamiltonian matrix, see Eq. (2.11). The inclusion of these modes to the VC models described earlier is, therefore, straightforward.

In the E×E JT case the N_t tuning modes are represented by

$$H^t_{\mathrm{JT}} = \sum_{i=1}^{N_t}\left[\left(\frac{\partial^2}{\partial Q_i^2} + Q_i^2\right)\mathbf{1}_2 + \begin{pmatrix} \kappa_i^E & \\ & \kappa_i^E \end{pmatrix} Q_i\right] \tag{2.31}$$

where the Q_i are totally symmetric modes and the κ_i^E are the gradients of the adiabatic PE functions of the E state with respect to the ith tuning mode.

For linear triatomic molecules, the stretching modes are the totally symmetric modes. The Hamiltonian corresponding to the tuning modes in case of RT coupling is

$$H^t_{\mathrm{RT}} = \sum_{i=1,3} \left[\left(\frac{\partial^2}{\partial Q_i^2} + Q_i^2 \right) \mathbf{1}_2 + \begin{pmatrix} \kappa_i^{\Pi} & \\ & \kappa_i^{\Pi} \end{pmatrix} Q_i \right]. \tag{2.32}$$

For the Σ-Π coupling, it is

$$H^t_{\Sigma-\Pi} = \sum_{i=1,3} \left[\left(\frac{\partial^2}{\partial Q_i^2} + Q_i^2 \right) \mathbf{1}_3 + \begin{pmatrix} \kappa_i^{\Pi} & & \\ & \kappa_i^{\Sigma} & \\ & & \kappa_i^{\Pi} \end{pmatrix} Q_i \right]. \tag{2.33}$$

From Eqs. (2.21), (2.27), (2.29), (2.31), (2.32), and (2.33), we have

$$\left[H_{\mathrm{JT}}, H^t_{\mathrm{JT}}\right] = \left[H_{\mathrm{RT}}, H^t_{\mathrm{RT}}\right] = 0, \quad \text{but} \quad \left[H_{\Sigma-\Pi}, H^t_{\Sigma-\Pi}\right] \neq 0. \tag{2.34}$$

From the above relations, the stretching and the bending motion of linear triatomic molecules can be decoupled if the VC of an isolated degenerate Π electronic state is considered. This decoupling, however, is not possible when the VC of Σ and Π electronic states are considered.

2.2 Calculation of spectra

We consider a molecule that is initially in the state $|\Psi_0\rangle$ and is excited by some operator $\mathcal{T}$ into a manifold of vibronically coupled electronic states. According to Fermi's golden rule, the excitation spectrum is described by the transition probability per unit time

$$P(E) = 2\pi \sum_{\nu} |\langle \Psi_0 | \mathcal{T} | \Psi_\nu \rangle|^2 \, \delta(E - E_0 - E_\nu) \tag{2.35}$$

where E_0 denotes the energy of the reference state $|\Psi_0\rangle$ and E_ν is the energy of the final molecular vibronic state $|\Psi_\nu\rangle$. Assuming the reference state to be energetically separated and vibronically decoupled from the excited states, we can apply the adiabatic approximation and write

$$|\Psi_0\rangle = |\Phi_0\rangle|\mathbf{0}\rangle, \tag{2.36}$$

where $|\Phi_0\rangle$ and $|\mathbf{0}\rangle$ represent the electronic and nuclear wave functions of the reference state $|\Psi_0\rangle$. The final vibronic states $|\Psi_\nu\rangle$ are obtained by a numerical exact solution of the time-independent Schrödinger equation for the VC Hamiltonian H

$$H|\Psi_\nu\rangle = E_\nu|\Psi_\nu\rangle. \tag{2.37}$$

We determine $|\Psi_\nu\rangle$ via an expansion in terms of a direct product basis of diabatic electronic states $|\phi_n\rangle$ and nuclear wave functions $|\chi_{\mathbf{v}}(Q)\rangle$, i.e.,

$$\begin{aligned} |\Psi_\nu\rangle &= \sum_n C^\nu_{n,\mathbf{v}} |\phi_n\rangle |\chi_{\mathbf{v}}(Q)\rangle \\ &= \sum_n \sum_{v_1 v_2 \ldots} C^\nu_{n,v_1,v_2,\ldots} |\phi_n\rangle |\chi_{v_1}(Q_1)\rangle |\chi_{v_2}(Q_2)\rangle \ldots \\ &= \sum_n \sum_{v_1 v_2 \ldots} C^\nu_{n,v_1,v_2,\ldots} |n\rangle \prod_j |v_j\rangle \end{aligned} \tag{2.38}$$

where $|v_j\rangle$ are one (for nondegenerate mode)- or two (for doubly degenerate mode)-dimensional harmonic oscillator basis functions for the jth mode. The determination of the Hamiltonian matrix elements is straightforward for unperturbed harmonic oscillator basis functions [106]. In many cases, the vibronic Hamiltonian commutes with a total angular momentum operator J_z, see, for example, Eqs. (2.24), (2.28), and (2.30) for the JT, RT, and $\Sigma - \Pi$ Hamiltonians, respectively. In these cases the full Hamiltonian matrix decouples into submatrices corresponding to different eigenvalues of j'_z which are the good quantum numbers. The real symmetric Hamiltonian matrix is constructed and diagonalized for a given value of the good quantum number. The vibrational basis is increased until convergence of the eigenvalues of interest has been achieved.

Insertion of Eq. (2.38) in Eq. (2.37) yields the following eigenvalue problem

$$H\mathbf{C}^\nu = E_\nu \mathbf{C}^\nu, \tag{2.39}$$

where $\mathbf{C}^\nu$ is the column matrix of coefficients $C^\nu_{n,v_1,v_2\ldots}$. Within the Condon approximation, only the coefficients $C_{n,0,0\ldots}$ need to be obtained when the initial state is assumed to be vibrationless. The intensity is given by

$$P(E) = 2\pi \sum_\nu \tau_n^2 \left|\langle \mathbf{0}|\chi_{\mathbf{0}}\rangle\right|^2 \delta(E - E_0 - E_\nu). \tag{2.40}$$

Here $\tau_n = \langle \phi_0 | \mathcal{T} | \phi_n \rangle$ is the electronic transition matrix element.

The eigenvalue problem (2.39) becomes difficult to solve for multi-mode VC models when the dimension of the Hamiltonian matrix becomes too large to be stored and diagonalized using standard routines. To circumvent this problem, one often uses the Lanczos method of diagonalizing matrices of very large dimension [107, 108]. The method uses an iterative matrix-vector multiplication to reduce the sparse Hamiltonian matrix to a tridiagonalized form which is then diagonalized yielding the eigenvalues and eigenvectors of interest. The details of this procedure are given in Appendix A.

The excitation spectrum (2.40) exhibits a series of lines that are represented by δ functions. To account for the finite experimental resolution and rotational broadening, the final form of the theoretical spectrum is obtained by convolution with a normalized Lorentzian of full width at half maximum (FWHM) Γ

$$L(E) = \frac{1}{\pi} \frac{\Gamma/2}{E^2 + (\Gamma/2)^2}. \tag{2.41}$$

When all the interstate coupling constants are put equal to zero, all the nonadiabatic effects vanish and the spectrum is particularly simple. For each final electronic state ϕ_f, the spectrum is the well-known spectrum of a shifted harmonic oscillator. All nuclear motions decouple and consequently the spectrum is a convolution of the spectra of individual one-dimensional oscillators. Each of the latter spectra can be written as [40]

$$P(E) = 2\pi|\tau_f|^2 \sum_{n=0}^{\infty} \left(\exp\left(-a_f\right) \frac{a_f^n}{n!} \right) \delta(E - E_f + a_f\omega - n\omega) \tag{2.42}$$

which is a series of equidistant peaks weighted by a Poisson distribution with a Poisson parameter $a_f = (\kappa_f^2/2\omega^2)$i, where κ_f is the intra-state coupling constant defined in Eq. (2.12).

2.3 Relativistic quantum mechanics

Relativistic effects arise from the difference in the true velocity of light (c=137.0359895 au) as opposed to infinite velocity, which is the assumption in nonrelativistic quantum mechanics. Since the speed of an electron in a lighter element of the periodic table is small compared to the speed of light, the infinite speed of light is a good approximation for the lighter elements. This approximation, however, is inadequate for heavier elements where the electrons lying close to the nucleus attain velocities which can be comparable to that of light. Thus the central theme of relativity is the constant value of the speed of light in all inertial frames. Since the physical laws are required to be identical in such frames, the time and space coordinates become equivalent and the relativistic description of a particle require four coordinates: three spatial and one temporal [109, 110]. The requirement that the physical laws have to be equivalent in all inertial frames, the equations describing the relativistic quantum mechanics must be invariant with respect to the Lorentz transformation which describes the change between different coordinates in the four-dimensional space-time coordinate system [109, 110, 35].

The time-dependent Schrödinger equation, given below for one electron, is not relativistically correct, since the derivative with respect to the space coordinate is of second order, whereas the time derivative is of first order,

$$\left[-\frac{1}{2m}\nabla^2 + V\right]\psi = i\frac{\partial\psi}{\partial t}, \tag{2.43}$$

where ∇ is the Laplacian operator, m is the mass of the electron, and V is the PE of the system. The failure of the Schrödinger equation to be Lorentz invariant necessitates the formulation of its relativistic analog.

The starting point of relativistic quantum mechanics is the energy-mass-momentum relation of Einstein,

$$(E - V)^2 = m^2c^4 + p^2c^2. \tag{2.44}$$

Replacing the appropriate quantum-mechanical operators for E and p, one obtains the Klein-Gordon equation [110],

$$(m^2c^4 + \hat{p}^2c^2)\psi = \left(i\frac{\partial}{\partial t} - V\right)^2\psi. \tag{2.45}$$

This equation is Lorentz invariant, but has serious drawbacks, e.g., the probability density $\psi^*\psi$ can have negative values and the equation does not describe SO coupling [111]. The Klein-Gordon equation is, however, used for mesons (which have no spin).

The deficiency of the Klein-Gordon equation is due to its nonlinear space and time derivatives. Thus, Dirac started from the linear expression of the energy of Eq. (2.44). He used a new type of square root and obtained [112],

$$E = \underline{\beta}mc^2 + c\underline{\alpha}\cdot p + V, \tag{2.46}$$

where

$$\left[\underline{\alpha}_i, \underline{\alpha}_j\right]_+ {}^1 = 2\delta_{ij}, \quad \left[\underline{\alpha}_i, \underline{\beta}\right]_+ = 0, \quad \underline{\beta}^2 = 1. \tag{2.47}$$

Using appropriate quantum-mechanical operators,

$$\underbrace{\left[\underline{\beta}mc^2 + c\underline{\alpha}\cdot\hat{p} + V\right]}_{H_D}\psi = i\frac{\partial\psi}{\partial t}. \tag{2.48}$$

The above equation is known as Dirac equation and is the relativistic analog of the Schrödinger equation. The Dirac equation is suitable for the relativistic

[1] anti-commutation

description of electrons. $\underline{\alpha}$ and $\underline{\beta}$ are conventionally represented as,

$$\underline{\alpha}_x = \begin{pmatrix} \mathbf{0} & \sigma_x \\ \sigma_x & \mathbf{0} \end{pmatrix} \quad \underline{\alpha}_y = \begin{pmatrix} \mathbf{0} & \sigma_y \\ \sigma_y & \mathbf{0} \end{pmatrix} \quad \underline{\alpha}_z = \begin{pmatrix} \mathbf{0} & \sigma_z \\ \sigma_z & \mathbf{0} \end{pmatrix} \quad \underline{\beta} = \begin{pmatrix} \mathbf{1}_2 & \mathbf{0} \\ \mathbf{0} & -\mathbf{1}_2 \end{pmatrix}, \tag{2.49}$$

where σ_x, σ_y, and σ_z are the well-known Pauli matrices:

$$\sigma_x = \begin{pmatrix} 0 & 1 \\ 1 & 0 \end{pmatrix} \quad \sigma_y = \begin{pmatrix} 0 & -i \\ i & 0 \end{pmatrix} \quad \sigma_z = \begin{pmatrix} 1 & 0 \\ 0 & -1 \end{pmatrix}, \tag{2.50}$$

and

$$\mathbf{0} = \begin{pmatrix} 0 & 0 \\ 0 & 0 \end{pmatrix}.$$

The Dirac Hamiltonian in matrix notation reads

$$H_D = \begin{pmatrix} V + mc^2 & 0 & c\hat{p}_z & c(\hat{p}_x - i\hat{p}_y) \\ 0 & V + mc^2 & c(\hat{p}_x + i\hat{p}_y) & -c\hat{p}_z \\ c\hat{p}_z & c(\hat{p}_x - i\hat{p}_y) & V - mc^2 & 0 \\ c(\hat{p}_x + i\hat{p}_y) & -c\hat{p}_z & 0 & V - mc^2 \end{pmatrix}. \tag{2.51}$$

The Dirac equation is first order in time and space and is Lorentz invariant [112, 35, 110]. Since the one-particle Dirac Hamiltonian involves 4×4 matrices instead of scalar functions, the solution of the Dirac equation is a vector of four components known as four-component spinor. Two of the degrees of freedom are accounted for by assigning an intrinsic magnetic moment (spin), while the other two are interpreted as two different particles: electrons (positive energy) and positrons (negative energy).

The time-independent Dirac equation can be written as,

$$H_D \Psi = E\Psi, \tag{2.52}$$

where

$$\Psi = \begin{pmatrix} \psi_{L\alpha} \\ \psi_{L\beta} \\ \psi_{S\alpha} \\ \psi_{S\beta} \end{pmatrix}. \tag{2.53}$$

Here ψ_L and ψ_S are the so-called large and small components, respectively, of wave function Ψ, while α and β are spin functions. In the nonrelativistic limit, i.e., $c \to \infty$, for electrons, the large component reduces to the solutions of Schrödinger equation and the small component vanishes. The opposite applies for positrons.

Separating the large and small components of the Dirac equation followed by the normalization of the large component wave function and keeping terms up to order c^{-2}, one arrives at the well-known Pauli Hamiltonian [36, 110, 35],

$$H_P = T - \underbrace{\frac{\hat{p}^2 V}{8m^2c^2}}_{\text{Darwin}} - \underbrace{\frac{\hat{p}^4}{8m^3c^2}}_{\text{mass-velocity}} + \underbrace{i\frac{\sigma \cdot (\hat{p}V) \times \hat{p}}{4m^2c^2}}_{\text{spin-orbit}} + V. \tag{2.54}$$

So far, we have considered only one-electron operators. For molecular applications, however, electron-electron interactions in the PE operator are important. The simplest form of the electron-electron interaction is the (non-relativistic) Coulomb operator

$$V = \sum_{i<j} \frac{1}{r_{ij}}. \tag{2.55}$$

This form of the PE operator is not correct in relativistic theory, since it is not Lorentz invariant. It implies an instantaneous interaction between two electrons, which is forbidden in relativistic theory as nothing can move faster than light. Hence a retardation term is introduced [113].

In order to obtain a two-electron interaction term which is consistent with special relativity, it is necessary to turn to quantum electrodynamics. The electron-electron interaction term is expanded in a Taylor series in $1/c$ and the terms up to $1/c^2$ are retained. In this approximation the PE operator for the electron-electron interaction becomes [114, 115],

$$V_{12} = \underbrace{\frac{1}{r_{12}}}_{\text{Coulomb term}} \overbrace{- \frac{1}{2r_{12}} \left[\underbrace{(\underline{\alpha}_1 \cdot \underline{\alpha}_2)}_{\text{Gaunt term}} + \underbrace{\frac{(\underline{\alpha}_1 \cdot r_{12})(\underline{\alpha}_2 \cdot r_{12})}{r_{12}^2}}_{\text{retardation term}} \right]}^{\text{Breit term}}. \tag{2.56}$$

The above operator is known as the Coulomb-Breit operator. $\underline{\alpha}_1$ and $\underline{\alpha}_2$ represent the $\underline{\alpha}$ matrices of Eq. (2.47) for electron 1 and 2.

Using the Coulomb-Breit form of PE in the Pauli Hamiltonian of Eq. (2.54), one obtains the well-known Breit-Pauli operator. For the application in VC theory, the scalar terms like Darwin and mass-velocity corrections are less important than the SO term. Using the last term of Eq. (2.54) and Eq. (2.56), the one- and two-electron Breit-Pauli SO operator can be written as [116],

$$
\begin{aligned}
H_{\mathrm{BP}}^{\mathrm{SO}} = \frac{1}{2m^2c^2}\Bigg[& \sum_i \left(-\hat{p}_i \left(\sum_I \frac{Z_I}{r_{iI}} \right) \times \hat{p}_i \right) \cdot \sigma_i \\
& + \sum_i \sum_{j \neq i} \left(\hat{p}_i \left(\frac{1}{r_{ij}} \right) \times \hat{p}_i \right) \cdot \sigma_i \\
& + \sum_i \sum_{j \neq i} \left(\hat{p}_j \left(\frac{1}{r_{ij}} \right) \times \hat{p}_j \right) \cdot \sigma_i \\
& + \sum_j \sum_{i \neq j} \left(\hat{p}_i \left(\frac{1}{r_{ji}} \right) \times \hat{p}_i \right) \cdot \sigma_j \Bigg] .
\end{aligned} \tag{2.57}
$$

The first two terms represent the spin-same-orbit part, of which, the former is the one-electron term that describes the interaction of the spin-magnetic moment of an electron i with the magnetic moment that arises from its orbiting in the field of nucleus I and the latter is the two-electron analog relating the motion of electron i in the field of electron j. The last two terms are the spin-other-orbit terms. They describe the coupling between the spin moment of electron i and the orbital moment of electron j and vice versa.

2.4 Electronic structure methods

The use of the Dirac Hamiltonian as the relativistic substitute for the one electron terms of the nonrelativistic many-electron Hamiltonian yields the Dirac-Coulomb Hamiltonian. The relativistic corrections to the Coulomb term give rise to the Dirac-Coulomb-Breit Hamiltonian. This Hamiltonian may be utilized to construct a Hartree-Fock (HF)-like wave function, which is known as the Dirac-Hartree-Fock (DHF) method. In a manner analogous to HF theory, DHF begins with the assumption that an n-electron wave function can be represented as an antisymmetrized product of n single-particle functions. These single-particle functions are four-component spinors. The requirement that the wave function should be stationary with respect to a variation in the spinors results in an equation which is formally equivalent to the nonrelativistic Hartree-Fock-Roothan equation [117]. However, the presence of solutions for the positronic states means that the desired solution is no longer the global minimum. If positronic states are occupied in the variational construction of Dirac-Fock operator, the single particle spinors will collapse to the negative energy minimum. An essential ingredient in this context is, therefore, the choice of the basis set. The basis sets for large and

small components have to be properly balanced. This is known as "kinetic balance" where the small component basis sets contain functions which are derivatives of the large component basis sets [118]. The use of kinetic balance ensures that the relativistic solution smoothly reduces to the nonrelativistic wave function as the speed of light is increased to infinite.

2.4.1 Electron correlation and spin-orbit coupling

The DHF method represents a technique for obtaining single-determinant wave functions which account for the most important consequences of special relativity. For chemical purposes, however, a single-determinant method is inadequate. Therefore methods accounting for correlation effects such as multi-configuration self-consistent field (MCSCF), many-body perturbation theory (MBPT), configuration interaction (CI), and coupled cluster (CC) have been developed which use a DHF reference wave function [119, 120].

The positronic solutions of the Dirac Hamiltonian as well as the approximate multi-electron Hamiltonians such as Dirac-Coulomb or Dirac-Coulomb-Breit Hamiltonians give rise to equations which are more complicated to interpret physically and more difficult to implement computationally. The relatively large basis set (due to the presence of small and large components and their kinetic balance) and the mixed real and imaginary part of wave function (due to the presence of spin) render the four-component methods computationally very expensive [118].

Therefore, methods which decouple the positronic and electronic solutions have been employed with a great deal of success. Though it is not possible to exactly separate the two parts of the DHF wave functions, methods such as the Foldy-Wouthoysen transformation [121] and the related Douglas-Kroll(-Hess) transformation [122, 123] can produce a molecular Hamiltonian which is decoupled (to a certain order of $1/c$) to two-component Hamiltonians [124, 125]. The resultant Hamiltonian and the two-component solutions represent the interaction of only electrons (or positrons) and nuclei. The two-component methods are thus variationally stable and account for the main relativistic effects. The operators appearing in the two-component Hamiltonians are quite complicated and the analytical calculation of matrix elements is no longer possible. In addition, the two-electron terms in these methods are hard to evaluate [116, 118].

The simultaneous treatment of relativistic effects and electron correlation is very computationally demanding and is, therefore, limited to systems containing at most two heavy atoms. To improve the efficiency of the calculations, one uses a different method known as spin-orbit CI or SOCI [118, 126, 111, 116]. In this method, usual orbitals are employed in-

stead of spinors. Here, the SO coupling is considered as a perturbation to the spin-free (or scalar-relativistic) Hamiltonian H_{SR}. The total Hamiltonian is thus the sum of a scalar-relativistic part and a SO part. The electrostatic and SO interactions are in general computed independently. The treatment of the electronic correlation is carried out in a scalar-relativistic scheme within a Schrödinger like formalism and takes advantage of nonrelativistic symmetries, which simplifies the CI calculations. In this scheme, the CI matrix without the SO interaction is diagonalized in a first step, providing nonrelativistic wave functions expanded in terms of Slater determinants. These correlated wave functions form a basis set, in which the SO Hamiltonian is represented in a second step. The simplest way to compute the SO interactions between spin-free correlated states is to employ correlated wave functions as zero-order basis functions to compute the SO splitting to first order within degenerate perturbation theory [118].

A straightforward generalization of the perturbation treatment is to use the correlated scalar relativistic functions ϕ_m^{SR} of the scalar Hamiltonian H_{SR} as a truncated set of contracted many-electron basis functions for the total Hamiltonian. Introducing the subscript i_m for a given ϕ_m^{SR} wave functions to indicate the spatial and spin components of this multiplet, the matrix representation of the Hamiltonian reads [118]

$$\begin{aligned}\langle\phi_{m,i_m}^{\mathrm{SR}}|H|\phi_{n,j_n}^{\mathrm{SR}}\rangle &= \langle\phi_{m,i_m}^{\mathrm{SR}}|H^{\mathrm{SR}}+H^{\mathrm{SO}}|\phi_{n,j_n}^{\mathrm{SR}}\rangle \\ &= \delta_{m,n}\delta_{i_m,j_n}E_m \\ &\quad +(1-\delta_{i_k,j_k})\langle\phi_{k,i_k}^{\mathrm{SR}}|H^{\mathrm{SO}}|\phi_{k,j_k}^{\mathrm{SR}}\rangle, \end{aligned} \tag{2.58}$$

where $m,n \in [1,N]$ and $k=m,n$. N is the number of correlated multiplet states coupled by the SO interaction and the total number of states in the matrix representation is $N_t = \sum_{m=1,N} N_m$ where N_m is the degeneracy of the mth multiplet ($i_m \in [1,N_m]$). The block-diagonal elements $E_m\delta_{m,n}\delta_{i_m,j_n}$ contain N_m identical E_m values. The off-diagonal SO elements $(1-\delta_{i_k,j_k})\langle\phi_{k,i_k}^{\mathrm{SR}}|H^{\mathrm{SO}}|\phi_{k,j_k}^{\mathrm{SR}}\rangle$ (where $k=m$ or n) allow the coupling between components of either a given multiplet or even different multiplets. When $N=1$, the basis functions in Eq. (2.58) are just the degenerate components of a multiplet.

The diagonalization of the total Hamiltonian is split into two reduced diagonalizations: the first one for H^{SR} concerns the SCF and the CI treatment and is not burdened by the SO interaction, while the diagonalization of H^{SO} benefits from a small number of basis correlated functions. This method is the best compromise to describe relativistic effects and electron correlation for systems with not too heavy elements.

2.4.2 Effective core potentials

The chemical similarity of elements in the same column of the periodic table leads to a fundamental assumption in chemistry, i.e., the low-lying core electrons are relatively inert and are not perturbed by a molecular environment. Since most of the important chemical properties of atoms and molecules are determined by the interaction of their valence electrons, a frozen-core approximation is found reasonable. Therefore the core orbitals are often replaced by a suitable potential, called effective potential, so that the number of two-electron integrals reduces drastically. The objective of the effective core potential (ECP) method is to construct potentials which are solely depending upon the coordinates of the valence electrons, but take into account the influence of the inert core electrons.

For an n-electron system, the antisymmetrized Hartree product wave function can be written as

$$\psi_{\mathrm{HF}} = \mathcal{A}(\phi_1, \phi_2, \cdots, \phi_n), \tag{2.59}$$

where $\mathcal{A}$ is the antisymmetrized operator and $\{\phi_i\}$ are single-particle eigenfunctions of the Fock operator

$$-\frac{\nabla_r^2}{2} - \frac{Z}{r} + \frac{l(l+1)}{2r^2} + \sum_{j=1}^{n} J_j - K_j. \tag{2.60}$$

where Z is nuclear charge, J and K are Coulomb and exchange operators, respectively. If we divide the orbitals to a group of N_c core and N_v valence orbitals, we can write the Fock operator as

$$-\frac{\nabla_r^2}{2} - \frac{Z}{r} + \frac{l(l+1)}{2r^2} + \underbrace{\sum_{a=1}^{N_c} J_a - K_a}_{V_{\mathrm{core}}} + \underbrace{\sum_{i=1}^{N_v} J_i - K_i}_{V_{\mathrm{val}}}. \tag{2.61}$$

The V_{core} term is now replaced by effective potential (V^{eff}) and nuclear charge Z by Z^{eff} such that:

$$\left[-\frac{\nabla_r^2}{2} - \frac{Z^{\mathrm{eff}}}{r} + \frac{l(l+1)}{2r^2} + V_{\mathrm{val}} + V^{\mathrm{eff}}\right]\phi_i = E_l\phi_i. \tag{2.62}$$

The next step is to consider the above equation for a valence atomic orbital of angular momentum l, ϕ_i^l, and to obtain an analytical form for V^{eff}. By inverting Eq. (2.62) we have

$$V_l^{\mathrm{eff}} = E_l + \frac{Z^{\mathrm{eff}}}{r} - \frac{l(l+1)}{2r^2} + \frac{(\nabla_r^2/2 - V_{\mathrm{val}})\phi_i^l}{\phi_i^l}. \tag{2.63}$$

The above expression for V_l^{eff} is, however, valid only for $\phi_i \neq 0$. This requires the valence orbitals $\{\phi_i\}$ to be replaced by approximate pseudo orbitals $\{\chi_i\}$ which are nodeless. Ideally, the V_l^{eff} is obtained such that the atomic valence pseudo orbitals $\{\chi_i\}$ are as close as possible to the original orbitals $\{\phi_i\}$. Using the nodeless pseudo orbitals, we can write,

$$\left[-\frac{\nabla_r^2}{2} - \frac{Z^{\text{eff}}}{r} + \frac{l(l+1)}{2r^2} + V'_{\text{val}} + V_l^{\text{eff}}\right]\chi_i^l = E_i^l \chi_i^l. \tag{2.64}$$

The ECP obtained in this way take care of the core-core and core-valence interactions. The valence-valence interaction, however, can be considered by minimizing the difference between V_{val} and V'_{val} which arises because of the replacement of the true orbitals by the pseudo orbitals. This is achieved by using pseudo orbitals that resemble the true valence orbitals $\{\phi_i\}$ for $r \geq R_{\text{max}}$, where R_{max} is the radius at which ϕ_i experiences its outermost maximum. Inside this region the wave function is fitted to a smooth polynomial function. This procedure gives rise to the so-called shape-consistent ECP [127]. By solving Eq. (2.64) we obtain

$$V_l^{\text{eff}} = E_i^l + \frac{Z^{\text{eff}}}{r} - \frac{l(l+1)}{2r^2} + \frac{(\nabla_r^2/2 - V'_{\text{val}})\chi_i^l}{\chi_i^l}. \tag{2.65}$$

There exists another way to obtain effective potential. In this approach, the analytical expression of V_l^{eff} is fitted to reproduce either the experimental atomic spectrum or the atomic spectrum obtained from an all-electron calculation at a given level of theory. The effective potentials obtained from this method are called energy-consistent ECP [127].

The ECP for a given element can be written in a semilocal form

$$V_{\text{eff}} = \sum_l V_{\text{eff}}^l(r) \sum_{m=-l}^{l} |lm\rangle\langle lm|, \tag{2.66}$$

where $|lm\rangle$ are the usual spherical harmonic eigenfunctions. Finally the effective potential is obtained by fitting to a semilocal Gaussian-type function for a given value of l.

2.4.3 Relativistic effective core potentials

The electrons close to the nucleus possess a large value of the kinetic energy and hence are more affected by relativity than the slow-moving valence electrons. Therefore, an ECP method which incorporates the direct relativistic effects experienced by the core orbitals is of great practical interest [111, 126, 118].

The starting point for the relativistic ECP (RECP) is the atomic Dirac-Coulomb Fock equations. The valence solutions $\{\phi_i\}$ are four-component spinors. Since the large components account for most of the electron density, the renormalized large components are used to obtain relativistic pseudo orbitals $\{\chi_i\}$. Since the DHF eigenstates are eigenstates of the total angular momentum operator $\hat{j} = \hat{l} + \hat{s}$, the resultant RECPs are no longer uniquely defined for a particular value of l. Instead, the RECPs are dependent on l and j. In order to use the RECP within a nonrelativistic frame-work, it is desirable to have only l-dependent RECP. This is usually done by statistically averaging over all of the appropriate j-dependent RECPs which are associated with a particular l value. The resulting RECPs are called l-averaged RECP (AREP's). The AREPs take into account the nuclear shielding and core contraction effects. The SO effects, on the other hand, are described by the so-called SO relativistic effective potentials (SOREP) which are obtained as the difference between the RECP and the AREP [111, 126, 118].

2.4.4 Core-polarization potential

One of the main approximations used in pseudo-potential theory is based on the core-valence separation. The correlation effects corresponding to core-core, core-valence, and valence-valence interactions are known to influence the SO coupling with respect to the core-valence separation. The separation becomes less obvious for the elements with a highly polarizable atomic core. In these cases, a core-polarization potential (CPP) is applied to describe accurately the interaction between the core and valence spaces [118].

The CPP is extracted from the experimental data (the core polarizability) and accounts for all effects which are not present in the pseudo potential, namely, core polarization, core-core, and core-valence correlation effects. The CPP is recommended in calculations involving a large core where the separation of core and valence parts may be problematic [118, 127].

Chapter 3

Renner-Teller and spin-orbit vibronic-coupling effects

3.1 Vibronic Hamiltonian in the diabatic basis

Let us consider the RT VC problem in a $^2\Pi$ electronic state of a linear triatomic molecule with a single unpaired electron. Following the analysis of Poluyanov and Domcke [128], the vibronic Hamiltonian of this single-electron system can be written as ($\hbar = 1$),

$$\begin{aligned}
H &= T_{\mathrm{N}} + H_{\mathrm{el}} \\
&= T_{\mathrm{N}} + H_{\mathrm{es}} + H_{\mathrm{SO}} \qquad (3.1) \\
T_{\mathrm{N}} &= \left[-\frac{\omega_2}{2}\left(\frac{1}{\rho}\frac{\partial}{\partial\rho}\rho\frac{\partial}{\partial\rho} + \frac{1}{\rho^2}\frac{\partial^2}{\partial\phi^2}\right) + \frac{\omega_2}{2}\rho^2\right] \\
&\quad + \sum_{i=1,3}\left(-\frac{\omega_i}{2}\frac{\partial^2}{\partial Q_i^2} + \frac{\omega_i}{2}Q_i^2\right) \qquad (3.2) \\
H_{\mathrm{es}} &= -\frac{1}{2}\nabla^2 - \sum_{n=1}^{3}\frac{eq_n}{r_n} \qquad (3.3) \\
H_{\mathrm{SO}} &= -\frac{i}{2m^2c^2}\sum_{n=1}^{3}\frac{q_n}{r_n^3}\left[r\sin\phi\frac{\partial}{\partial z} - z_n\left(\sin\phi\frac{\partial}{\partial r} + \frac{\cos\phi}{r}\frac{\partial}{\partial\phi}\right)\right]\cdot\sigma_x \\
&\quad -\frac{i}{2m^2c^2}\sum_{n=1}^{3}\frac{q_n}{r_n^3}\left[z_n\left(\cos\phi\frac{\partial}{\partial r} - \frac{\sin\phi}{r}\frac{\partial}{\partial\phi}\right) - r\cos\phi\frac{\partial}{\partial z}\right]\cdot\sigma_y \\
&\quad -\frac{i}{2m^2c^2}\sum_{n=1}^{3}\frac{q_n}{r_n^3}\frac{\partial}{\partial\phi}\cdot\sigma_z \\
&= A_x\cdot\sigma_x + A_y\cdot\sigma_y + A_z\cdot\sigma_z. \qquad (3.4)
\end{aligned}$$

Here $H_{\rm es}$ is the electrostatic part of the electronic Hamiltonian that includes the electronic kinetic energy and the electronic nuclear interaction term. The SO coupling of the electron in the field of three nuclei is given by the $H_{\rm SO}$ which is described within the single-electron approximation of the Breit-Pauli SO operator (2.57), expressed in cylindrical coordinates. Here the q_n are the effective nuclear charges. A_x, A_y, and A_z are differential operators in electronic coordinate space introduced to simplify the expression for $H_{\rm SO}$. m is the mass of the electron. The σ_x, σ_y, and σ_z are the Pauli spin matrices introduced in Eq. (2.50). $T_{\rm N}$ is the nuclear kinetic energy operator. ω_1 and ω_3 are the the harmonic frequencies associated with the totally symmetric stretching modes Q_1 and Q_3, respectively, whereas ω_2 is the averaged bending frequency associated with the degenerate bending mode, described in polar coordinates (ρ, ϕ). ρ and ϕ represent the radial and angular part of the degenerate bending vibrational mode, respectively, whose relationship with the complex valued Cartesian coordinates $Q_\pm$ is given in Eq. (2.17).

The electronic Hamiltonian $H_{\rm el}$ can be shown to commute with the z-component of the electronic angular momentum operator

$$j_z = -i\frac{\partial}{\partial\theta} + \sigma_z, \tag{3.5}$$

where θ is the angular electronic coordinate and σ is the spin angular momentum. j_z describes a continuous symmetry, generating an one-parametrical group of unitary transformations

$$J_z(\epsilon) = e^{i\epsilon j_z}. \tag{3.6}$$

Here ϵ is the angular group parameter.

The electronic Hamiltonian $H_{\rm el}$ also possesses the TR symmetry. For odd-electronic systems, the TR operator $\hat{T}$ is an antiunitary operator that satisfies [129, 130],

$$\langle\hat{T}\psi_1|\hat{T}\psi_2\rangle = \langle\psi_1|\psi_2\rangle^*. \tag{3.7}$$

The full Hamiltonian H of Eq. (3.1), satisfies, in addition to the TR property,

$$[H, j_z'] = 0 \tag{3.8}$$

with

$$j_z' = j_z - i\frac{\partial}{\partial\phi}. \tag{3.9}$$

Here j_z' is the z-component of the total angular momentum operator (including the nuclear angular momentum). The eigenvalues (μ) of j_z' are half integers ($\mu = \pm 1/2, \pm 3/2, \cdots$). The eigenvalues of H are doubly degenerate (Kramer's degeneracy [131]), which is a consequence of the TR symmetry.

Lets define $|\psi_{\pm}\rangle$ as diabatic [95, 96, 97] electronic basis set associated with the two components of the degenerate $^2\Pi$ electronic state. The coupling of the spin motion with the orbital motion of the electron gives rise to four SO coupled states. Hence, a complete diabatic electronic basis set is given by $|\psi_{\pm\alpha}\rangle$ and $|\psi_{\pm\beta}\rangle$ where the notation $|\psi_{\pm\alpha}\rangle$ stands for $|\psi_{\pm}\rangle|\alpha\rangle$. Here α and β represent the two spin eigenstates of the single unpaired electron.

For linear molecules with cylindrical symmetry, the following relationship is fulfilled by the diabatic electronic basis,

$$J_z(\epsilon)|\psi_{\Lambda,\sigma}\rangle = e^{i\epsilon(\Lambda+\sigma)\phi}|\psi_{\Lambda,\sigma}\rangle. \tag{3.10}$$

The TR operator $\hat{T}$ has the following effect on the diabatic electronic basis functions:

$$\begin{aligned} \hat{T}|\psi_{\pm\alpha}\rangle &= |\psi_{\mp\beta}\rangle \\ \hat{T}|\psi_{\pm\beta}\rangle &= -|\psi_{\mp\alpha}\rangle. \end{aligned} \tag{3.11}$$

The electronic Hamiltonian in this diabatic electronic basis can be written as

$$H_{\rm el} = \begin{array}{c|cccc} & \psi_{+\alpha} & \psi_{-\alpha} & \psi_{+\beta} & \psi_{-\beta} \\ \hline \psi_{+\alpha} & H^{++}_{\alpha\alpha} & H^{+-}_{\alpha\alpha} & H^{++}_{\alpha\beta} & H^{+-}_{\alpha\beta} \\ \psi_{-\alpha} & H^{-+}_{\alpha\alpha} & H^{--}_{\alpha\alpha} & H^{-+}_{\alpha\beta} & H^{--}_{\alpha\beta} \\ \psi_{+\beta} & H^{++}_{\beta\alpha} & H^{+-}_{\beta\alpha} & H^{++}_{\beta\beta} & H^{+-}_{\beta\beta} \\ \psi_{-\beta} & H^{-+}_{\beta\alpha} & H^{--}_{\beta\alpha} & H^{-+}_{\beta\beta} & H^{--}_{\beta\beta} \end{array} . \tag{3.12}$$

While the totally symmetric stretching modes can contribute only to the diagonal elements, the nontotally symmetric degenerate bending mode can contribute to both diagonal and off-diagonal matrix elements.

Diagonal elements:

Let us expand the diagonal matrix element $H^{++}_{\alpha\alpha}$ in a Taylor series around the reference geometry up to second order in the two totally symmetric stretching modes $Q_{1,3}$ and the degenerate bending coordinate ($Q_{\pm}$),

$$\begin{aligned} H^{++}_{\alpha\alpha} &= H^{++(0)}_{\alpha\alpha} + \left(\frac{\partial H^{++}_{\alpha\alpha}}{\partial Q_{\pm}}\right)_0 Q_{\pm} + \sum_{i=1,3}\left(\frac{\partial H^{++}_{\alpha\alpha}}{\partial Q_i}\right)_0 Q_i \\ &+\frac{1}{2}\left(\frac{\partial^2 H^{++}_{\alpha\alpha}}{\partial Q^2_{\pm}}\right)_0 Q^2_{\pm} + \sum_{i=1,3}\frac{1}{2}\left(\frac{\partial^2 H^{++}_{\alpha\alpha}}{\partial Q^2_i}\right)_0 Q^2_i \\ &+\frac{1}{2}\left(\frac{\partial^2 H^{++}_{\alpha\alpha}}{\partial Q_+ \partial Q_-}\right)_0 Q_+ Q_- + \frac{1}{2}\left(\frac{\partial^2 H^{++}_{\alpha\alpha}}{\partial Q_1 \partial Q_3}\right)_0 Q_1 Q_3 \cdots \end{aligned} \tag{3.13}$$

Since $H_{\rm el}$ must be totally symmetric, it can be shown that only the totally symmetric terms in the above expansion can contribute to the matrix element $H^{++}_{\alpha\alpha}$. Thus, the second and the fourth term in the right-hand side of

the above equation vanish. Considering the tuning modes in the linear-VC approximation, we neglect the last term. By using the following definitions;

$$H^{++}_{\alpha\alpha}(\mathrm{es})^{(0)} = 0,$$

$$H^{++}_{\alpha\alpha}(\mathrm{SO})^{(0)} = \frac{\zeta}{2},$$

$$\frac{1}{2}\left(\frac{\partial^2 H^{++}_{\alpha\alpha}(\mathrm{es})}{\partial Q_+ \partial Q_-}\right)_0 = \frac{\omega_2}{2},$$

$$\sum_{i=1,3}\left(\frac{\partial H^{++}_{\alpha\alpha}(\mathrm{es})}{\partial Q_i}\right)_0 = \sum_{i=1,3}\kappa_i,$$

$$\sum_{i=1,3}\frac{1}{2}\left(\frac{\partial^2 H^{++}_{\alpha\alpha}(\mathrm{es})}{\partial Q_i^2}\right)_0 = \sum_{i=1,3}\frac{\omega_i}{2},$$

we have,

$$H^{++}_{\alpha\alpha} = \frac{\zeta}{2} + \frac{1}{2}\omega_2\rho^2 + \sum_{i=1,3}\left(\kappa_i Q_i + \frac{1}{2}\omega_i Q_i^2\right). \tag{3.14}$$

Note that in the above equation we have neglected the quadratic SO-coupling terms and also the SO contribution to the linear stretching coupling terms, as they are expected to be small compared to other terms.

Similarly we can write

$$H^{--}_{\alpha\alpha} = -\frac{\zeta}{2} + \frac{1}{2}\omega_2\rho^2 + \sum_{i=1,3}\left(\kappa_i Q_i + \frac{1}{2}\omega_i Q_i^2\right). \tag{3.15}$$

Using the TR symmetry relations of Eqs. (3.7) and (3.11), we have

$$H^{++}_{\alpha\alpha} = H^{--}_{\beta\beta}; \quad H^{--}_{\alpha\alpha} = H^{++}_{\beta\beta}. \tag{3.16}$$

Off-diagonal elements:

Using the TR symmetry, Eqs. (3.7) and (3.11), we have

$$H^{+-}_{\alpha\beta} = H^{-+}_{\alpha\beta} = 0. \tag{3.17}$$

We define

$$H^{+-}_{\alpha\alpha} = (H^{-+}_{\beta\beta})^* = H^{+-}_{\beta\beta} = (H^{-+}_{\alpha\alpha})^* = \mathcal{C}, \tag{3.18}$$

$$H^{++}_{\alpha\beta} = -(H^{--}_{\beta\alpha})^* = -H^{--}_{\alpha\beta} = (H^{++}_{\beta\alpha})^* = \mathcal{D}. \tag{3.19}$$

Using the above definitions, Eq. (3.12) can be written as

$$H_{\rm el} = \begin{array}{c|cccc} & \psi_{+\alpha} & \psi_{-\alpha} & \psi_{+\beta} & \psi_{-\beta} \\ \hline \psi_{+\alpha} & \zeta/2 & \mathcal{C} & \mathcal{D} & 0 \\ \psi_{-\alpha} & & -\zeta/2 & 0 & -\mathcal{D} \\ \psi_{+\beta} & & & -\zeta/2 & \mathcal{C} \\ \psi_{-\beta} & & & & \zeta/2 \end{array} \tag{3.20}$$

The electrostatic part of the electronic Hamiltonian $H_{\rm es}$ contributes to matrix elements with the basis functions involving identical spin eigenstates. Hence the matrix element $\mathcal{C}$ will have contributions from the electrostatic Hamiltonian. The contribution of $H_{\rm SO}$ to the matrix elements of the electronic Hamiltonian is determined in the following way,

$$\mathcal{C}_{\rm SO} = \langle\psi_{+\alpha}|H_{\rm SO}|\psi_{-\alpha}\rangle = \frac{1}{2}\langle\psi_{+}|A_z|\psi_{-}\rangle = 0 \tag{3.21}$$

$$\mathcal{D}_{\rm SO} = \langle\psi_{+\alpha}|H_{\rm SO}|\psi_{+\beta}\rangle = \frac{1}{2}\langle\psi_{+}|A_x - iA_y|\psi_{+}\rangle \neq 0. \tag{3.22}$$

The matrix elements of the electronic Hamiltonian are expanded in a Taylor series up to second order in the degenerate bending mode ($Q_\pm$). The terms with appropriate symmetry with respect to the symmetry operation $J_z(\epsilon)$ of the corresponding electronic matrix elements survive. Using Eq. (3.10), it is found that the matrix element $\mathcal{C}$ is of second order in the expansion, whereas $\mathcal{D}$ is of first order.

Using the definitions

$$\left(\frac{\partial\mathcal{D}}{\partial Q_+}\right)_0 = d \quad \text{and} \quad \left(\frac{\partial\mathcal{C}}{\partial Q_+\partial Q_+}\right)_0 = c, \tag{3.23}$$

we obtain the following form of the 4×4 RT-SO VC Hamiltonian

$$H = \left(T_{\rm N} + \sum_{i=1,3}\kappa_i Q_i\right)\mathbf{1}_4 + \begin{pmatrix} \zeta/2 & c\rho^2 e^{2i\phi} & d\rho e^{i\phi} & 0 \\ c\rho^2 e^{-2i\phi} & -\zeta/2 & 0 & -d\rho e^{i\phi} \\ d\rho e^{-i\phi} & 0 & -\zeta/2 & c\rho^2 e^{2i\phi} \\ 0 & -d\rho e^{-i\phi} & c\rho^2 e^{-2i\phi} & \zeta/2 \end{pmatrix}. \tag{3.24}$$

Here ζ is the SO splitting of the $^2\Pi$ state. c is the well-known nonrelativistic quadratic RT coupling constant [17, 18, 19, 20], The parameter d, on the other hand, is a relativistic term of first order in the bending displacement. The coupling term d is absent when the phenomenological form of SO operator (1.1) is used [30] instead of the microscopic Breit-Pauli SO operator. This

linear-VC term has not been considered so far in the theory of the RT effect. The zeros appearing along the cross diagonal are a consequence of the TR symmetry.

In literature, the RT coupling is often characterized by the dimensionless RT parameter ϵ. It is defined as [132]

$$\epsilon = \frac{\left(\omega_2^+\right)^2 - \left(\omega_2^-\right)^2}{\left(\omega_2^+\right)^2 + \left(\omega_2^-\right)^2}. \tag{3.25}$$

where $\omega_2^{\pm}$ are the harmonic frequencies associated with the two RT components of the bending PE curve and related to the averaged bending frequency ω_2 via [132]

$$\omega_2 = \sqrt{\frac{1}{2}\left[\left(\omega_2^+\right)^2 + \left(\omega_2^-\right)^2\right]}. \tag{3.26}$$

The dimensionless RT parameter ϵ is related to the nonrelativistic coupling constant c via

$$\epsilon = \frac{2\omega_2 c}{\omega_2^2 + c^2}. \tag{3.27}$$

It should be noted that the stretching and bending modes remain decoupled when one restricts the discussion to an isolated Π electronic state. This is evident from the Eq. (3.24) where the stretching part of the vibronic Hamiltonian is diagonal and hence the stretching and bending Hamiltonians commute with each other.

3.2 Vibronic Hamiltonian in the adiabatic representation

For fixed nuclei, let us transform the vibronic matrix of Eq. (3.24) to diagonal form, i.e.,

$$\mathbf{W}^\dagger H \mathbf{W} = \mathbf{U}, \tag{3.28}$$

where the transformation matrix $\mathbf{W}$ is given by [128]

$$\begin{aligned}\mathbf{W} &= \mathbf{W}(\phi)\times\mathbf{W}(\rho)\\ &= \frac{1}{\sqrt{2}}\begin{pmatrix} e^{(\frac{3i\phi}{2}-i\frac{\pi}{4})} & 0 & 0 & e^{(\frac{3i\phi}{2}-i\frac{\pi}{4})}\\ 0 & e^{(-\frac{i\phi}{2}+i\frac{\pi}{4})} & -e^{(-\frac{i\phi}{2}+i\frac{\pi}{4})} & 0\\ 0 & e^{(\frac{i\phi}{2}-i\frac{\pi}{4})} & e^{(\frac{i\phi}{2}-i\frac{\pi}{4})} & 0\\ -e^{(-\frac{3i\phi}{2}+i\frac{\pi}{4})} & 0 & 0 & e^{(-\frac{3i\phi}{2}+i\frac{\pi}{4})}\end{pmatrix}\times\\ &\quad\begin{pmatrix} e^{i\tilde{\theta}}\cos\gamma & 0 & -e^{i\tilde{\theta}}\sin\gamma & 0\\ 0 & e^{i\tilde{\theta}}\cos\gamma & 0 & e^{i\tilde{\theta}}\sin\gamma\\ e^{-i\tilde{\theta}}\cos\gamma & 0 & e^{-i\tilde{\theta}}\cos\gamma & 0\\ 0 & -e^{-i\tilde{\theta}}\sin\gamma & 0 & e^{-i\tilde{\theta}}\cos\gamma\end{pmatrix}. \qquad (3.29)\end{aligned}$$

Here γ and $\tilde{\theta}$ are defined by

$$\tan(2\gamma) = 2\rho\sqrt{d^2+c^2\rho^2}/\zeta \qquad \tan(2\tilde{\theta}) = -\rho c/d.$$

The diagonal elements of $\mathbf{U}$ are the adiabatic PE functions given by

$$U_{1,2}(\rho) = \pm\frac{1}{2}\sqrt{\zeta^2+4\rho^2(d^2+\rho^2c^2)}. \qquad (3.30)$$

Both adiabatic terms $U_1(\rho)$ and $U_2(\rho)$ are two-fold degenerate, representing Kramers doublets [106, 129]. This degeneracy is a consequence of the TR symmetry.

Using the above transformation matrix $\mathbf{W}$, the diabatic spin-electronic states can be transformed to obtain the corresponding adiabatic spin-electronic states [128]

$$\begin{aligned}\sqrt{2}\psi_1^{\rm ad} &= e^{i\tilde{\theta}}\cos\gamma\left(e^{(\frac{3i\phi}{2}-i\frac{\pi}{4})}\psi_{+\alpha}-e^{(-\frac{3i\phi}{2}+i\frac{\pi}{4})}\psi_{-\beta}\right)\\ &\quad+e^{-i\tilde{\theta}}\sin\gamma\left(e^{(\frac{i\phi}{2}-i\frac{\pi}{4})}\psi_{+\beta}-e^{(-\frac{i\phi}{2}+i\frac{\pi}{4})}\psi_{-\alpha}\right)\\ \sqrt{2}\psi_2^{\rm ad} &= e^{i\tilde{\theta}}\sin\gamma\left(-e^{(\frac{3i\phi}{2}-i\frac{\pi}{4})}\psi_{+\alpha}+e^{(-\frac{3i\phi}{2}+i\frac{\pi}{4})}\psi_{-\beta}\right)\\ &\quad+e^{-i\tilde{\theta}}\cos\gamma\left(e^{(\frac{i\phi}{2}-i\frac{\pi}{4})}\psi_{+\beta}-e^{(-\frac{i\phi}{2}+i\frac{\pi}{4})}\psi_{-\alpha}\right)\\ \sqrt{2}\psi_3^{\rm ad} &= e^{-i\tilde{\theta}}\sin\gamma\left(-e^{(\frac{3i\phi}{2}-i\frac{\pi}{4})}\psi_{+\alpha}-e^{(-\frac{3i\phi}{2}+i\frac{\pi}{4})}\psi_{-\beta}\right)\\ &\quad+e^{i\tilde{\theta}}\cos\gamma\left(e^{(\frac{i\phi}{2}-i\frac{\pi}{4})}\psi_{+\beta}+e^{(-\frac{i\phi}{2}+i\frac{\pi}{4})}\psi_{-\alpha}\right)\\ \sqrt{2}\psi_4^{\rm ad} &= e^{-i\tilde{\theta}}\cos\gamma\left(e^{(\frac{3i\phi}{2}-i\frac{\pi}{4})}\psi_{+\alpha}+e^{(-\frac{3i\phi}{2}+i\frac{\pi}{4})}\psi_{-\beta}\right)\\ &\quad+e^{i\tilde{\theta}}\sin\gamma\left(e^{(\frac{i\phi}{2}-i\frac{\pi}{4})}\psi_{+\beta}-e^{(-\frac{i\phi}{2}+i\frac{\pi}{4})}\psi_{-\alpha}\right). \qquad (3.31)\end{aligned}$$

The TR operator $\hat{T}$ transforms these states within both Kramers doublets:

$$\begin{aligned} \hat{T}\psi_1^{\rm ad} &= \psi_4^{\rm ad} \quad : \text{adiabatic terms } U_1, \\ \hat{T}\psi_2^{\rm ad} &= \psi_3^{\rm ad} \quad : \text{adiabatic terms } U_2. \end{aligned} \tag{3.32}$$

An interesting property of the SO adiabatic states of Eq. (3.31) is the existence of a nontrivial topological phase: when ϕ is varying from 0 to 2π, the adiabatic states change their sign. It is noteworthy that this nontrivial topological phase exists despite the absence of a conical intersection of the adiabatic PE surfaces.

3.3 Generic aspects of relativistic linear Renner-Teller coupling

In this section, we discuss the generic effects of the LRVC term $d\rho e^{\pm i\phi}$ on RT spectra. For simplicity, we have neglected the totally symmetric stretching modes. Since d will be small for molecules with not too heavy atoms, the effect of the LRVC term is expected to become significant only when the potentially interacting unperturbed levels are nearly degenerate. Since d couples, in first order, levels with different spin quantum number which differ by one quantum of the bending frequency, we expect near-degeneracy effects when the absolute value of ω_2 and ζ are nearly equal. We shall refer to the case $\omega_2 \simeq \zeta$ as the "resonant case" in the following.

As is well known in RT theory [30, 22, 23, 24, 16, 133], two limiting cases can be considered. In case A, the SO splitting ζ is small compared with the nonrelativistic RT coupling constant c, which in turn is small compared with the bending frequency ω_2. In case B, the SO splitting ζ is comparable to or larger than ω_2 and/or c. We shall be concerned here with a special case of case B, in which $\zeta \simeq \omega_2$ and $c < \omega_2$.

Figure 3.1 shows the energy levels of such a system with $d = 0$. The parameter values are $\zeta/\omega_2 = -0.8$, $c/\omega_2 = 0.08$. The negative sign of the SO splitting implies that the 3/2 component of the $^2\Pi$ state lies below the 1/2 component. The unperturbed bending levels are shown in column (a). Column (b) gives the energy levels of the nonrelativistic RT system. The energy levels obtained with inclusion of the SO splitting ζ are given in column (c), assigned by usual spectroscopic terms [30, 22, 23, 24, 16, 133, 37, 38].

It is seen that the energy levels (000) $^2\Pi_{1/2}$ and (010) μ $^2\Sigma_{1/2}$ are close in energy, as a consequence of $\omega_2 \simeq \zeta$ and $c < \omega_2, \zeta$. The same applies for the level pairs (020) μ $^2\Pi_{3/2}$, (010) $^2\Delta_{3/2}$, and (010) κ $^2\Sigma_{1/2}$, (020) μ $^2\Pi_{1/2}$. These

Figure 3.1: Energy levels of a RT system with SO coupling in the resonant case ($\zeta \simeq \omega_2$).

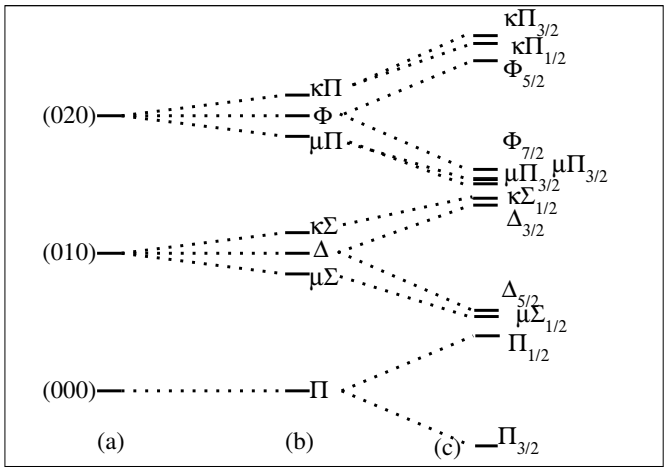

quasi-degenerate energy levels interact with each other when the coupling term $d\rho e^{\pm i\phi}$ is taken into account.

Figure 3.2 displays the energy levels of this system (complete up to two quanta in the bending mode) as a function of the dimensionless parameter d/ω_2. The energy levels corresponding to different values of μ, i.e., $\mu = \pm 1/2, \pm 3/2, \pm 5/2$, are shown by the full, dash-dotted, and dashed lines, respectively. The figure reveals significant level repulsions within the $\mu = 1/2$ manifold: the pairs (000) $^2\Pi_{1/2}$ / (010) μ $^2\Sigma_{1/2}$, (010) κ $^2\Sigma_{1/2}$ / (020) μ $^2\Pi_{1/2}$, and (030) μ $^2\Sigma_{1/2}$ / (020) κ $^2\Pi_{1/2}$ are seen to repel each other with increasing d/ω_2. Similar, but less pronounced level-repulsion effects are seen in the $\mu = 3/2$ manifold. The lowest $^2\Delta_{5/2}$ level, on the other hand, is isolated and its energy is essentially independent of d/ω_2. As a result, the (010) μ $^2\Sigma_{1/2}$ and (010) $^2\Delta_{5/2}$ levels cross as function of d/ω_2. Numerous other level crossings occur among the higher energy levels, see Fig. 3.2.

Figure 3.2 reveals that even weak LRVC ($d \ll \omega_2, \zeta$) can lead to a significant rearrangement of the vibronic energy levels in resonant cases ($\zeta \simeq \omega_2$). Such perturbations of the vibronic energy levels of $^2\Pi$ states of linear triatomic molecules with moderate RT and SO coupling have been observed experimentally, in particular in the spectra of NCS and GeCH, and have

Figure 3.2: Effect of d on the vibronic levels. Solid, dashed-dotted, and dashed lines represent energy levels with $\mu = 1/2$, $3/2$, and $5/2$, respectively.

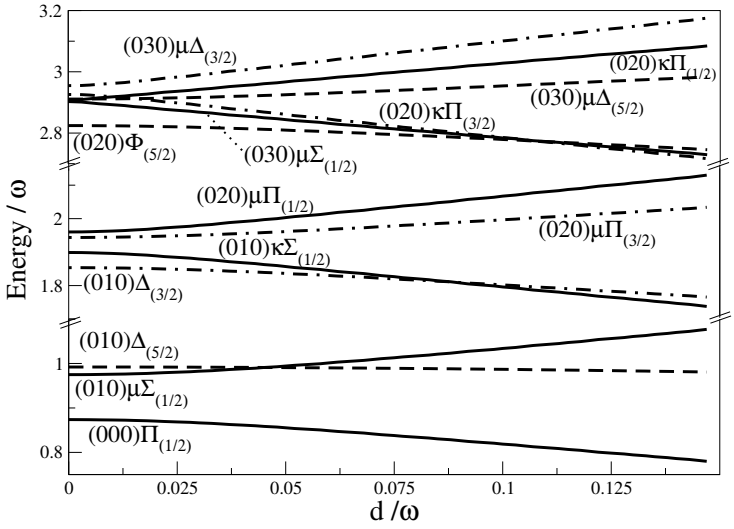

been termed "Sears resonances" [37, 39].

The mixing of the zero-order energy levels also has a significant effect on the intensity of the spectral lines. We shall consider here the case of electronic excitation from the (000) vibrational ground state of some nondegenerate electronic state into the $^2\Pi$ manifold. In the Condon approximation, only the (000) $^2\Pi_{3/2}$ and (000) $^2\Pi_{1/2}$ zero-order levels then carry spectral intensity. As is well known [23, 24, 16, 133], the RT coupling leads to a redistribution of intensity, but only among levels with an even number of quanta in the bending mode, reflecting the second-order (quadratic in ρ) character of the RT coupling. The relativistic vibronic coupling term $d\rho e^{\pm i\phi}$, on the other hand, being of first order in ρ, transfers spectroscopic intensity to vibronic levels with an odd number of quanta in the bending mode.

This phenomenon is illustrated in Fig. 3.3, for a resonant case with the parameter values $\zeta/\omega_2 = -1$, $c/\omega_2 = 0.2$, and $d/\omega_2 = 0, 0.1, 0.2$. The full and dashed-dotted lines represent levels with $\mu = 1/2$ and $\mu = 3/2$, respectively. Figure 3.3a reveals that the (020) μ $^2\Pi_{1/2}$ level borrows intensity from the (000) $^2\Pi_{1/2}$ level via RT coupling (the intensities of the other vibronic levels are too low to be visible in the figure). Figures 3.3b and 3.3c illustrate an example of strong mixing of the quasi-degenerate (000) $^2\Pi_{1/2}$ and (010) μ $^2\Sigma_{1/2}$

Figure 3.3: Redistribution of the spectral intensity by the LRVC parameter d. Solid and dashed-dotted lines represent energy levels with $\mu = 1/2$ and $\mu = 3/2$ respectively.

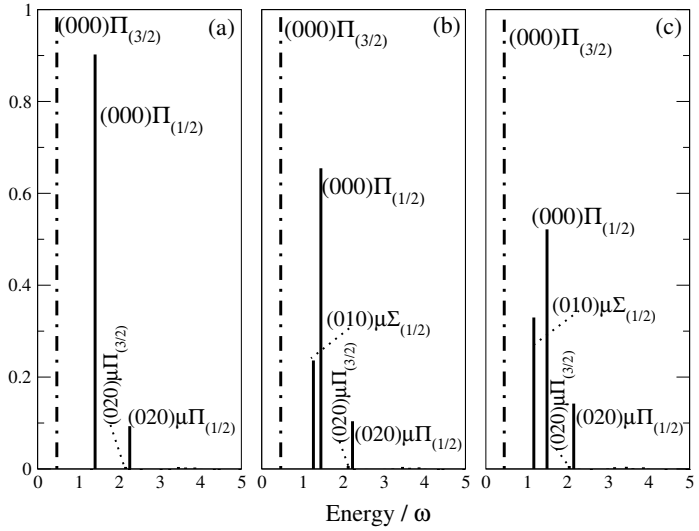

levels via LRVC. In such cases of quasi-degeneracy of nonrelativistic RT vibronic levels, the intensity of levels with an odd number of quanta of the bending mode (such as (010) $\mu\ ^2\Sigma_{1/2}$) can become comparable to those with an even number of quanta, see Fig. 3.3.

3.4 Applications of the Renner-Teller spin-orbit vibronic-coupling model

In this section, we describe the relevance of the LRVC mechanism in different molecular systems, e.g., BS_2, CS_2^+, OCS^+, OBS, GeCH, FCN^+, $ClCN^+$, and $BrCN^+$. The details of *ab initio* calculations are presented in the following subsection.

Ab initio calculation of the coupling parameters

The electronic basis states obtained by *ab initio* electronic-structure calculations are the nonrelativistic *adiabatic* states, which correspond to the diagonalization of the nonrelativistic fixed-nuclei electronic Hamiltonian,

$$H_{\rm es} = \begin{pmatrix} 0 & c\rho^2 e^{2i\phi} & 0 & 0 \\ c\rho^2 e^{-2i\phi} & 0 & 0 & 0 \\ 0 & 0 & 0 & c\rho^2 e^{2i\phi} \\ 0 & 0 & c\rho^2 e^{-2i\phi} & 0 \end{pmatrix}. \tag{3.33}$$

The unitary matrix S which diagonalizes $H_{\rm es}$, i.e.,

$$S^+ H_{\rm es} S = \begin{pmatrix} -c\rho^2 & 0 & 0 & 0 \\ 0 & -c\rho^2 & 0 & 0 \\ 0 & 0 & c\rho^2 & 0 \\ 0 & 0 & 0 & c\rho^2 \end{pmatrix} \tag{3.34}$$

is

$$S = \frac{1}{\sqrt{2}} \begin{pmatrix} e^{i\phi} & -e^{i\phi} & 0 & 0 \\ e^{-i\phi} & e^{-i\phi} & 0 & 0 \\ 0 & 0 & e^{i\phi} & -e^{i\phi} \\ 0 & 0 & e^{-i\phi} & e^{-i\phi} \end{pmatrix}. \tag{3.35}$$

The correspondingly transformed relativistic vibronic Hamiltonian reads

$$S^+ H_{\rm SO} S = \begin{pmatrix} 0 & 0 & -i\frac{\zeta}{2} & -id\rho e^{-i\phi} \\ 0 & 0 & -id\rho e^{i\phi} & i\frac{\zeta}{2} \\ i\frac{\zeta}{2} & id\rho e^{-i\phi} & 0 & 0 \\ id\rho e^{i\phi} & -i\frac{\zeta}{2} & 0 & 0 \end{pmatrix}. \tag{3.36}$$

The matrix (3.36) represents the matrix elements of the Breit-Pauli operator with nonrelativistic *adiabatic* electronic states. The SO splitting is directly obtained from the SO-matrix elements at the linear geometry ($\rho = 0$). The parameter d can be extracted from the slope of the corresponding SO-matrix elements as a function of the bending coordinate.

BS_2, CS_2^+, OCS^+, OBS, and GeCH

The electronic-structure calculations have been carried out using the MOLPRO package [134]. The ground-state geometry of the system under consideration is first optimized with the coupled-cluster method including single and double excitations with perturbative triple excitations [CCSD(T)] [135], employing the correlation-consistent polarized-valence-quadruple zeta (cc-pVQZ) [136, 137] basis set. The nonrelativistic parameters ω_2 and ϵ are obtained from the bending force constants of the two components of the PE surface of the degenerate Π state, using Eqs. (3.26) and (3.25), respectively. The SO-matrix elements have been computed with CASSCF wave functions. A state-averaged full-valence CASSCF calculation of the two components of the $^2\Pi$ state has been performed. These wave functions are then used to calculate the matrix elements of the Breit-Pauli operator. These calculations were performed for a few bent geometries and the parameter d was extracted as described above.

XCN^+ (X=F, Cl, and Br)

The XCN are closed-shell linear molecules in their ground electronic state $\tilde{X}\ ^1\Sigma$ with the following valence-shell electronic configuration: $1\sigma^2\ 2\sigma^2\ 1\pi^4\ 3\sigma^2\ 2\pi^4$. Removal of an electron from the highest occupied π-type molecular orbital gives rise to the ground electronic state of the corresponding cation, i.e., the $\tilde{X}\ ^2\Pi$ state.

We have employed the augmented correlation-consistent polarized valence triple-zeta (aug-cc-pVTZ) basis set of Dunning [136, 137] for all atoms except Br, which is described by RECP, where the core orbitals (i.e. 1s-3d, with 28 electrons) are described by a semilocal energy-adjusted pseudo potential of energy-consistent variety [138]. The valence orbitals of Br are described by optimized contracted s, p, d, and f type functions of augmented triple-zeta quality [138]. Using this basis set, we have optimized the geometry of the neutral molecules as well as their cations in their respective ground states and have calculated the harmonic frequencies with DFT method using Becke's three parameter hybrid functional with the LYP correlation functional (B3LYP) [139]. The DFT calculations have been performed using the

GAUSSIAN package [140]. In addition to the DFT calculations, we also have performed CCSD(T) calculations [141] to determine the optimized geometries of the neutral and the cationic species. The coupled-cluster calculations have been performed with the MOLPRO program suite [134].

The averaged bending frequency (ω_2), the RT coupling parameter c, the SO splitting of the $\tilde{\mathrm{X}}\ ^2\Pi$ state, and the LRVC term d are obtained as described earlier. The two $\tilde{\mathrm{X}}\ ^2\Pi$ bending PE curves have been obtained from CCSD(T) [141] calculations at the ground-state reference geometry of the stretching modes. The matrix elements of the Breit-Pauli SO operator with nonrelativistic wave functions [142] have been computed, yielding the SO splitting ζ as well as the LRVC parameter d. The nonrelativistic wave functions have been obtained by performing a state-averaged (over the two components of the $\tilde{\mathrm{X}}\ ^2\Pi$ state) full-valence complete-active-space self-consistent-field (CASSCF) calculation [143, 144]. Here, all the inner valence electrons are kept frozen, resulting in the correlation of 15 electrons in 12 orbitals, i.e., a $(15, 12)$ CASSCF calculation. In the case of BrCN, the SO-matrix elements are determined by employing the SO pseudo operator of Dolg [145] for the Br atom, adapted to the above cited scalar RECP. The MOLPRO software has been used for the SO calculations [134, 142].

The linear-VC constants of the stretching modes have been calculated according to the expression

$$\kappa_i = \sqrt{\frac{\hbar}{\omega_i}} \sum_{j=1,3} L_{ij} \left(\frac{\partial V(Q)}{\partial R_j} \right)_0, i = 1, 3. \tag{3.37}$$

Here, the R_j are the two bond distances. The L matrix is obtained by the simultaneous diagonalization of the F and the G matrices [146]. The G matrix has been constructed from the molecular geometry parameters and atomic masses [146], while the F matrix has been obtained from a force-field calculation using the DFT/B3LYP method. The gradients $\partial V/\partial R_j$ have been determined by a CCSD(T) calculation for the cations. The vertical ionization potential (IP) of the $\tilde{\mathrm{X}}\ ^2\Pi$ state of the title molecules has been calculated with the outer-valence Green's function (OVGF) method, [147, 148] using the cc-pVTZ basis set and the frozen-core approximation. The OVGF calculation has been performed using the GAUSSIAN package [140]. In addition, a state-averaged $(15, 12)$ CASSCF followed by a $(15, 8)$ multi-reference-configuration-interaction (MRCI) [149, 150] calculation has been performed at the equilibrium geometry of the ground state of the neutral XCN molecules. The vertical IP of the $\tilde{\mathrm{X}}\ ^2\Pi$ state of XCN^+ has been obtained from the difference of the MRCI energies of this state and the $\tilde{\mathrm{X}}\ ^1\Sigma$ state of XCN, and is denoted by ΔMRCI.

Table 3.1: Structural, vibrational, VC and SO-coupling parameters for BS_2, CS_2^+, OCS^+, and OBS. Numbers in parentheses are the absolute values in units of ω_2.

Parameter		BS_2	CS_2^+	OCS^+	OBS
r_1	/Å	1.6760	1.5647	1.1583	1.2142
r_2	/Å	$--$	$--$	1.5690	1.7583
ω_2	/cm^{-1}	284.78	331.84	442.65	370.04
ϵ		-0.2257	-0.1912	-0.1590	-0.1383
c	/cm^{-1}	32.56 (0.12)	32.02 (0.10)	35.42 (0.08)	26.72 (0.07)
ζ	/cm^{-1}	-394.90 (1.39)	-417.40 (1.26)	-347.55 (0.78)	-345.04 (0.93)
d	/cm^{-1}	13.31	13.39	26.96	29.08

3.4.1 A comparative study of BS_2, CS_2^+, OCS^+, and OBS

We consider relativistic VC in molecules with a second-row atom (S) : BS_2, CS_2^+, OCS^+, OBS. All four systems possess a well isolated $\tilde{X}\ ^2\Pi$ ground state. The *ab initio* calculated vibrational, VC and SO-coupling parameters of the four systems are given in Table 3.1.

In the case of BS_2, the SO splitting of the $\tilde{X}^2\Pi$ state is calculated to be -395 cm^{-1}, which is larger than the bending frequency (285 cm^{-1}). This is accompanied by a relatively strong Renner coupling $c/\omega_2 = 0.12$. The calculations predict a rather small value of d (13.3 cm^{-1}). The differences between the energies of the vibronic levels with and without inclusion of d are given in Table 3.2.

In the case of BS_2, we observe a very small effect of d on the energy levels (less than 2 cm^{-1}). This is the consequence of the nonresonant character of BS_2 ($\zeta/\omega_2 \simeq 1.4$) and the rather small value of d ($d/\zeta < 0.03$). The situation is similar in CS_2^+, although ζ/ω_2 is closer to unity than in BS_2. In addition, the Renner coupling is weaker in CS_2^+. However, this system still is too far from $\zeta \sim \omega_2$ resonance to exhibit strong relativistic VC effects.

In OCS^+, the bending frequency (443 cm^{-1}) is larger than the SO splitting (-348 cm^{-1}). The Renner coupling is weaker than in BS_2 and CS_2^+. The value of d is 27 cm^{-1}. The more favorable ζ/ω_2 ratio of 0.78, weaker RT coupling, and the larger value of d render relativistic VC effects more conspicuous than in BS_2 and CS_2^+ (see Table 3.1). The difference in the energy levels is sometimes as large as 20 cm^{-1}. The relativistic VC effects are largest in OBS. It has a favorable ζ/ω_2 ratio (0.93), a weak Renner coupling ($c/\omega_2 = 0.07$),

Table 3.2: Calculated $\tilde{X}\ ^2\Pi$ vibronic energy levels (in cm^{-1}). δ is the difference in energy with and without inclusion of the LRVC.

$(\nu_1\nu_2\nu_3)$ State		BS_2		CS_2^+		OCS^+		OBS	
		with d	δ	with d	δ	with d	δ	with d	δ
(000)	$^2\Pi_{1/2}$	386.09	1.4	412.72	1.9	338.26	-6.6	323.45	-19.4
(010)	$\mu\ ^2\Sigma_{1/2}$	272.69	-1.4	320.27	-1.8	435.87	7.3	382.81	20.3
(010)	$^2\Delta_{5/2}$	280.03	-0.3	327.75	-0.2	437.62	-0.9	366.40	-1.2
(010)	$^2\Delta_{3/2}$	648.60	1.1	728.30	1.7	772.47	-5.7	687.30	-18.9
(010)	$\kappa\ ^2\Sigma_{1/2}$	680.98	2.2	754.98	3.0	785.88	-15.6	685.69	-34.8
(020)	$\mu\ ^2\Pi_{3/2}$	543.02	-1.5	639.12	-1.8	860.40	5.9	742.23	19.3
(020)	$\mu\ ^2\Pi_{1/2}$	558.30	-2.2	649.70	-2.9	878.60	16.3	764.11	35.7
(020)	$^2\Phi_{7/2}$	557.83	-0.5	653.58	-0.5	873.22	-1.8	731.60	-2.3
(020)	$^2\Phi_{5/2}$	812.18	-1.5	956.88	-1.8	1202.76	-4.4	1049.25	-17.2
(020)	$\kappa\ ^2\Pi_{1/2}$	821.11	-1.6	960.93	-2.3	1227.90	-20.3	1049.89	-32.3
(020)	$\kappa\ ^2\Pi_{3/2}$	852.56	-2.5	986.54	-3.6	1233.51	-25.4	1052.21	-45.2

and a relatively large value of d (29 cm^{-1}). The calculated vibronic levels of OBS with and without inclusion of d are depicted in Fig. 3.4. It can be seen that the levels are shifted by up to 30 cm^{-1} by the relativistic VC. Moreover, a complete rearrangement of the energy levels take place.

It is worthwhile to point out some observations which are common to all four systems. In all cases, we observe a very small change in the energy of the (010) $^2\Delta_{5/2}$ level upon the inclusion of d. A similar observation applies for the (020) $^2\Phi_{7/2}$ level. Both levels are little affected because of the absence of close-lying levels of the same symmetry. Another common observation is the nearly symmetric splitting of the energy levels which are coupled by the linear relativistic term, for example (010) $\mu\ ^2\Sigma_{1/2}$ and (000) $^2\Pi_{1/2}$. This symmetric splitting is also observed for higher levels (see Fig. 3.4).

3.4.2 Calculation of the vibronic energy levels of GeCH

GeCH is a linear radical with an orbitally degenerate $\tilde{X}\ ^2\Pi$ electronic ground state. Apart from the RT effect, there are other effects which complicate the vibronic structure of the $\tilde{X}\ ^2\Pi$ state. The SO splitting of the $\tilde{X}\ ^2\Pi$ state is significant, being of the order of the bending frequency. A Fermi resonance between the bending mode and the Ge-C stretching mode and possible vibronic interactions with the close-lying electronically excited $\tilde{A}\ ^2\Sigma$

Figure 3.4: Comparison of vibronic energy levels of the $\tilde{X}\ ^2\Pi$ state of OBS, calculated with and without inclusion of LRVC, respectively.

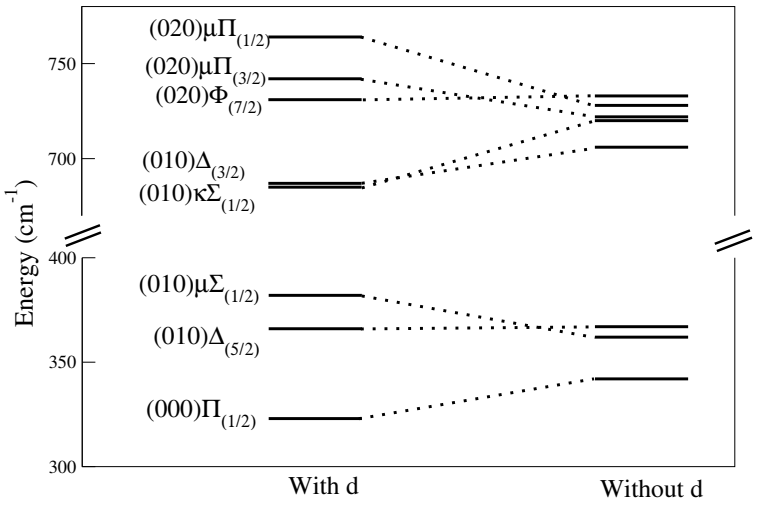

state are further perturbations [151].

The geometry of GeCH in the electronic ground state has been optimized at the CCSD(T)/cc-pVQZ level. GeCH is found to be a linear molecule with r_0(HC)=1.079 Å, r_0(CGe)=1.769 Å, in good agreement with the experimental values 1.067 Å and 1.776 Å [151], respectively. These results agree with the results obtained by other authors [152] with the same basis set and method. The bending vibrational frequencies associated with the $^2A'$ and $^2A''$ components of the $\tilde{X}\ ^2\Pi$ state are found to be 476.6 cm^{-1} and 523.7 cm^{-1} respectively. The averaged harmonic bending frequency (ω_2) is obtained as 500.7 cm^{-1}, in good agreement with Ref. [152]. The RT parameter ϵ, defined in Eq. (3.25), is obtained as -0.0940, which compares well with the value of -0.1046 reported in Ref. [152]. The negative sign of ϵ reflects the fact that the $^2A'$ energy lies below the $^2A''$ energy.

The relativistic parameters were determined with the procedure described in Chapter 3.4. The SO splitting is found to be -325 cm^{-1}, in good agreement with the spectroscopically determined value of -334.6 cm^{-1} [151]. The parameter d is calculated as 41.06 cm^{-1}, which is more than 10% of the SO splitting. The calculated parameters are given in Table 3.3.

Although we have employed elaborate electronic-structure methods and

Table 3.3: Vibrational, VC and SO-coupling parameters for the $\tilde{X}\ ^2\Pi$ state of GeCH. ω_2, ζ, d are given in cm^{-1}, ϵ is dimensionless.

Parameter	Expt.	Calc.	fitted
ω_2		500.7[a]	435.6[a]
		500[b]	434.8[c]
ϵ		−0.0940[a]	−0.1090[a]
		−0.1046[b]	−0.1135[c]
ζ	−334.6[d]	−325.0[a]	−348.76[a]
			−383.8[c]
d		41.06[a]	40.48[a]

[a] this work.
[b] Ref. [152].
[c] Ref. [39].
[d] Ref. [151].

an extended basis set in the *ab initio* electronic structure calculations, one cannot expect that the obtained vibronic and SO parameters are of the spectroscopic accuracy. We therefore have performed an independent determination of the parameters by a least-squares fit of the energy levels of the Hamiltonian (3.1) to the observed energy levels [39]. The fitted parameters are also given in Table 3.3. The fitted bending frequency (435.6 cm^{-1}) is lower than the *ab initio* calculated value (500.7 cm^{-1}). The fit of Ref. [39] has given a similar value of bending frequency (434.8 cm^{-1}). The fitted value of ϵ (-0.1090) is in good agreement with the fitted value (-0.1135) of Ref. [39].

The fitted and *ab initio* calculated values for ϵ are in satisfactory agreement with each other. For the SO splitting, the present fitting yields -348.76 cm^{-1}, which is quite close to the *ab initio* calculated value (-325 cm^{-1}) and the observed (-334.6 cm^{-1}) splitting of the (000) $^2\Pi_{3/2}$ and (000) $^2\Pi_{1/2}$ levels [151]. In Ref. [39], anharmonic as well as Fermi resonance effects were included in the fit, resulting in a somewhat larger value of the SO splitting. The parameter d is obtained as 40.48 cm^{-1} from the fit of the experimental spectrum, which is in very good agreement with its *ab initio* calculated value (41.06 cm^{-1}).

The $\tilde{X}\ ^2\Pi$ vibronic energy levels obtained with the fitted parameters are compared in Table 3.4 with the observed energy levels [39]. We have restricted our analysis to the lowest few bending excitations, because at higher excitation levels anharmonicity effects, which are not included in our vibronic model, may become important. The overall quality of the fit is determined

Table 3.4: The $\tilde{X}\ ^2\Pi$ vibronic energy levels of GeCH. The differences between the calculated and experimentally observed values are given in cm^{-1}.

GeCH				
$(\nu_1\nu_2\nu_3)$	State	Obs.	Obs. - Calc.	
			with d	without d
(000)	$^2\Pi_{1/2}$	334.9	1.8	-12.6
(010)	$^2\Delta_{5/2}$	440.0	6.1	4.1
(010)	$\mu\ ^2\Sigma_{1/2}$	444.5	-1.0	15.1
(010)	$\kappa\ ^2\Sigma_{1/2}$	755.6	-5.5	-34.1
(010)	$^2\Delta_{3/2}$	765.1	-1.1	-13.9
(020)	$\mu\ ^2\Pi_{3/2}$	869.7	-1.4	12.5
(020)	$\mu\ ^2\Pi_{1/2}$	889.8	-1.6	28.8
(020)	$\kappa\ ^2\Pi_{1/2}$	1193.0	-4.8	-34.5

from the square root of the mean squared deviation of the calculated energy levels from the observed energy levels, which is found to be 3.5 cm^{-1}. To reveal the effect of LRVC, we have included in Table 3.4 the deviations of the calculated from the observed energy levels obtained with and without inclusion of d. As can be seen, most of the calculated vibronic levels are in good agreement with the observed values. In most cases, the difference is below 2 cm^{-1} which is well within the experimental error. It can be seen that the levels obtained with the inclusion of d match the observed levels much better than for $d = 0$. Several levels are shifted measurably by the effect of the LRVC. The (000) $^2\Pi_{1/2}$ and (010) $\mu\ ^2\Sigma_{1/2}$ levels, for example, exhibit significant level repulsion. A similar level repulsion can be observed for the (010) $\kappa\ ^2\Sigma_{1/2}$ and (020) $\mu\ ^2\Pi_{1/2}$ levels. The ordering of the (010) $^2\Delta_{3/2}$ and (010) $\kappa\ ^2\Sigma_{1/2}$ levels is interchanged by the inclusion of d (see Fig. 3.5).

The $\tilde{X}\ ^2\Pi$ state of GeCH clearly represents a resonant case: $\zeta/\omega_2 = -0.88$. The Renner coupling is relatively weak. As discussed earlier, these circumstances are favorable for the observation of the relativistic linear-VC effects.

In studies of the vibronic spectrum of the $\tilde{X}\ ^2\Pi$ state of NCS, Northrup and Sears [37] have analyzed the repulsion of certain levels, e.g. (010) $^2\Delta_{3/2}$ and (020) $\mu\ ^2\Pi_{3/2}$ in terms of a mixed second-order perturbation treatment, considering the SO coupling within the $^2\Pi$ state as well as nonrelativistic VC of the $^2\Pi$ state with a distant $^2\Sigma$ state. Since the $\Sigma - \Pi$ coupling is of first order in ρ and the SO coupling is of zeroth order in ρ, the combined effect of both perturbations is of first order in ρ [37]. The analysis of Northrup and Sears thus is equivalent to a perturbative treatment of the LRVC term

Figure 3.5: Comparison of calculated and observed energy levels for GeCH. Solid, dashed-dotted, and dashed lines represent energy levels with $\mu = 1/2, 3/2$, and $5/2$, respectively.

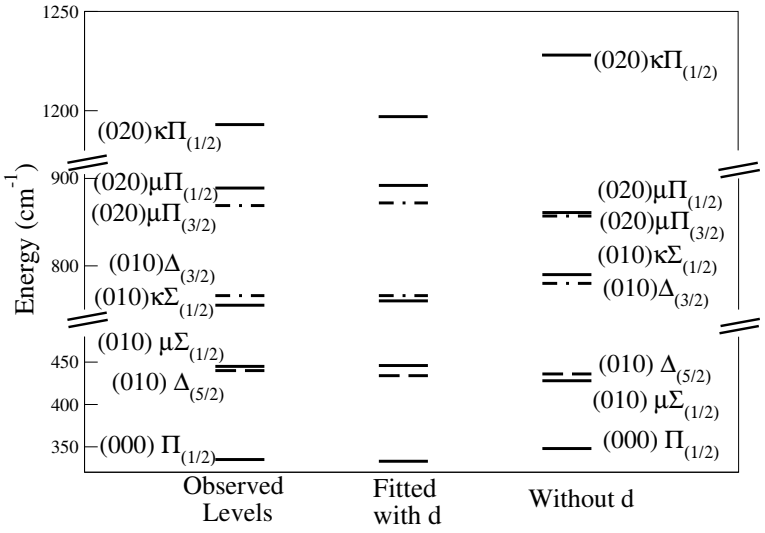

$d\rho e^{\pm i\phi}$. It should be noted that the perturbative approach of Ref. [37] is bound to break down when the energy gap of the $^2\Sigma$ and $^2\Pi$ states is of the order of (or smaller than) the SO splitting of the $^2\Pi$ state.

3.4.3 Calculation of the vibronic structure of the $\tilde{X}\ ^2\Pi$ photoelectron spectra of XCN, X= F, Cl, and Br

FCN

The FC and CN bond distances in the ground electronic state of FCN have been experimentally determined as 1.264 and 1.157 Å, respectively [153]. The DFT calculation reproduces the experimental geometry satisfactorily, see Table 3.5, while the CCSD(T) method seems to over-estimate the bond lengths. The geometry of the $\tilde{X}\ ^2\Pi$ state of FCN^+ is calculated to be linear with decreased FC and increased CN bond distances, reflecting the bonding and anti-bonding character of the 2π orbital with respect to the FC and CN bonds, respectively. The calculated vibrational frequencies of FCN and FCN^+ are compared with experimental data in Table 3.5. Ionization of FCN leads to a substantial reduction of ω_1, whereas the corresponding changes in ω_2 and ω_3 are less pronounced, see Table 3.5. The dimensionless RT coupling parameter is calculated as -0.2485, see Table 3.6, corresponding to a rather weak RT effect. The calculated SO splitting is 91 cm^{-1}. The LRVC parameter is determined as 6 cm^{-1}, about a fifteenth of the SO splitting, see Table 3.6. The dimensionless VC parameters of the stretching modes are $(\kappa_1/\omega_1) = -1.62$ and $(\kappa_3/\omega_3) = 0.30$. The negative value for (κ/ω) for the ν_1 mode (CN stretch) indicates a stretching of CN bond distance upon ionization. The vertical $\tilde{X}\ ^2\Pi$ IP of FCN obtained by the OVGF and ΔMRCI calculations are compared with the experimental estimates in Table 3.7.

ClCN

The experimentally observed bond lengths of ClCN, R_0(ClC) = 1.629 Å and R_0(CN) = 1.160 Å [47], are well produced by the *ab initio* calculations, see Table 3.5. The vibrational frequencies obtained with DFT compare well with their experimental values, see Table 3.5. In the $\tilde{X}\ ^2\Pi$ state of $ClCN^+$, the ClC bond distance is shorter and the CN bond distance is longer than in the neutral molecule, which reflects the bonding and antibonding characters of the 2π orbital with respect to the CN and ClC bonds, respectively. The calculated vibrational frequencies agree well with the experimental data, see Table 3.5. The dimensionless RT parameter is calculated as -0.2015. The calculated SO splitting is 269 cm^{-1}, in good agreement with the observed

Table 3.5: Bond distances (in Å) and vibrational frequencies (in cm^{-1}) of the ground state of neutral and cationic XCN.

Parameter	FCN		ClCN		BrCN	
	$\tilde{X}\ ^1\Sigma$	$\tilde{X}\ ^2\Pi$	$\tilde{X}\ ^1\Sigma$	$\tilde{X}\ ^2\Pi$	$\tilde{X}\ ^1\Sigma$	$\tilde{X}\ ^2\Pi$
R_0(XC)	1.2663[a]	1.2029[a]	1.6368[a]	1.5698[a]	1.7899[a]	1.7304[a]
	1.2715[b]	1.2299[b]	1.6430[b]	1.5672[b]	1.7966[b]	1.7218[b]
	1.264[c]		1.629[d]	1.555[e]	1.789[f]	1.745[g]
						1.736[h]
R_0(CN)	1.1504[a]	1.2168[a]	1.1528[a]	1.1994[a]	1.1531[a]	1.1868[a]
	1.1628[b]	1.2058[b]	1.1647[b]	1.2155[b]	1.1662[b]	1.2039[b]
	1.157[c]		1.160[d]	1.207[e]	1.158[f]	1.195[g]
						1.2006[h]
ω_1	2408[a]	2183[a]	2308[a]	1987.58[a]	2289[a]	1989[a]
						1925[h]
	2318[i]		2201[j]	1916[j]	2187[j]	1906[j]
				1915[k]	2198[l]	1940[m]
ω_2	484[a]	426.49[a]	403[a]	366[a]	365[a]	325[a]
	451[i]	411.4[b]		341.22[b]	368[j]	290.12[b]
						280[h]
			397[j]		341[l]	288[j]
ω_3	1093[a]	1162.16[a]	743[a]	820.93[a]	585[a]	640[a]
						640[h]
	1076[i]		729[j]	823[j]	580[j]	650[j]
			741[d]	827[k]	587[l]	640[m]

[a] DFT/B3LYP.
[b] CCSD(T).
[c] Ref. [153].
[d] Ref. [47].
[e] Ref. [48].
[f] Ref. [154].
[g] Ref. [155].
[h] Ref. [156].
[i] Ref. [157] and [158].
[j] Ref. [44].
[k] Ref. [46].
[l] Ref. [159].
[m] Ref. [51].

Table 3.6: VC parameters of the $\tilde{X}\ ^2\Pi$ state of XCN^+. ζ and d are in cm^{-1}; the other parameters are dimensionless.

Parameter	FCN^+	$ClCN^+$	$BrCN^+$
ϵ	-0.2145[a]	-0.1776[a]	-0.1853[a]
	-0.2485[b]	-0.2015[b]	-0.2328[b]
			-0.1989[c]
			-0.1850[d]
ζ	91	269.2	1758
			1475[c]
		277[e]	1477[e]
		275[f]	1480[h]
		276[g]	1490[i]
			1420[j]
d	6.0	22.3	22.0
(κ_1/ω_1)	-1.62	-1.24	-0.93
(κ_3/ω_3)	0.30	0.89	0.83

[a] DFT/B3LYP.
[b] CCSD(T).
[c] Ref. [156].
[d] Ref. [160].
[e] Ref. [44].
[f] Ref. [45].
[g] Ref. [46].
[h] Ref. [49].
[i] Ref. [51].
[j] Ref. [52].

Table 3.7: Vertical ionization potential of the $\tilde{X}\ ^2\Pi$ state of XCN^+ (in eV).

Method	FCN^+	$ClCN^+$	$BrCN^+$
ΔMRCI	13.59	12.47	12.02
OVGF	13.51	12.42	11.90
Expt.[a]	13.34	12.37	12.08

[a] Ref. [50].

splitting (277 cm^{-1})[44]. The LRVC parameter d is calculated as 22 cm^{-1}, which is about one tenth of the SO splitting. The dimensionless coupling parameters (κ_i/ω_i) of the stretching modes are -1.24 and 0.89 for ν_1 and ν_3, respectively. The calculated and observed vertical IP of the $\tilde{X}\ ^2\Pi$ state of $ClCN^+$ are given in Table 3.7.

BrCN

The optimized geometry as well as the vibrational frequencies obtained with the DFT method are given in Table 3.5. The agreement with experimental geometries in both neutral and cation of BrCN is excellent. Upon ionization, the BrC bond distance decreases, whereas CN bond distance increases, see Table 3.5. The averaged bending frequency and the dimensionless RT parameter of the $\tilde{X}\ ^2\Pi$ state of $BrCN^+$ are determined as 290 cm^{-1} and -0.2328 respectively. The calculated SO splitting is 1758 cm^{-1}, which is larger than the experimentally determined values [44, 49, 51, 52], see Table 3.6. The recent theoretical work by Biczysko and Tarroni [156] reveals the origin of this discrepancy. Their analysis shows that the SO splitting decreases with increasing CN stretching coordinate and increases with the BrC coordinate. As a result, the effective SO splitting of the $\tilde{X}\ ^2\Pi$ state of $BrCN^+$ is smaller than the calculated value at the equilibrium geometry of neutral BrCN. The LRVC parameter is determined as 22 cm^{-1}, which is smaller than the SO splitting by two orders of magnitude. We have also performed a CPP calculation [138] for Br to determine the SO-matrix elements. The SO splitting of this calculation is larger by 20 cm^{-1}, while the effect on the LRVC parameter is negligible. The dimensionless linear-VC parameters (κ/ω) of the two stretching modes ν_1 and ν_3 are -0.93 and 0.83, respectively, see Table 3.6. The calculated vertical IP of the $\tilde{X}\ ^2\Pi$ state are in good agreement with the experimental estimates, see Table 3.7.

Discussion of the photoelectron spectra

The vibronic spectra for bending and stretching modes are calculated separately and the final spectrum is obtained as a convolution of the two, as described in Chapter 2.2. The theoretically calculated stick spectrum is finally convoluted with a normalized Lorentzian of finite width to account for rotational broadening and the finite resolution of the experimental photoelectron spectra. Since we are concerned with relativistic VC, which sometimes has very small effects on the line positions and the spectral intensities, a rather small value has been chosen for the FWHM (1 meV $\sim$ 8 cm^{-1}).

In the following figures the stretching progressions in the photoelectron spectra are indicated by the dotted lines, whereas the peaks corresponding to the bending vibration and their combination bands with stretching modes are labeled by $(\nu_1\nu_1\nu_3)$. Levels with $\mu = 1/2$ are distinguished from $\mu = 3/2$ by an overbar.

FCN

The calculated $\tilde{\mathrm{X}}\ ^2\Pi$ photoelectron spectrum of FCN is shown in Fig. 3.6. Most of the peaks appear as closely spaced doublets, reflecting the small SO splitting. In the case of FCN, the SO splitting is 6 times smaller than the bending frequency. The spectrum is dominated by a long progression in the mode ν_1, while the mode ν_3 forms a very short progression. The tiny peak assigned as $(\overline{020})$ reflects the nonrelativistic RT coupling. There are some peaks in the spectrum which have very small intensities and hence are not labeled. The calculated spectrum in Fig. 3.6 is in very good agreement with the experimental spectrum, see Refs. [49, 50].

ClCN

The calculated photoelectron spectrum of the $\tilde{\mathrm{X}}\ ^2\Pi$ state of ClCN^+ is shown in Fig. 3.7a. The spectrum is dominated by a long progression in the mode ν_1 and also to some extent by a progression in the mode ν_3. The peaks appear as doublets reflecting the SO splitting of about 270 cm^{-1}. In addition to the peaks from the stretching modes, the spectrum also exhibits peaks corresponding to the bending mode. The peaks with even quanta of bending excitation, such as $(\overline{020})$, arise from the nonrelativistic quadratic RT coupling. In addition to these, the calculated spectrum also shows peaks corresponding to excitation of odd quanta of the bending mode, e.g., $(\overline{010})$ and its combination bands, see Fig. 3.7a. These lines arise from the LRVC mechanism. As has been discussed in Chapter 3.3, the LRVC mechanism plays an important role in the spectroscopy of quasi-linear triatomic molecule when

Figure 3.6: Calculated $\tilde{X}\ ^2\Pi$ photoelectron spectrum of FCN^+. The stretching progressions are indicated by the dotted lines. The bending levels along with their combination bands are labeled as $(\nu_1\nu_2\nu_3)$. Levels with an overbar correspond to μ=1/2.

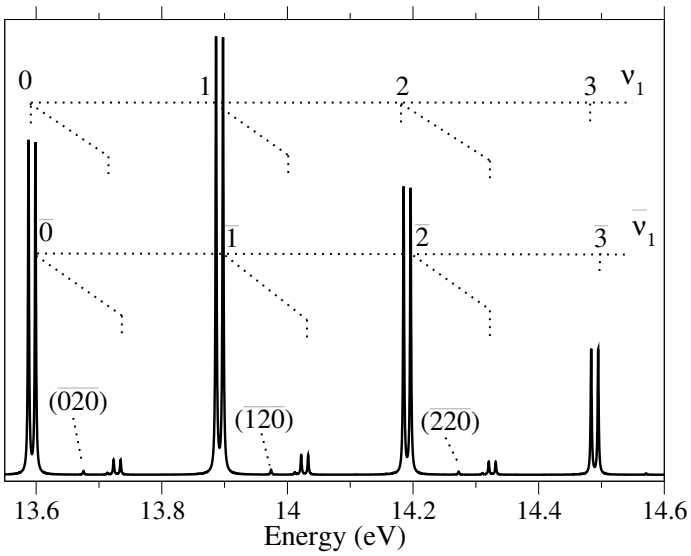

the SO splitting (ζ) is of the same order of magnitude as the bending frequency (ω_2). This VC mechanism has been shown to reorder vibronic energy levels as well as to redistribute spectral intensities among various vibronic levels, see Chapter 3.3. It is this VC mechanism that enables vibronic level with odd quanta of bending excitation to carry intensity in the $\tilde{X}\ ^2\Pi$ photoelectron spectrum of $ClCN^+$. Here, the SO splitting (270 cm^{-1}) is of the same order of magnitude as the bending frequency (341 cm^{-1}) and hence the ($\overline{000}$) and ($\overline{010}$) levels lie close to each other. These two levels interact with each other through the coupling term $d\rho e^{\pm i\phi}$. This interaction leads to a transfer of intensity from the intensity carrying ($\overline{000}$) to the dark ($\overline{010}$) level. This transfer of intensity is reflected by the lower intensity of the ($\overline{000}$) line compared to that of the (000) line, see Fig. 3.7a. To reveal explicitly the effects of the LRVC mechanism, we show in Fig. 3.7b the spectrum obtained for $d = 0$. The excitation of odd quanta of the bending mode is absent in this case. The line positions and relative spectral intensities of the $\tilde{X}\ ^2\Pi$ photoelectron spectrum of ClCN with and without inclusion of LRVC term are given in tabular form in Table 3.8.

The experimentally observed stretching progression and the relative intensities of the vibronic levels in the photoelectron spectrum of ClCN are correctly reproduced by the calculated photoelectron spectrum. A high-resolution experimental recording of the photoelectron spectrum of the $\tilde{X}\ ^2\Pi$ state of $ClCN^+$ in which the close-lying vibronic levels are resolved is not yet available for comparison with our calculated spectrum. However, the low resolution spectrum in Refs. [48, 49] exhibits some unassigned shoulders at the positions where the present calculation predicts intensity from the excitation of odd quanta of the bending mode.

BrCN

The calculated photoelectron spectrum of the $\tilde{X}\ ^2\Pi$ state of $BrCN^+$ is shown in Fig. 3.8. The progression in mode ν_1 (CN-stretch) is considerably shorter and that in mode ν_3 (BrC-stretch) is more pronounced than in FCN^+ and $ClCN^+$, see Figs. 3.6 and 3.7, respectively. In $BrCN^+$, the two stretching modes exhibit progressions of the equal length. The doublet structure of the vibronic peaks seen in FCN^+ and $ClCN^+$ is not present here because of the large SO splitting ($\sim$ 1758 cm^{-1}).

The stretching progressions as well as their relative intensities of the experimental photoelectron spectrum of Ref. [52] are well produced in our calculated spectrum. However, some bending vibronic levels have been observed in the experimental photoelectron spectrum which are absent in the calculated spectrum. The reason for the absence of bending excitations in the calculated

Figure 3.7: Calculated $\tilde{X}\,^2\Pi$ photoelectron spectrum of $ClCN^+$ (a) with LRVC and (b) without LRVC. The stretching progressions are indicated by the dotted lines. The bending levels along with their combination bands are labeled as ($\nu_1\nu_2\nu_3$). Levels with an overbar correspond to μ=1/2.

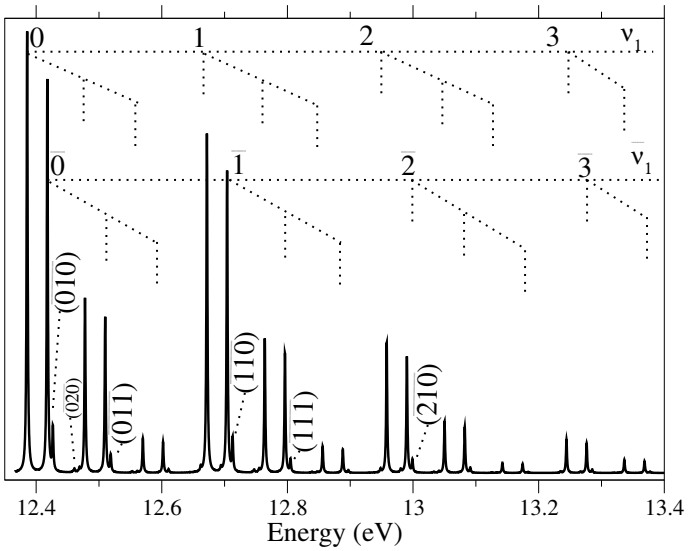

(a)

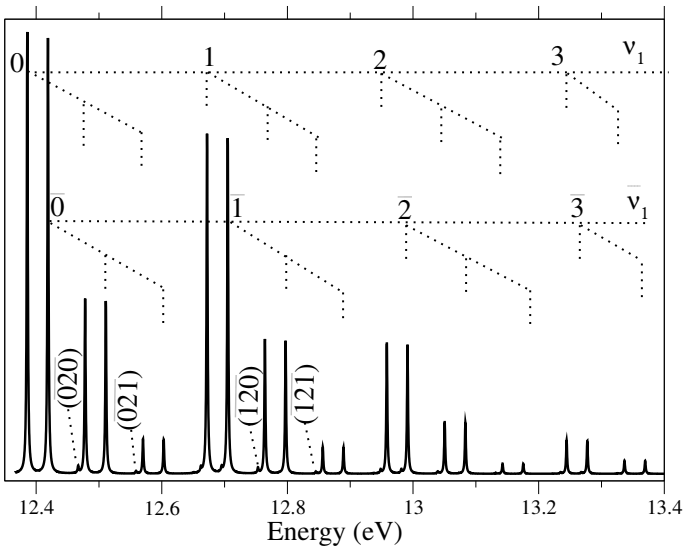

(b)

Table 3.8: Line positions (in eV) and relative spectral intensities of the photoelectron spectrum of the $\tilde{X}\ ^2\Pi$ state of $ClCN^+$ with and without inclusion of the LRVC term.

With LRVC (Fig. 3.7a)			Without LRVC (Fig. 3.7b)		
Label	Energy	Intensity	Label	Energy	Intensity
(000)	12.470	100.00	(000)	12.470	100.00
($\overline{000}$)	12.502	89.05	($\overline{000}$)	12.503	98.74
($\overline{010}$)	12.511	9.69	($\overline{020}$)	12.551	1.49
($\overline{020}$)	12.545	0.80	(001)	12.562	39.60
(001)	12.562	39.61	($\overline{001}$)	12.595	39.11
($\overline{001}$)	12.594	35.27	($\overline{201}$)	12.643	0.59
($\overline{011}$)	12.603	3.84	(002)	12.654	7.84
($\overline{021}$)	12.645	0.33	($\overline{002}$)	12.687	7.74
(002)	12.654	7.84	(100)	12.756	76.88
($\overline{002}$)	12.686	6.98	($\overline{100}$)	12.789	75.91
(100)	12.756	76.88	($\overline{120}$)	12.837	1.15
($\overline{100}$)	12.788	68.46	(101)	12.848	30.45
($\overline{110}$)	12.797	7.45	($\overline{101}$)	12.881	30.06
(101)	12.848	30.45	(102)	12.940	6.03
($\overline{101}$)	12.880	27.11	($\overline{102}$)	12.973	5.95
($\overline{111}$)	12.889	2.95	(200)	13.042	29.55
(102)	12.940	6.03	($\overline{200}$)	13.075	29.18
($\overline{102}$)	12.973	5.37	(201)	13.134	11.70
(200)	13.042	29.55	($\overline{201}$)	13.167	11.56
($\overline{200}$)	13.074	26.32	(202)	13.227	2.32
($\overline{210}$)	13.083	2.86	($\overline{202}$)	13.260	2.29
(201)	13.134	11.70	(300)	13.329	7.57
($\overline{201}$)	13.167	10.42	($\overline{300}$)	13.362	7.48
(202)	13.227	2.32	(301)	13.421	3.00
($\overline{202}$)	13.259	2.06	($\overline{301}$)	13.454	2.96
(300)	13.329	7.57			
($\overline{300}$)	13.361	6.74			
(301)	13.421	3.00			
($\overline{301}$)	13.453	2.67			

Figure 3.8: Calculated $\tilde{X}\ ^2\Pi$ photoelectron spectrum of $BrCN^+$. The stretching progressions are indicated by the dotted lines. Levels with an overbar correspond to μ=1/2.

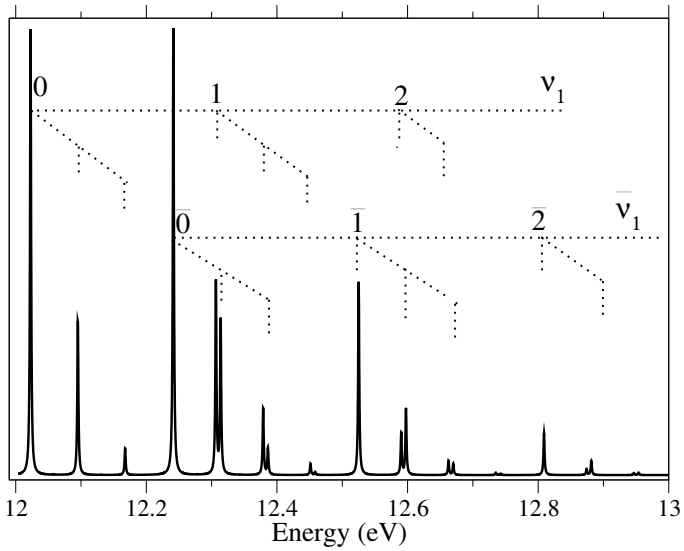

spectrum is the large value of SO splitting, which completely quenches the nonrelativistic RT coupling. Moreover, since $\zeta \gg \omega_2$, the LRVC mechanism is not effective in $BrCN^+$. This further justifies the neglect of the RT effect in the analysis of low-resolution spectra [42, 44, 45].

It is likely that the origin of intensity of bending vibronic levels in the $\tilde{X}\ ^2\Pi$ photoelectron spectrum of BrCN is due to Σ-Π coupling rather than RT coupling. While the strong SO splitting of the $\tilde{X}\ ^2\Pi$ state quenches the RT effect, the quenching effect is less pronounced for Σ-Π coupling, since the bending vibrational angular momentum is coupled with the orbital angular momentum associated with the $\tilde{X}\ ^2\Pi$ and $\tilde{A}\ ^2\Sigma^+$ states. The analysis of Σ-Π coupling with inclusion of SO-coupling effects will be the subject of future work.

Chapter 4

$\Sigma - \Pi$ and spin-orbit vibronic-coupling effects

4.1 Vibronic Hamiltonian in diabatic basis

Herein, we formulate the Hamiltonian of a single unpaired electron in a quasi-linear molecule. We focus on the situation where a degenerate $^2\Pi$ electronic state and a nondegenerate $^2\Sigma$ state of a linear triatomic molecule are closely spaced and coupled by the degenerate bending mode.

The vibronic Hamiltonian of this system is written as ($\hbar = 1$),

$$\begin{aligned} H &= T_{\rm N} + H_{\rm el} \\ &= T_{\rm N} + H_{\rm es} + H_{\rm SO}. \end{aligned} \tag{4.1}$$

The nuclear kinetic energy T_N, electrostatic $H_{\rm es}$, and the SO $H_{\rm SO}$ operators and their symmetry properties are described in Chapter 3.1 Eqs. (3.2)-(3.9).

Lets define $|\psi_\pm\rangle$ and $|\psi_0\rangle$ as diabatic [95, 96, 97] electronic basis set associated with the two components of the degenerate $^2\Pi$ electronic state (with electronic orbital angular momentum quantum numbers $\Lambda = \pm 1$) and the nondegenerate $^2\Sigma$ state ($\Lambda = 0$), respectively. The coupling of the spin motion with the orbital motion of the electron gives rise to six SO coupled states. Hence, a complete diabatic electronic basis set is given by $|\psi_{\pm\alpha}\rangle$, $|\psi_{\pm\beta}\rangle$, $|\psi_{0\alpha}\rangle$, and $|\psi_{0\beta}\rangle$, where the notation $|\psi_{\pm\alpha}\rangle$ stands for $|\psi_\pm\rangle|\alpha\rangle$. Here α and β represent the two spin eigenstates of the single unpaired electron.

The TR operator $\hat{T}$ has the following effect on the diabatic electronic basis functions:

$$\begin{aligned} \hat{T}|\psi_{\pm\alpha}\rangle = |\psi_{\mp\beta}\rangle \quad &, \quad \hat{T}|\psi_{0\alpha}\rangle = |\psi_{0\beta}\rangle, \\ \hat{T}|\psi_{\pm\beta}\rangle = -|\psi_{\mp\alpha}\rangle \quad &, \quad \hat{T}|\psi_{0\beta}\rangle = -|\psi_{0\alpha}\rangle. \end{aligned} \tag{4.2}$$

Using the above defined six diabatic spin-electronic basis functions, the electronic Hamiltonian can be written as a 6×6 vibronic matrix. The determination of the vibronic matrix elements can be simplified by using the TR symmetry, Eqs. (3.7) and (4.2), and the Hermitian property of $H_{\rm el}$.

The electronic Hamiltonian in the diabatic electronic basis can be written as follows

$$H_{\rm el} = \begin{array}{c|cccccc} & \psi_{+\alpha} & \psi_{0\alpha} & \psi_{-\alpha} & \psi_{+\beta} & \psi_{0\beta} & \psi_{-\beta} \\ \hline \psi_{+\alpha} & H^{++}_{\alpha\alpha} & H^{+0}_{\alpha\alpha} & H^{+-}_{\alpha\alpha} & H^{++}_{\alpha\beta} & H^{+0}_{\alpha\beta} & H^{+-}_{\alpha\beta} \\ \psi_{0\alpha} & H^{0+}_{\alpha\alpha} & H^{00}_{\alpha\alpha} & H^{0-}_{\alpha\alpha} & H^{0+}_{\alpha\beta} & H^{00}_{\alpha\beta} & H^{0-}_{\alpha\beta} \\ \psi_{-\alpha} & H^{-+}_{\alpha\alpha} & H^{-0}_{\alpha\alpha} & H^{--}_{\alpha\alpha} & H^{-+}_{\alpha\beta} & H^{-0}_{\alpha\beta} & H^{--}_{\alpha\beta} \\ \psi_{+\beta} & H^{++}_{\beta\alpha} & H^{+0}_{\beta\alpha} & H^{+-}_{\beta\alpha} & H^{++}_{\beta\beta} & H^{+0}_{\beta\beta} & H^{+-}_{\beta\beta} \\ \psi_{0\beta} & H^{0+}_{\beta\alpha} & H^{00}_{\beta\alpha} & H^{0-}_{\beta\alpha} & H^{0+}_{\beta\beta} & H^{00}_{\beta\beta} & H^{0-}_{\beta\beta} \\ \psi_{-\beta} & H^{-+}_{\beta\alpha} & H^{-0}_{\beta\alpha} & H^{--}_{\beta\alpha} & H^{-+}_{\beta\beta} & H^{-0}_{\beta\beta} & H^{--}_{\beta\beta} \end{array} . \tag{4.3}$$

Diagonal elements:
Following the procedure described for the RT-SO system in Eq. (3.13), we can write

$$H^{++}_{\alpha\alpha} = \underbrace{-\frac{\Delta}{2} + \frac{\zeta}{2}}_{E_{\Pi,3/2}} + \frac{1}{2}\omega_2\rho^2 + \sum_{i=1,3}\left(\kappa^{\Pi}_i Q_i + \frac{1}{2}\omega_i Q_i^2\right), \tag{4.4}$$

where $H^{++}_{\alpha\alpha}(\mathrm{es})^{(0)} = -\frac{\Delta}{2}$.

Similarly,

$$H^{--}_{\alpha\alpha} = \underbrace{-\frac{\Delta}{2} - \frac{\zeta}{2}}_{E_{\Pi,1/2}} + \frac{1}{2}\omega_2\rho^2 + \sum_{i=1,3}\left(\kappa^{\Pi}_i Q_i + \frac{1}{2}\omega_i Q_i^2\right), \tag{4.5}$$

$$H^{00}_{\alpha\alpha} = \underbrace{\frac{\Delta}{2}}_{E_{\Sigma,1/2}} + \frac{1}{2}\omega_2\rho^2 + \sum_{i=1,3}\left(\kappa^{\Sigma}_i Q_i + \frac{1}{2}\omega_i Q_i^2\right). \tag{4.6}$$

Using the TR symmetry relations of Eqs. (3.7) and (4.2), we have

$$H^{++}_{\alpha\alpha} = H^{--}_{\beta\beta}; \quad H^{--}_{\alpha\alpha} = H^{++}_{\beta\beta}; \quad H^{00}_{\alpha\alpha} = H^{00}_{\beta\beta}. \tag{4.7}$$

Off-diagonal elements:
Using the TR symmetry, Eqs. (3.7) and (4.2), we have

$$H^{+-}_{\alpha\beta} = H^{-+}_{\alpha\beta} = H^{00}_{\alpha\beta} = 0. \tag{4.8}$$

We define

$$\begin{aligned} H^{+0}_{\alpha\alpha} = (H^{-0}_{\beta\beta})^* = H^{0-}_{\beta\beta} = (H^{0+}_{\alpha\alpha})^* &= \\ H^{0-}_{\alpha\alpha} = (H^{+0}_{\beta\beta})^* = H^{+0}_{\beta\beta} = (H^{-0}_{\alpha\alpha})^* &= \mathcal{L} \end{aligned} \tag{4.9}$$

$$H^{+-}_{\alpha\alpha} = (H^{-+}_{\beta\beta})^* = H^{+-}_{\beta\beta} = (H^{-+}_{\alpha\alpha})^* = \mathcal{C} \tag{4.10}$$

$$H^{++}_{\alpha\beta} = -(H^{--}_{\beta\alpha})^* = -H^{--}_{\alpha\beta} = (H^{++}_{\beta\alpha})^* = \mathcal{D} \tag{4.11}$$

$$H^{0+}_{\alpha\beta} = -(H^{0-}_{\beta\alpha})^* = -H^{-0}_{\alpha\beta} = (H^{+0}_{\beta\alpha})^* = \mathcal{G} \tag{4.12}$$

$$H^{+0}_{\alpha\beta} = -(H^{-0}_{\beta\alpha})^* = -H^{0-}_{\alpha\beta} = (H^{0+}_{\beta\alpha})^* = \mathcal{H}. \tag{4.13}$$

Using the above definitions, Eq. (4.3) can be written as

$$H_{\mathrm{el}} = \begin{array}{c|cccccc} & \psi_{+\alpha} & \psi_{0\alpha} & \psi_{-\alpha} & \psi_{+\beta} & \psi_{0\beta} & \psi_{-\beta} \\ \hline \psi_{+\alpha} & E_{\Pi,3/2} & \mathcal{L} & \mathcal{C} & \mathcal{D} & \mathcal{H} & 0 \\ \psi_{0\alpha} & & E_{\Sigma,1/2} & \mathcal{L} & \mathcal{G} & 0 & -\mathcal{H} \\ \psi_{-\alpha} & & & E_{\Pi,1/2} & 0 & -\mathcal{G} & -\mathcal{D} \\ \psi_{+\beta} & & & & E_{\Pi,1/2} & \mathcal{L} & \mathcal{C} \\ \psi_{0\beta} & & & & & E_{\Sigma,1/2} & \mathcal{L} \\ \psi_{-\beta} & & & & & & E_{\Pi,3/2} \end{array} . \tag{4.14}$$

The electrostatic part of the electronic Hamiltonian H_{es} contributes to matrix elements with the basis functions involving identical spin eigenstates. Hence the matrix elements $\mathcal{L}$ and $\mathcal{C}$ will have contributions from the electrostatic Hamiltonian. The contribution of H_{SO} to the matrix elements of the electronic Hamiltonian is determined in the following way,

$$\mathcal{L}_{\mathrm{SO}} = \langle\psi_{+\alpha}|H_{\mathrm{SO}}|\psi_{0\alpha}\rangle = \frac{1}{2}\langle\psi_{+}|A_z|\psi_0\rangle = 0 \tag{4.15}$$

$$\mathcal{C}_{\mathrm{SO}} = \langle\psi_{+\alpha}|H_{\mathrm{SO}}|\psi_{-\alpha}\rangle = \frac{1}{2}\langle\psi_{+}|A_z|\psi_{-}\rangle = 0 \tag{4.16}$$

$$\mathcal{D}_{\mathrm{SO}} = \langle\psi_{+\alpha}|H_{\mathrm{SO}}|\psi_{+\beta}\rangle = \frac{1}{2}\langle\psi_{+}|A_x - iA_y|\psi_{+}\rangle \neq 0 \tag{4.17}$$

$$\mathcal{G}_{\mathrm{SO}} = \langle\psi_{0\alpha}|H_{\mathrm{SO}}|\psi_{+\beta}\rangle = \frac{1}{2}\langle\psi_{0}|A_x - iA_y|\psi_{+}\rangle \neq 0 \tag{4.18}$$

$$\mathcal{H}_{\mathrm{SO}} = \langle\psi_{0\alpha}|H_{\mathrm{SO}}|\psi_{-\beta}\rangle = \frac{1}{2}\langle\psi_{0}|A_x - iA_y|\psi_{-}\rangle \neq 0. \tag{4.19}$$

The matrix elements of the electronic Hamiltonian are expanded in a Taylor series up to second order in the degenerate bending mode ($Q_{\pm}$). The terms with appropriate symmetry with respect to the symmetry operation $J_z(\epsilon)$ on the corresponding electronic matrix elements survive. Using Eq. (3.10), it is

found that the matrix element $\mathcal{G}$ is of zeroth-order in the expansion; $\mathcal{L}$ and $\mathcal{D}$ are of first order; while $\mathcal{C}$ and $\mathcal{H}$ are of second-order.

By using the abbreviations

$$\begin{aligned} \mathcal{G}^{(0)} &= g \\ \left(\frac{\partial \mathcal{L}}{\partial Q_+}\right)_0 &= \lambda \qquad \left(\frac{\partial \mathcal{D}}{\partial Q_+}\right)_0 = d \\ \left(\frac{\partial \mathcal{C}}{\partial Q_+ \partial Q_+}\right)_0 &= c \qquad \left(\frac{\partial \mathcal{H}}{\partial Q_+ \partial Q_+}\right)_0 = h, \end{aligned} \tag{4.20}$$

we obtain the 6×6 spin-vibronic Hamiltonian as

$$H = T_{\mathrm{N}} \mathbf{1}_6 + H_{\mathrm{b}} + H_{\mathrm{t}} \tag{4.21}$$

where

$$H_{\mathrm{b}} = \begin{pmatrix} E_{\Pi,3/2} & \lambda\rho e^{i\phi} & c\rho^2 e^{2i\phi} & d\rho e^{i\phi} & h\rho^2 e^{2i\phi} & 0 \\ \lambda\rho e^{-i\phi} & E_{\Sigma,1/2} & \lambda\rho e^{i\phi} & g & 0 & -h\rho^2 e^{2i\phi} \\ c\rho^2 e^{-2i\phi} & \lambda\rho e^{-i\phi} & E_{\Pi,1/2} & 0 & -g & -d\rho e^{i\phi} \\ d\rho e^{-i\phi} & g & 0 & E_{\Pi,1/2} & \lambda\rho e^{i\phi} & c\rho^2 e^{2i\phi} \\ h\rho^2 e^{-2i\phi} & 0 & -g & \lambda\rho e^{-i\phi} & E_{\Sigma,1/2} & \lambda\rho e^{i\phi} \\ 0 & -h\rho^2 e^{-2i\phi} & -d\rho e^{-i\phi} & c\rho^2 e^{-2i\phi} & \lambda\rho e^{-i\phi} & E_{\Pi,3/2} \end{pmatrix}, \tag{4.22}$$

and

$$H_{\mathrm{t}} = \sum_{i=1,3} \begin{pmatrix} \kappa_i^{\Pi} & & & & & \\ & \kappa_i^{\Sigma} & & & & \\ & & \kappa_i^{\Pi} & & & \\ & & & \kappa_i^{\Pi} & & \\ & & & & \kappa_i^{\Sigma} & \\ & & & & & \kappa_i^{\Pi} \end{pmatrix} Q_i. \tag{4.23}$$

Here $E_{\Pi,3/2}$, $E_{\Pi,1/2}$, and $E_{\Sigma,1/2}$ are the electronic energies at the reference geometry ($\rho = 0$). To simplify the notation, we introduce the $\Sigma - \Pi$ energy gap Δ and the SO splitting ζ as follows

$$\Delta = E_{\Pi} - E_{\Sigma}, \tag{4.24}$$

$$\zeta = E_{\Pi,3/2} - E_{\Pi,1/2}. \tag{4.25}$$

Here E_{Π} and E_{Σ} are the electrostatic energies at the reference geometry, while $E_{\Pi,1/2}$ and $E_{\Pi,3/2}$ are the reference energies with inclusion of SO coupling. c is the well-known nonrelativistic quadratic RT coupling constant [17, 18, 19, 20], λ is the linear $\Sigma - \Pi$ coupling constant [57], while g and h are purely relativistic $\Sigma - \Pi$ coupling constants of zeroth and second order in

bending coordinate, respectively. The parameter d is the relativistic linear RT coupling constant introduced in Chapter 3. The zeros appearing along the cross diagonal are a consequence of the TR symmetry. The two 3×3 diagonal blocks of the vibronic Hamiltonian (4.22) have the same form as the nonrelativistic $\Sigma - \Pi$ Hamiltonian (ζ=0) [57]. The off-diagonal 3×3 blocks of the vibronic Hamiltonian (4.22) are, necessarily, of purely relativistic origin.

H_{t} is the Hamiltonian of the two stretching modes with dimensionless normal coordinates Q_1 and Q_3. The κ_i's for the $^2\Sigma$ and $^2\Pi$ states are the linear electron-vibrational coupling constants [41, 40] which are given by the first derivatives of the corresponding PE terms with respect to the respective dimensionless normal coordinates.

For linear geometry ($\rho = 0$), all off-diagonal elements of the Hamiltonian matrix (4.22) vanish, with the exception of the zeroth-order off-diagonal coupling SO-matrix element g. This special case of the $\Sigma - \Pi$ SO Hamiltonian has been considered in Ref. [161]. It has been shown that the 6×6 matrix can be block-diagonalized in this case to two 3×3 matrices by a constant (ρ independent) unitary transformation. It should be realized, however, that this transformation mixes the $^2\Sigma$ and $^2\Pi$ diabatic states. The transformed basis states thus are no longer diabatic electronic states, if, for example, a $\Sigma - \Pi$ crossing occurs as a function of the stretching coordinates. In the general case ($\rho \neq 0$) the Hamiltonian matrix (4.22) cannot be decoupled into smaller submatrices.

Although the adiabatic approximation fails to describe the vibronic energy levels of nearly degenerate electronic states, the adiabatic PE surfaces are nevertheless very helpful for the qualitative interpretation of the vibronic spectra. The adiabatic PE surfaces are obtained by diagonalizing $H - T_{\mathrm{N}}$ at a fixed nuclear geometry. The derivation of analytic expressions for the eigenvalues of the 6×6 matrix is unfeasible even with the help of symbolic-mathematical tools. The adiabatic PE surfaces therefore have been obtained by numerical diagonalization of the 6×6 matrix.

4.2 Generic aspects of $\Sigma - \Pi$ spin-orbit vibronic-coupling terms

In this section, we analyze the influence of the $\Sigma - \Pi$ VC and SO coupling on the energy levels and the spectral intensity distribution for the photoinduced transition from an unperturbed initial state into the vibronically coupled $^2\Sigma$ and $^2\Pi$ final states. Since under Condon approximation the vibronic energy levels corresponding to $\mu = 1/2$ and $3/2$ can only carry intensity,

the vibronic spectra are calculated only for $\mu = 1/2$ and $3/2$ as described in Chapter 2.2. While $\mu = 3/2$ levels gain intensity only from the $^2\Pi_{3/2}$ state, $\mu = 1/2$ levels gain intensity from both the $^2\Sigma_{1/2}$ and $^2\Pi_{1/2}$ states (we assume equal oscillator strengths of all three states). For $\mu = 3/2$, the square of the eigenvector element corresponding to the $|^2\Pi_{3/2}\rangle|00\rangle$ basis state gives the intensity. For $\mu = 1/2$, on the other hand, two eigenvector components, corresponding to the $|^2\Pi_{1/2}\rangle|00\rangle$ and $|^2\Sigma_{1/2}\rangle|00\rangle$ basis states, may give intensity.

In this study we have suppressed the totally symmetric stretching modes in the Hamiltonian (4.1). The stretching modes generally "tune" the energy gap of the vibronically coupled $^2\Sigma$ and $^2\Pi$ states and are, therefore, not separable from the bending motion in the $\Sigma - \Pi$ VC problem [41]. Since the aim of this section is to understand the generic effects of $\Sigma - \Pi$ VC as well as SO coupling rather than to calculate spectra of specific molecular systems, the omission of the stretching modes is appropriate for simplicity and clarity. For brevity, we consider only the case where the $^2\Sigma$ state is higher in energy than the $^2\Pi$ state. The 6×6 $\Sigma - \Pi$ vibronic Hamiltonian contains several VC terms. We, however, will limit ourselves to the investigation of a few selected and particularly interesting cases.

The effect of nonrelativistic RT coupling (parameter c) and LRVC (parameter d) within a $^2\Pi$ state is described in Chapter 3. Therefore, we do not consider these coupling mechanisms in the present study. The coupling term h is purely relativistic and quadratic in the bending distortion and hence will be ignored in the following discussion. It should be kept in mind that all coupling parameters, in particular Δ and ζ, may be functions of the stretching modes, which is not taken into account here.

4.2.1 Variation of the $\Sigma - \Pi$ coupling strength

The nonrelativistic $\Sigma - \Pi$ VC mechanism has been analyzed in detail in Ref. [57]. For weak SO coupling, it is straightforward to include the SO effects by perturbation theory. Hence we shall focus here on the cases where the SO splitting (ζ) of the $^2\Pi$ state is relatively large, being comparable to the $\Sigma - \Pi$ energy gap (Δ).

Case I

Here we discuss a system with $\Delta/\omega_2 = 5.0$ and $\zeta/\omega_2 = -2.0$. This represents a typical case of a relatively large $\Sigma - \Pi$ gap and moderate SO splitting of a $^2\Pi$ state, which can be found in many linear molecules with moderately heavy atoms. Figure 4.1(a-c) shows the adiabatic PE curves of this system

Figure 4.1: Adiabatic PE curves of the $^2\Pi_{3/2}$ (solid), $^2\Pi_{1/2}$ (dashed), and $^2\Sigma_{1/2}$ (dotted) states for $\Delta/\omega_2 = 5.0$, $\zeta/\omega_2 = $ -2.0, and $\lambda/\omega_2 = 0$ (a), 2.0 (b), and 4.0 (c).

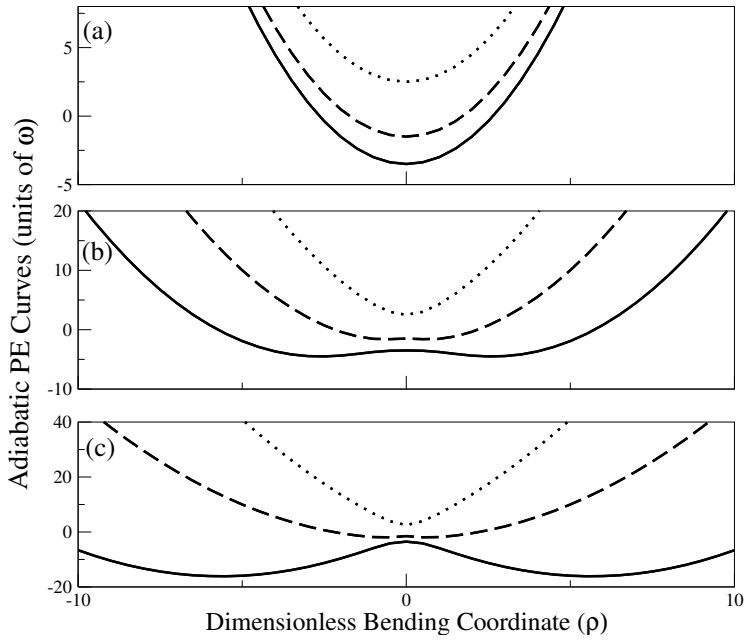

for $\lambda/\omega_2 = 0$, 2.0, and 4.0, respectively. All other coupling parameters in Eq. (4.22) are set to zero. The solid, dashed, and dotted lines correspond to the $^2\Pi_{3/2}$, $^2\Pi_{1/2}$, and $^2\Sigma_{1/2}$ states, respectively. For $\lambda = 0$, the adiabatic PE curves are parabolae which are separated by the zeroth-order splittings (Δ and ζ). With increasing λ/ω_2 the $^2\Pi_{3/2}$ PE functions develop a double-minimum shape, while the PE function of the $^2\Pi_{1/2}$ state becomes very flat in the vicinity of $\rho = 0$.

The corresponding vibronic spectra are shown in Fig. 4.2(a-c). For $\lambda/\omega_2 = 0$, the result is trivial, showing three purely electronic transitions of equal intensity, see Fig. 4.2a. The intensities of these lines get distributed over vibronic levels when λ/ω_2 becomes nonzero. The increase in the curvature of the uppermost adiabatic PE curve (the $^2\Sigma_{1/2}$ state), leads to a substantial increase of the zero-point energy, thus shifting the corresponding lines to higher energy. The VC effects are most pronounced in the $^2\Pi$ state, where the adiabatic PE function develops a bent geometry. Strong $\Sigma - \Pi$ coupling ($\lambda/\omega_2 = 4.0$) leads to very complicated vibronic structures of the $^2\Pi_{3/2}$ and $^2\Pi_{1/2}$ states, see Fig. 4.2c. It is noteworthy that the vibronic spectra of the two components of the $^2\Pi$ state are very different from each other in this

Figure 4.2: $\Sigma - \Pi$ vibronic spectra for $\Delta/\omega_2 = 5.0$, ζ/ω_2 = -2.0, and $\lambda/\omega_2 =$ 0 (a), 2.0 (b), and 4.0 (c). The solid, dashed, and dotted lines represent the vibronic levels which gain intensity from the $^2\Pi_{3/2}$, $^2\Pi_{1/2}$, and $^2\Sigma_{1/2}$ states, respectively.

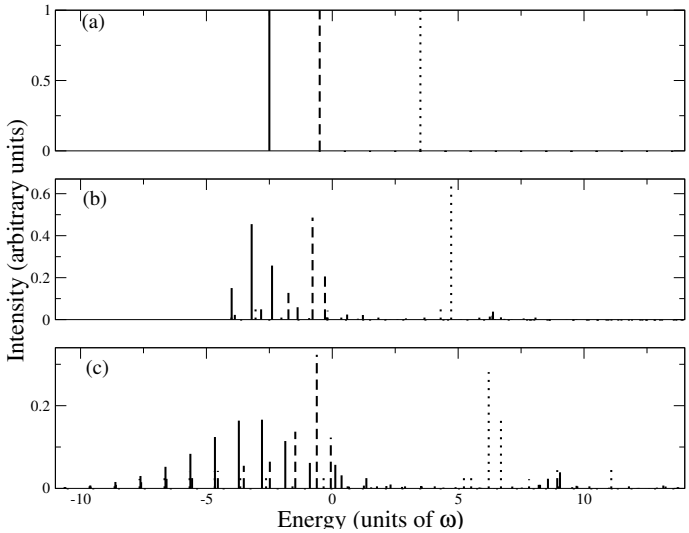

case. This possibility of very different vibronic structures of the two SO components of a $^2\Pi$ state apparently has never been considered so far in the assignment of observed spectra.

Case II

Here we investigate the case of very large SO splitting (ζ/ω_2 = -20.0) and moderate $\Sigma - \Pi$ gap ($\Delta/\omega_2 = 5.0$). This combination of parameters leads to the interesting situation where the nondegenerate $^2\Sigma$ state lies between the two SO components of the $^2\Pi$ state. This situation may arise for excited states of molecules containing relatively heavy atoms [162], as is well known for diatomic molecules [163].

Figure 4.3(a-c) shows the adiabatic PE curves for $\lambda/\omega_2 = 0$, 2.0, and 4.0. For $\lambda/\omega_2 = 0$, the adiabatic PE curves are harmonic and the $^2\Sigma_{1/2}$ state lies in between the two SO components of the $^2\Pi$ state, see Fig. 4.3a. For $\lambda/\omega_2 =$ 2.0, the PE function of the $^2\Pi_{3/2}$ state becomes very flat near $\rho = 0$, while the PE function of the $^2\Sigma_{1/2}$ state has developed a slight double minimum. With further increasing λ/ω_2, both the $^2\Pi_{3/2}$ as well as the $^2\Sigma_{1/2}$ PE functions develop minima at bent geometries, see Fig. 4.3c. Figure 4.4(a-c) shows the corresponding absorption spectra. For $\lambda/\omega_2 = 2.0$, the close-lying $^2\Sigma_{1/2}$ and

Figure 4.3: Adiabatic PE curves of the $^2\Pi_{3/2}$ (solid), $^2\Pi_{1/2}$ (dashed), and $^2\Sigma_{1/2}$ (dotted) states for $\Delta/\omega_2 = 5.0$, ζ/ω_2 = -20.0, and $\lambda/\omega_2 = 0$ (a), 2.0 (b), and 4.0 (c).

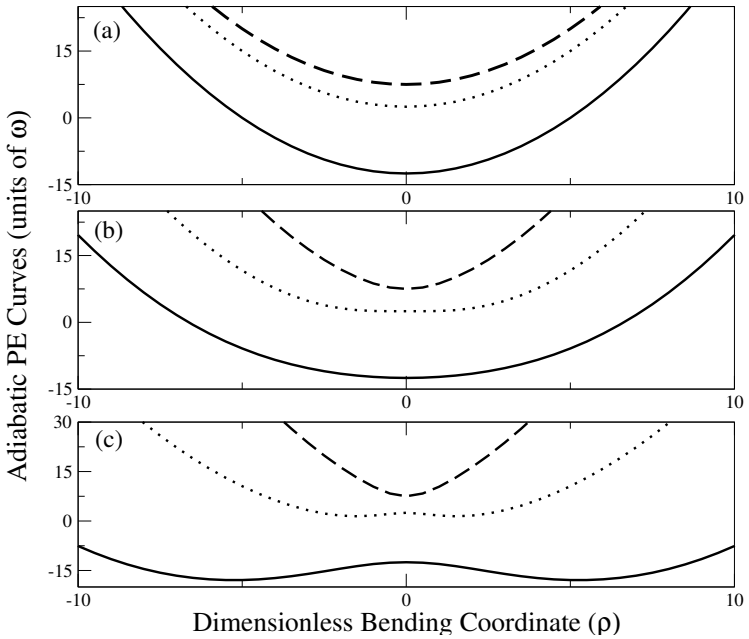

Figure 4.4: $\Sigma-\Pi$ vibronic spectra for $\Delta/\omega_2 = 5.0$, ζ/ω_2 = -20.0, and $\lambda/\omega_2 =$ 0 (a), 2.0 (b), and 4.0 (c). The solid, dashed, and dotted lines represent the vibronic levels which gain intensity from the $^2\Pi_{3/2}$, $^2\Pi_{1/2}$, and $^2\Sigma_{1/2}$ states, respectively.

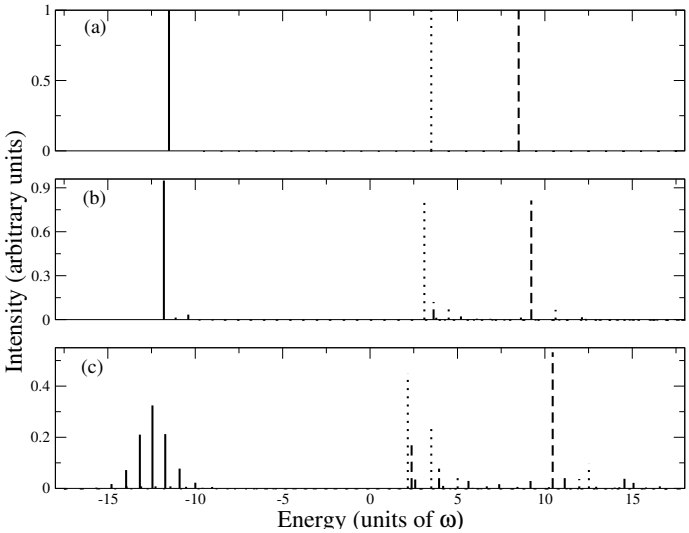

$^2\Pi_{1/2}$ states show weak indications of vibronic interaction, while the far-lying $^2\Pi_{3/2}$ state remains nearly unperturbed. Compared to Fig. 4.2b, the effect of $\Sigma-\Pi$ coupling is less pronounced here because of the larger SO splitting. For $\lambda/\omega_2 = 4.0$, the spectrum of the $^2\Pi_{3/2}$ state exhibits a pronounced progression in the bending mode, which reflects the nonlinear equilibrium geometry, see Fig. 4.3c. The $^2\Sigma_{1/2}$ and $^2\Pi_{1/2}$ states exhibit rather complex vibronic spectra which are dominated by quasi-degeneracy effects, see Fig. 4.4c. This again shows that the two SO components of the $^2\Pi$ state can exhibit completely different vibronic spectra.

4.2.2 The $^2\Pi_{1/2} - {}^2\Sigma_{1/2}$ resonance case

Here, we consider the case of accidental degeneracy of the $^2\Pi_{1/2}$ and $^2\Sigma_{1/2}$ states. The $\Sigma - \Pi$ gap (Δ) and the SO splitting (ζ) are adjusted such that the $^2\Pi_{1/2}$ component of the $^2\Pi$ state and the $^2\Sigma_{1/2}$ state are degenerate at the reference geometry. For a sufficiently large value of Δ, the $^2\Pi_{3/2}$ can be considered to be decoupled from the $^2\Pi_{1/2}$ and $^2\Sigma_{1/2}$ states. The 6×6

Figure 4.5: Adiabatic PE curves of the $^2\Pi_{3/2}$ (solid), $^2\Pi_{1/2}$ (dashed), and $^2\Sigma_{1/2}$ (dotted) states for Δ/ω_2 = 5.0, ζ/ω_2 = -10.0, and λ/ω_2 = 1.0 with g/ω_2 = 0 (a), 0.2 (b), and 0.5 (c).

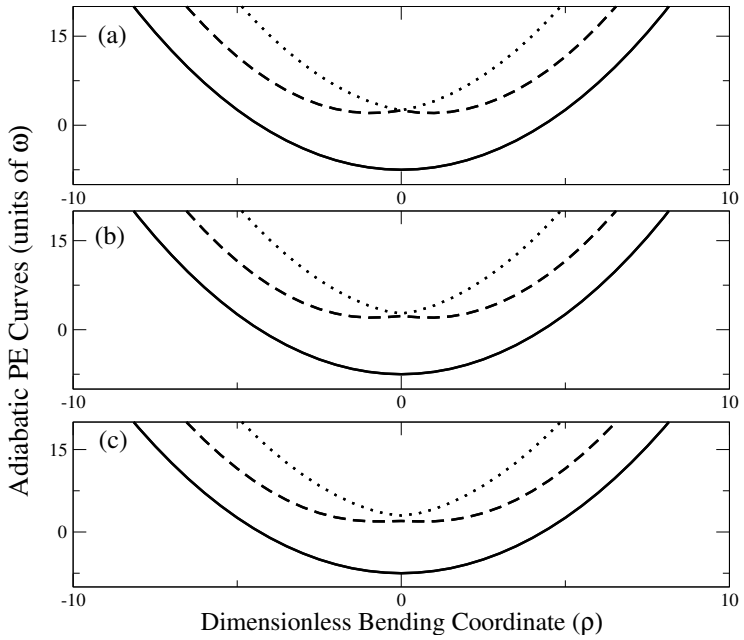

vibronic Hamiltonian can thus be truncated to 4×4 form

$$H = T_{\mathrm{N}}\mathbf{1} + \begin{pmatrix} E_{\Sigma,1/2} & \lambda\rho e^{i\phi} & g & 0 \\ \lambda\rho e^{-i\phi} & E_{\Pi,1/2} & 0 & -g \\ g & 0 & E_{\Pi,1/2} & \lambda\rho e^{i\phi} \\ 0 & -g & \lambda\rho e^{-i\phi} & E_{\Sigma,1/2} \end{pmatrix}. \qquad (4.26)$$

where $\mathbf{1}$ is the 4-dimensional unit matrix. The above Hamiltonian is isomorphic to the Hamiltonian of the linear E×E JT effect with SO coupling in trigonal symmetry, see Ref. [164]. λ is equivalent to the linear JT coupling parameter, while g is equivalent to the matrix elements of the $A_x\sigma_x + A_y\sigma_y$ term of the SO-coupling operator.

Case I

In this special case of accidental degeneracy of the $^2\Sigma_{1/2}$ and $^2\Pi_{1/2}$ states, we have investigated the effect of the zeroth-order coupling parameter g. Figure 4.5(a-c) exhibits the adiabatic PE curves of a system with Δ/ω_2 = 5.0, ζ/ω_2 = -10.0, λ/ω_2 = 1.0, while g/ω_2 takes the value 0, 0.2, and 0.5. Figure 4.5a shows that the $^2\Pi_{1/2}$ and $^2\Sigma_{1/2}$ PE functions touch each other at the

Figure 4.6: $\Sigma - \Pi$ vibronic spectra for Δ/ω_2 = 5.0, ζ/ω_2 = -10.0, and λ/ω_2 = 1.0 with g/ω_2 = 0 (a), 0.2 (b), and 0.5 (c). The solid and dashed lines represent the vibronic levels gaining intensity from the $^2\Pi_{3/2}$ and $^2\Pi_{1/2}$ states, respectively.

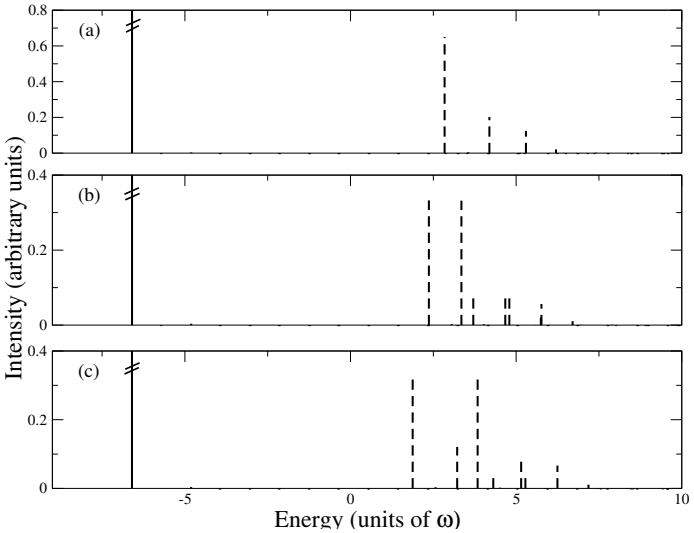

reference geometry (ρ=0). With increasing g, this degeneracy is removed, see Figures 4.5b and 4.5c, while the adiabatic PE curve of the $^2\Pi_{3/2}$ state remains essentially unchanged. Figure 4.6(a-c) shows the corresponding vibronic spectra, assuming vanishing oscillator strength of the $^2\Sigma_{1/2}$ state (the alternative case will lead to a spectrum with same line positions, but different intensities). In Fig. 4.5a, the $^2\Pi_{1/2}$ state exhibits a vibronic spectrum which corresponds to a moderately strong E×E JT effect, each vibronic line being doubly degenerate. With increasing g/ω, these degenerate vibronic lines split proportional to g/ω. The coupling parameter g thus removes the accidental degeneracy of the vibronic levels (due to the $^2\Sigma_{1/2}$-$^2\Pi_{1/2}$ accidental degeneracy) in zeroth order.

Case II

In this final example, we investigate the resonance case in the limit of very strong $\Sigma-\Pi$ nonrelativistic coupling ($\lambda/\omega_2 = 4.0$). Figure 4.7(a-c) shows the adiabatic PE functions for Δ/ω_2 = 5.0, ζ/ω_2 = -10.0, while g/ω_2 takes the values 0, 0.5, and 1.0. The lowest adiabatic PE curve develops a minimum at a strongly bent geometry as a consequence of the strong $\Sigma - \Pi$ coupling, see Fig. 4.7a. The accidental degeneracy of the $^2\Pi_{1/2}$ and $^2\Sigma_{1/2}$ states in

Figure 4.7: Adiabatic PE curves of the $^2\Pi_{3/2}$ (solid), $^2\Pi_{1/2}$ (dashed), and $^2\Sigma_{1/2}$ (dotted) states for $\Delta/\omega_2 = 5.0$, ζ/ω_2 = -10.0, and $\lambda/\omega_2 = 4.0$ with $g/\omega_2 = 0$ (a), 0.5 (b), and 1.0 (c).

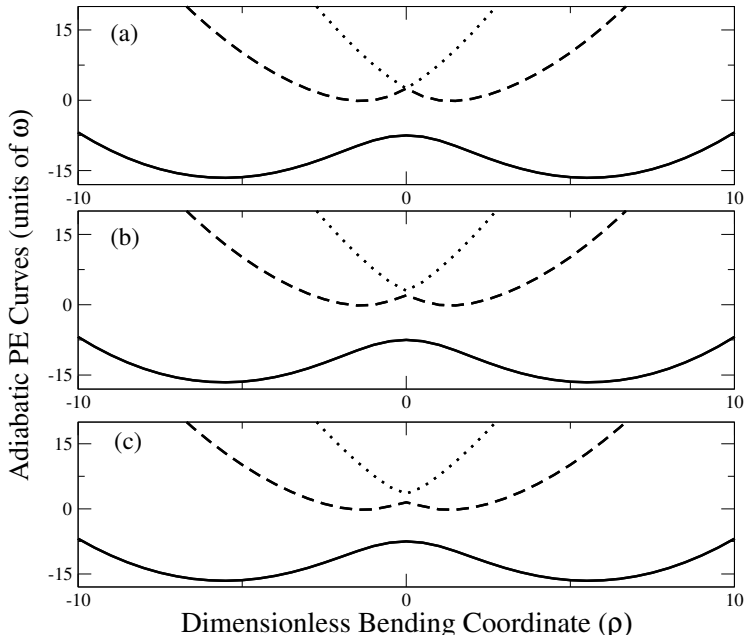

Figure 4.8: $\Sigma - \Pi$ vibronic spectra for Δ/ω_2 = 5.0, ζ/ω_2 = -10.0, and λ/ω_2 = 4.0 with g/ω_2 = 0 (a), 0.5 (b), and 1.0 (c). The solid and dashed lines represent the vibronic levels gaining intensity from the $^2\Pi_{3/2}$ and $^2\Pi_{1/2}$ states, respectively.

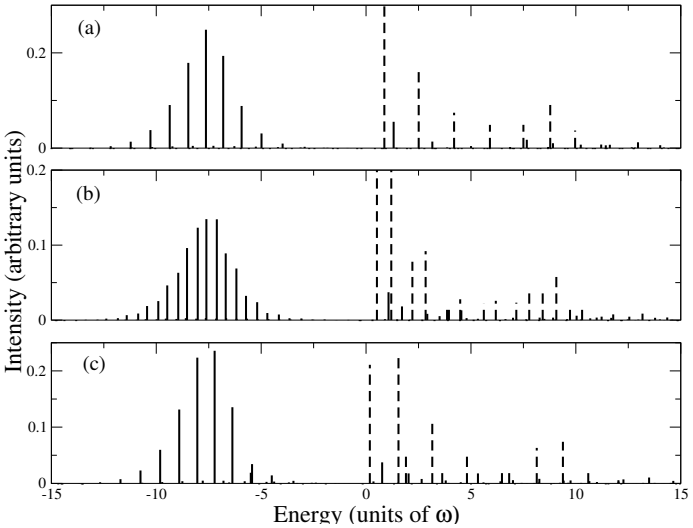

Fig. 4.7a is lifted by finite values of g/ω_2 , see Fig. 4.7c. Figure 4.8(a-c) shows the corresponding vibronic spectra. For $g/\omega_2 = 0$, the $^2\Pi_{1/2}$ state shows vibronic structure which is typical for strong JT coupling. Note in particular, the double-hump shape of the spectral envelope. The well separated $^2\Pi_{3/2}$ state, on the other hand, exhibits the characteristic extended Franck-Condon progression of a linear-to-bent transition. With increasing g/ω, each of the $^2\Pi_{1/2}$ lines splits into two, as described earlier. However, in addition to changes in the vibronic structure of the $^2\Pi_{1/2}$ state, the parameter g also strongly affects the vibronic structure of the $^2\Pi_{3/2}$ state, see Fig. 4.8b. In this case of large λ/ω, the $^2\Pi_{3/2}$ state cannot be decoupled from the $^2\Sigma_{1/2}$ and $^2\Pi_{1/2}$ states. For $g/\omega_2 = 0.5$, the density of intensity carrying lines in the $^2\Pi_{3/2}$ state is doubled, see Fig. 4.8b. Interestingly, further increase of g/ω_2 to 1.0 essentially restores the line density observed for $g/\omega_2 = 0$, see Fig. 4.8c. In the latter case, the levels of the $^2\Pi_{3/2}$ state are again doubly degenerate.

4.3 Photodetachment spectra of $CCCl^-$ and $CCBr^-$

Ab initio calculation of parameters

Computational methods

The VC terms of SO origin are obtained from the matrix elements of the Breit-Pauli SO operator with the nonrelativistic basis functions as described in Chapter 3.4. The electronic basis states obtained by the *ab initio* electronic-structure calculations are the nonrelativistic adiabatic states, which correspond to the diagonalization of the nonrelativistic fixed-nuclei electronic Hamiltonian $H_{\mathrm{b}}^{\mathrm{nr}}$. Using the unitary matrix that diagonalizes $H_{\mathrm{b}}^{\mathrm{nr}}$ and performing a corresponding similarity transformation of the relativistic part of the vibronic Hamiltonian (4.22), we arrive at the following transformed form of the SO part of the Hamiltonian

$$\begin{pmatrix} 0 & 0 & i\zeta/2 & 0 & -\frac{g-h\rho^2e^{2i\phi}}{\sqrt{2}} & id\rho e^{i\phi} \\ 0 & 0 & 0 & \frac{g-h\rho^2e^{2i\phi}}{\sqrt{2}} & 0 & i\frac{g+h\rho^2e^{2i\phi}}{\sqrt{2}} \\ -i\zeta/2 & 0 & 0 & -id\rho e^{i\phi} & -i\frac{g+h\rho^2e^{2i\phi}}{\sqrt{2}} & 0 \\ 0 & \frac{g-h\rho^2e^{-2i\phi}}{\sqrt{2}} & id\rho e^{-i\phi} & 0 & 0 & -i\zeta/2 \\ -\frac{g-h\rho^2e^{-2i\phi}}{\sqrt{2}} & 0 & i\frac{g+h\rho^2e^{-2i\phi}}{\sqrt{2}} & 0 & 0 & 0 \\ -id\rho e^{-i\phi} & -i\frac{g+h\rho^2e^{-2i\phi}}{\sqrt{2}} & 0 & i\zeta/2 & 0 & 0 \end{pmatrix}. \tag{4.27}$$

The matrix of Eq. (4.27) represents the matrix elements of the Breit-Pauli SO operator with nonrelativistic adiabatic electronic wave functions. The SO splitting ζ and the zeroth-order relativistic $\Sigma - \Pi$ coupling term g are obtained at the linear geometry. The parameters d and h can be extracted from the slope and the curvature of the corresponding SO-matrix elements as a function of the bending coordinate, respectively.

$CCCl^-$ and $CCBr^-$ are closed-shell linear systems in their ground electronic state $\tilde{\mathrm{X}}\ ^1\Sigma$ with the following valence-shell electronic configuration: $1\sigma^2\ 2\sigma^2\ 3\sigma^2\ 1\pi^4\ 2\pi^4\ 4\sigma^2$. While the 4σ molecular orbital is a nonbonding orbital localized on the terminal C atom, the 2π molecular orbital is essentially a CC π bonding orbital. Removal of an electron from the 4σ and 2π molecular orbital gives rise to the ground and first excited electronic states of the corresponding radical, i.e., the $\tilde{\mathrm{X}}\ ^2\Sigma^+$ and $\tilde{\mathrm{A}}\ ^2\Pi$ states, respectively.

We have employed the aug-cc-pVTZ basis set of Dunning [136, 137] for the C and Cl atoms. For Br, we have used the RECP described in Chapter 3.4. Using this basis set, we have optimized the geometry of the anions in their ground states and have calculated the harmonic frequencies with DFT using the B3LYP functional [139]. The DFT calculations have been performed

using the GAUSSIAN package [140]. In addition to the DFT calculations, we also have performed CCSD(T) calculations [141] to determine the optimized geometries of the anions. The coupled-cluster calculations have been performed with the MOLPRO program suite [134].

The averaged bending frequency ω_2, the nonrelativistic quadratic RT coupling parameter c, and the nonrelativistic $\Sigma - \Pi$ coupling term λ have been obtained by performing a nonlinear least-squares fit of the PE curves of the two components of the $\tilde{A}\ ^2\Pi$ state and the $\tilde{X}\ ^2\Sigma^+$ state as a function of the bending coordinate. The two $\tilde{A}\ ^2\Pi$ bending PE curves, which touch each other at the linear geometry, and that of the $\tilde{X}\ ^2\Sigma^+$ state have been obtained by performing a state-averaged full-valence CASSCF calculation at the ground-state reference geometry of the stretching modes [143, 144]. Here, all the inner valence electrons are kept frozen, resulting in the correlation of 15 electrons in 12 orbitals, i.e., a $(15, 12)$ CASSCF calculation.

The matrix elements of the Breit-Pauli SO operator with nonrelativistic wave functions have been computed, yielding the SO splitting ζ, the linear-relativistic RT parameter d as well as the zeroth- and second-order relativistic parameters (g and h), as described above. The nonrelativistic wave functions have been obtained by performing a state-averaged (over the degenerate $\tilde{A}\ ^2\Pi$ state and the nondegenerate $\tilde{X}\ ^2\Sigma^+$ state) full-valence (15,12) CASSCF calculation [143, 144]. In the case of CCBr, the SO-matrix elements have been determined by employing the SO pseudo operator of Dolg [145] for the Br atom, adapted to the above cited scalar RECP. The MOLPRO software has been used for the SO calculations [134, 142].

The linear-VC constants of the stretching modes (κ_i) for the $\tilde{X}\ ^2\Sigma^+$ state and the $\tilde{A}\ ^2\Pi$ state have been obtained from the gradients of the CCSD(T) calculated PE curves of the corresponding states, in a similar way described in Chapter 3.4. The vertical detachment energies of the $\tilde{X}\ ^2\Sigma^+$ and $\tilde{A}\ ^2\Pi$ states of the corresponding radicals at the ground-state equilibrium geometry of the anions have been obtained from the difference of the CCSD(T) energies of these states and the $\tilde{X}\ ^1\Sigma$ state of the corresponding anions, and is denoted by ΔCCSD(T). The difference between the energies of the $\tilde{X}\ ^2\Sigma^+$ and $\tilde{A}\ ^2\Pi$ states provides the $\Sigma - \Pi$ splitting Δ.

Results

$CCCl^-$

The CC and CCl bond distances in the ground electronic state of $CCCl^-$ have been obtained as 1.2404 Å and 1.6975 Å from the DFT calculation, while the CCSD(T) method predicts a slightly longer bond length for both CC and

Table 4.1: Bond distances (in Å) and harmonic vibrational frequencies (in cm^{-1}) of the ground state of CCX^-.

Parameter	$CCCl^-$	$CCBr^-$
R_0(CC)	1.2404[a]	1.2419[a]
	1.2566[b]	1.2585[b]
	1.2430[c]	
R_0(CX)	1.6975[a]	1.8490[a]
	1.7049[b]	1.8526[b]
	1.708[c]	
ω_1	2006.8[a]	1992.2[a]
	1937.1[b]	1918.2[b]
ω_2	254.1[a]	221.0[a]
	226.0[b]	203.1[b]
ω_3	640.3[a]	521.2[a]
	633.3[b]	512.7[b]

[a] DFT/B3LYP.
[b] CCSD(T).
[c] Ref. [91].

CCl bonds, see Table 4.1. The CC bond length of $CCCl^-$ is longer than the bond length of the triple bond of acetylene. This suggests that the CC bond order in $CCCl^-$ is less than three, which is expected due to the presence of an electronegative atom like Cl which also contains electrons in its p orbitals [86, 165]. The calculated bond distances are in good agreement with the values obtained in Ref. [91], see Table 4.1. The harmonic vibrational frequencies are obtained as 2006.8 cm^{-1} (CC stretch), 254.1 cm^{-1} (CCCl bend), and 640.3 cm^{-1} (CCl stretch) from the DFT/B3LYP calculation. The CCSD(T) method predicts smaller values of harmonic frequencies for all vibrational modes, see Table 4.1. From the nonlinear least-squares fit of the *ab initio* PE curves of the $\tilde{X}\ ^2\Sigma^+$ and $\tilde{A}\ ^2\Pi$ states along the bending coordinate obtained by a (15,12) CASSCF calculation, the averaged bending frequency, the quadratic RT parameter, and the linear $\Sigma - \Pi$ coupling parameter are obtained as: 377.8 cm^{-1}, 30.5 cm^{-1}, and 718.3 cm^{-1}, respectively. The overall quality of the fit, determined from the square root of the mean-squared deviation of the *ab initio* calculated energy from the adiabatic PE functions, is less than 1 cm^{-1}. Note the change in the averaged bending frequency of the $\tilde{X}\ ^2\Sigma^+$-$\tilde{A}\ ^2\Pi$ states of CCCl compared to the harmonic bending frequency of the $\tilde{X}\ ^1\Sigma$ state of $CCCl^-$. This change is a consequence of the nonlinear

Table 4.2: VC parameters (in cm^{-1}) of the $\tilde{X}\ ^2\Sigma^+$ and $\tilde{A}\ ^2\Pi$ states of CCX. The numbers in parentheses are the values in units of ω_2. See Eq. (4.22) for the definition of the coupling parameters.

Parameter	CCCl	CCBr
ω_2	377.8[a]	361.7[a]
	354.0[b]	
c	30.5(0.08)[a]	30.0(0.08)[a]
λ	718.3(1.90)[a]	714.6(1.98)[a]
ζ	-85 (0.23)[c]	-290.1 (0.81)[c]
	-101.2[d]	
d	1.6(0.00)[c]	20.7 (0.06)[c]
g	22.2(0.06)[c]	156.3 (0.43)[c]
h	0.0(0.00)[c]	0.0 (0.00)[c]

[a] From the least-squares fitting of the $\tilde{X}\ ^2\Sigma^+$ and $\tilde{A}\ ^2\Pi$ state averaged CASSCF PE functions.
[b] Ref. [73].
[c] From the matrix elements of the SO operator with the $\tilde{X}\ ^2\Sigma^+$ and $\tilde{A}\ ^2\Pi$ state-averaged CASSCF basis functions.
[d] Ref. [72].

Table 4.3: The linear electron-vibrational coupling constants of the $\tilde{X}\ ^2\Sigma^+$ and $\tilde{A}\ ^2\Pi$ states of CCX (in cm^{-1}) obtained from the CCSD(T)/AVTZ calculation. The numbers in parentheses are the so-called Poisson parameters $(\kappa_i^2/2\omega_i^2)$.

	CCCl		CCBr	
	$\tilde{X}\ ^2\Sigma^+$	$\tilde{A}\ ^2\Pi$	$\tilde{X}\ ^2\Sigma^+$	$\tilde{A}\ ^2\Pi$
κ_1	1405.0(0.25)	-1461.5(0.26)	1370.5(0.24)	-1403.6(0.25)
κ_3	684.4(0.57)	926.1(1.05)	520.5(0.50)	741.6(1.02)

ground-state equilibrium geometry of the CCCl radical, which has been the subject of discussion in several articles [93, 72, 89, 165, 86, 91, 73]. The large value of the nonrelativistic $\Sigma - \Pi$ coupling term (nearly twice the averaged bending frequency) implies a very strong vibronic interaction of the $\tilde{X}\ ^2\Sigma^+$ and $\tilde{A}\ ^2\Pi$ states. The quadratic RT coupling term has a rather moderate value, i.e., one tenth of the averaged bending frequency, see Table 4.2.

The SO splitting of the $\tilde{A}\ ^2\Pi$ state is calculated as -85 cm^{-1}. Tarroni and Carter have calculated the SO splitting as -101 cm^{-1} at the equilibrium geometry of the $^2\Pi$ state [72]. The negative value implies that the $^2\Pi_{3/2}$ component is lower in energy than the $^2\Pi_{1/2}$ component. The rather small value of the SO splitting is due to the fact that the $^2\Pi$ state is mostly a CC π orbital with small electron density on the Cl atom. The LRVC term d is small (1.6 cm^{-1}) and the SO splitting of the $^2\Pi$ state is considerably smaller than the averaged bending frequency. Therefore, no significant perturbations of the spectra by the LRVC term $d\rho e^{\pm i\phi}$ are expected. The zeroth-order relativistic $\Sigma - \Pi$ coupling term g is calculated as 22.2 cm^{-1}, which is nearly one tenth of the averaged bending frequency. The quadratic relativistic $\Sigma - \Pi$ coupling term h, on the other hand, is negligibly small.

The VC parameters of the stretching modes are given in Table 4.3. The so-called Poisson parameters $(\kappa_i^2/2\omega_i^2)$ are shown in parentheses. The vibrational couplings of the $\tilde{X}\ ^2\Sigma^+$ and $\tilde{A}\ ^2\Pi$ states are relatively weak along the CC stretching mode. The CCl stretching mode, on the other hand, is more strongly coupled, especially in the $\tilde{A}\ ^2\Pi$ state, see Table 4.3. The adiabatic PE functions of the linear-VC model are compared with the *ab initio* CCSD(T) energies in Fig. 4.9, as a function of the Q_1 and Q_3 modes. The excellent agreement between the two suggests that the linear-VC approximation is appropriate for the present problem.

The calculated vertical detachment energies of the $\tilde{X}\ ^2\Sigma^+$ and $\tilde{A}\ ^2\Pi$ states of the CCCl radical are given in Table 4.4. While the $^2\Sigma$ state is found to

Figure 4.9: Comparison of the adiabatic PE functions of the linear-VC model (solid lines) with *ab initio* CCSD(T) energies (crosses) for the stretching modes Q_1 and Q_3 of CCCl.

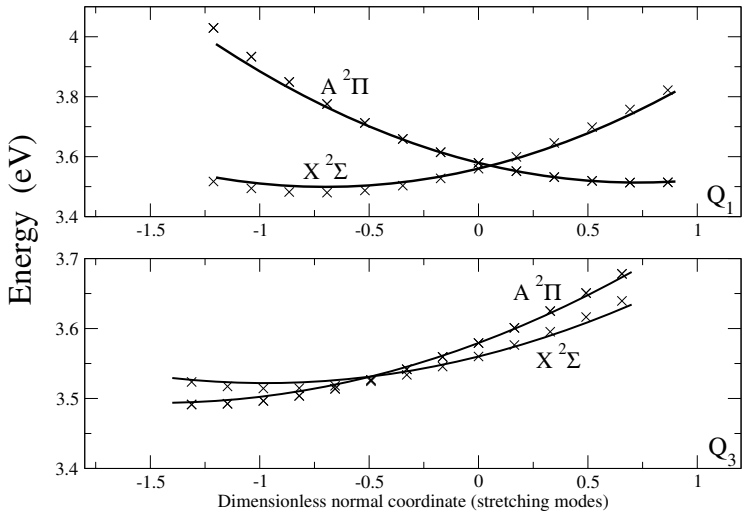

Table 4.4: Vertical detachment energy (VDE) and $\tilde{X}\ ^2\Sigma^+$ - $\tilde{A}\ ^2\Pi$ splitting (Δ) of CCX (in eV), obtained from CCSD(T)/AVTZ calculations. The numbers in parentheses are the values in cm^{-1}.

	CCCl		CCBr	
	$\tilde{X}\ ^2\Sigma^+$	$\tilde{A}\ ^2\Pi$	$\tilde{X}\ ^2\Sigma^+$	$\tilde{A}\ ^2\Pi$
VDE	3.5599	3.5792	3.5860	3.6021
Δ	0.0193(155.6)		0.0162(130.6)	
	0.0248(200.0)[a]			
	0.0609(491.0)[b]			

[a] Ref. [73].
[b] Ref. [72].

be 3.56 eV above the ground state of the anion at the equilibrium geometry of the latter, the $^2\Pi$ state is found only about 156 cm^{-1} above the $^2\Sigma$ state. The latter result is in very good agreement with the most recent experimental determination, where the $\tilde{A}\ ^2\Pi$ state is reported to be around 200 cm^{-1} above the $\tilde{X}\ ^2\Sigma^+$ state [73].

$CCBr^-$

The CC bond distance of $CCBr^-$ is nearly the same as in $CCCl^-$. The CBr bond distance is calculated as 1.8490 Å with the B3LYP functional. As found for $CCCl^-$, the CCSD(T) method predicts longer bond distances, see Table 4.1. The harmonic vibrational frequencies of $CCBr^-$, shown in Table 4.1, are smaller than the corresponding values of $CCCl^-$, as a consequence of the larger mass of Br. The nonlinear least-squares fit of the state-averaged CASSCF PE curves of the $\tilde{X}\ ^2\Sigma^+$ and $\tilde{A}\ ^2\Pi$ states yielded values for the averaged bending frequency (ω_2), the RT parameter (c), and the nonrelativistic $\Sigma - \Pi$ coupling parameter (λ) which are similar to those of $CCCl^-$. This is the consequence of the very limited contribution of the p orbitals of the halogen atom to the two highest occupied molecular orbitals of the anion. The large difference between the harmonic bending frequency of the anion and the averaged bending frequency of the radical suggests a nonlinear equilibrium geometry of the radical. The overall root-mean-square error of the fit is less than 1 cm^{-1}.

The SO splitting is calculated as -290 cm^{-1}, which is about 80% of the averaged bending frequency. The bending frequency and the SO splitting of the $^2\Pi$ state are thus nearly in resonance. The LRVC parameter d is

Figure 4.10: Comparison of the adiabatic PE functions of the linear-VC model (solid lines) with *ab initio* CCSD(T) energies (crosses) for the stretching modes Q_1 and Q_3 of CCBr.

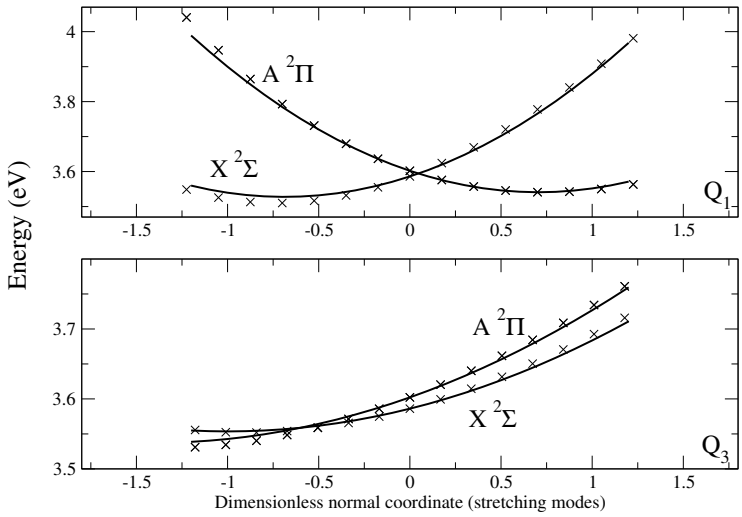

small, less than one tenth of the averaged bending frequency. On the other hand, we obtain a very large value for the zeroth-order relativistic $\Sigma - \Pi$ coupling parameter (g) which is nearly half the averaged bending frequency, see Table 4.2. The second-order relativistic $\Sigma - \Pi$ coupling parameter h again has a negligible value. We have also performed a CPP calculation [138] for Br to determine the SO-matrix elements. The effect of the core polarization is found to be negligible.

The VC parameters of the stretching modes are shown in Table 4.3 with the so-called Poisson parameters ($\kappa_i^2/2\omega_i^2$) in parentheses. The Poisson parameters have similar values as for $CCCl^-$, i.e., the coupling of the CC stretching mode is weak and that of the CBr mode is strong, see Table 4.3. The adiabatic PE curves of the linear-VC model are in excellent agreement with the *ab initio* CCSD(T) energies along both the stretching modes, (see Fig. 4.10) thus suggesting the validity of the linear-VC model.

The calculated vertical detachment energies of the $\tilde{X}\ ^2\Sigma^+$ and $\tilde{A}\ ^2\Pi$ states of the radical are given in Table 4.4. They are similar to those of CCCl. The $\Sigma - \Pi$ splitting is calculated as 131 cm^{-1}. To our knowledge, this is perhaps the smallest known vertical energy difference between the ground state and

the first excited state of any linear triatomic system.

Discussion of the photodetachment spectra

The photodetachment spectra are calculated by diagonalizing large symmetric Hamiltonian matrix by Lanczos method. The calculated spectrum is finally convoluted with a normalized Lorentzian of 1 meV width (FWHM) to account for rotational broadening and the finite resolution of the experimental photodetachment spectra. Since $CCCl^-$ and $CCBr^-$ have similar Poisson parameters for all vibrational modes, the number of harmonic oscillator basis functions used for the calculation of the final spectra are same. The appropriate values of the maximum vibrational quantum number of different modes are found as 25 (CCX bending), 14(CX stretching), and 7 (CC stretching). Thus a Hamiltonian matrix of dimension 14,700 has been diagonalized by performing 1,500 Lanczos iterations. The origin of the spectra is adjusted to the detachment energy of the $\tilde{X}\ ^2\Sigma^+$ state.

$CCCl^-$

The calculated vibronic structure of the photodetachment spectrum of $CCCl^-$ is shown in Fig. 4.11. In the upper panel, the pure bending spectrum is shown, i.e., the stretching modes are absent. The solid, dashed, and dotted lines represent vibronic levels which gain intensity from the $^2\Pi_{3/2}$, $^2\Pi_{1/2}$, and $^2\Sigma_{1/2}$ states, respectively. Most of the peaks of $^2\Pi$ origin appear as closely spaced doublets. This reflects the small SO splitting and moderate RT coupling. The $\tilde{X}\ ^2\Sigma^+$ ground state gives rise to the progression of dotted lines in Fig. 4.11a. It is noteworthy that this progression exhibits a double-hump spectral envelope which is typical for strongly coupled JT systems [20, 166, 11, 13, 14]. The pure bending spectrum is quite complicated with many quasi-degenerate levels. The reason for the complicated structure is primarily the very small $\Sigma - \Pi$ splitting and the strong nonrelativistic $\Sigma - \Pi$ coupling.

Figure 4.11b shows the calculated photodetachment spectrum with all the three modes included. The spectrum is unusually complex with many peaks of small or medium intensity. Several closely-spaced doublets, belonging to the $\tilde{A}\ ^2\Pi$ state, can still be identified. It is very difficult to assign the individual peaks due to the strong vibronic mixing of most levels. The low-energy part of the spectrum is mainly due to bending excitations, while the high-energy levels involve excitations of the stretching modes. The overall envelope of the spectrum exhibits two broad humps. This shape of the spectrum might suggest the assignment of the two bands as the spectral

Figure 4.11: Calculated vibronic structure of the $\tilde{X}\ ^2\Sigma^+$-$\tilde{A}\ ^2\Pi$ photodetachment spectrum of CCCl. (a) Only the bending vibrational mode is considered. The solid, dashed, and dotted lines represent vibronic levels which gain intensity from the $^2\Pi_{3/2}$, $^2\Pi_{1/2}$, and $^2\Sigma_{1/2}$ states, respectively. (b) All vibrational modes are included.

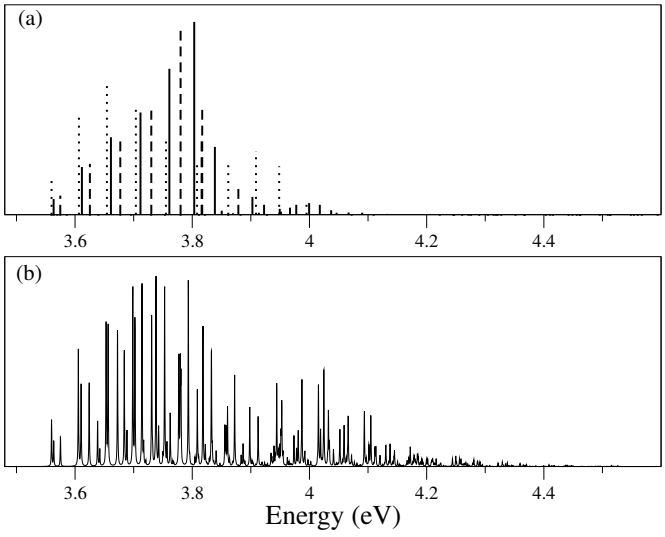

Figure 4.12: Calculated vibronic structure of the $\tilde{X}\ ^2\Sigma^+$-$\tilde{A}\ ^2\Pi$ photodetachment spectrum of CCBr. (a) Only the bending vibrational mode is considered. The solid, dashed, and dotted lines represent vibronic levels which gain intensity from the $^2\Pi_{3/2}$, $^2\Pi_{1/2}$, and $^2\Sigma_{1/2}$ states, respectively. (b) All vibrational modes are included.

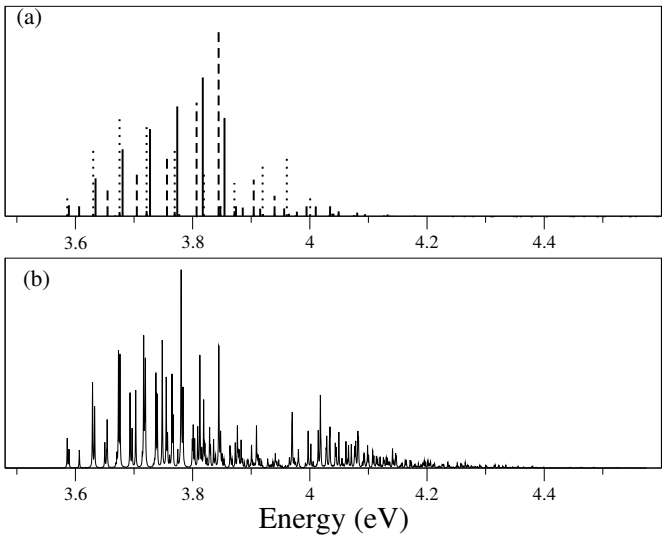

structures of two separate electronic states. In reality, however, the two electronic states are closely spaced and the double-hump shape arises from the strong $\Sigma - \Pi$ coupling of both nonrelativistic and relativistic origin.

$CCBr^-$

The calculated photodetachment spectrum of $CCBr^-$ is shown in Fig. 4.12. The upper panel of the figure shows the pure bending spectrum. In Fig. 4.12a, the solid, dashed, and dotted lines represent vibronic levels which gain intensity from the $^2\Pi_{3/2}$, $^2\Pi_{1/2}$, and $^2\Sigma_{1/2}$ states, respectively. The near degeneracy of the vibronic levels of the $^2\Sigma_{1/2}$ and the $^2\Pi_{3/2}$ states is the consequence of the accidental degeneracy of these two states. Similar to $CCCl^-$, the vibronic levels of the two SO components of the $\tilde{A}\ ^2\Pi$ state appear as doublets. The doublet splittings are larger owing to the larger SO splitting in CCBr. The $\tilde{X}\ ^2\Sigma^+$ state gives rise to a double-hump spectral envelope, see Fig. 4.12a.

Figure 4.12b shows the complete calculated photodetachment spectrum of

$CCBr^-$. The lower energy part of the spectrum is again dominated by bending excitations, whereas the high-energy part contains many densely spaced peaks with medium and low intensities. The spectrum is more complicated than that of the $CCCl^-$ because of a strong relativistic zeroth-order $\Sigma - \Pi$ VC in CCBr. The overall shape of the spectrum again appears as a double hump.

Chapter 5

Summary and Outlook

With the advent of high-resolution spectroscopic techniques and high-level computational capabilities, the overall understanding of highly complicated VC effects in isolated molecules has increased considerably. One of the most successful theoretical approaches in this regard is the adoption of simple VC model Hamiltonians. The essential simplifications are the assumption of harmonic diabatic potentials and low-order (in a Taylor series expansion in the nuclear coordinates) couplings of the diabatic electronic states. The advantages of this approach are its conceptual and technical simplicity and wide applicability. A critical shortcoming of this approach is the general practice to either neglect or consider only phenomenologically the SO coupling. In many cases, the SO coupling is treated as a weak perturbation of the VC problem. On the other hand, the SO coupling becomes increasingly important for molecules involving second-row (or heavier) elements.

The purpose of the present work is to treat the SO coupling and the VC in an equal footing with the electrostatic potentials. A Taylor series expansion of the matrix elements of the electronic Hamiltonian including the microscopic Breit-Pauli SO operator has been performed to obtain model Hamiltonians which are then used to analyze several molecular spectroscopic problems on the basis of high-level *ab initio* electronic-structure methods. Since a fully relativistic (i.e., four-component) *ab initio* treatment is computationally demanding, the present work employs the so-called SOCI method [118], in which electronic correlation and relativistic effects are treated separately.

The effect of SO coupling on the RT effect in a $^2\Pi$ electronic state of a linear molecule has been investigated, employing the microscopic expression for the SO operator in the single-electron approximation. In contrast to treatments which employ the phenomenological SO operator [30], the RT vibronic problem involves four coupled electronic states with spin-orbital angular momentum projections 3/2, 1/2, -1/2, -3/2. The Hamiltonian matrix

has been worked out in the diabatic representation. It has been found that in addition to the well-known nonrelativistic RT coupling term, which is of second order in the bending displacement, there exists a relativistic VC term of first order, which couples the two SO components (1/2 and 3/2) of the $^2\Pi$ electronic state. The symmetry properties of the relativistic RT problem have been analyzed. It has been shown that there exists a relativistic vibronic angular momentum operator which commutes with the vibronic Hamiltonian. As a result, the vibronic eigenstates can be classified by an angular momentum quantum number μ which is half integral. Time-reversal symmetry guarantees the degeneracy of energy levels with different sign of μ (vibronic Kramers degeneracy).

The vibronic Hamiltonian has been transformed to the adiabatic electronic representation. It has been shown that the adiabatic electronic wave functions carry a nontrivial topological phase, that is, they change sign along a closed loop in the plane of the degenerate bending mode. This remarkable feature, which is not found in the nonrelativistic RT effect and also not in the L_zS_z approximation for the SO operator, can be traced back to the existence of a linear-VC term in the relativistic RT effect. It is noteworthy that a nontrivial topological phase exists despite the absence of a conical intersection of the adiabatic PE surfaces.

The spectroscopic effects of the LRVC term d have been analyzed for a series of linear triatomic radicals and radical cations with $^2\Pi$ electronic ground states. It has been shown that the relativistic VC mechanism can lead to significant perturbations of the vibronic spectra when the $^2\Pi$ SO splitting and the bending vibrational frequency are of similar magnitude.

A brief survey of the *ab initio* calculated LRVC constants and the resulting vibronic spectra of the series BS_2, CS_2^+, OCS^+, OBS has been given. The survey illustrates the interplay of the parameters ζ (SO splitting of the $^2\Pi$ state), c (RT coupling constant), and d (LRVC term) in RT-SO spectra. Near degeneracy of ζ and the bending vibrational frequency ω_2 ($\zeta/\omega_2 \simeq 1$) as well as weak nonrelativistic RT coupling ($c/\omega_2 \ll 1$) are favorable circumstances for significant perturbations of RT-SO spectra by the relativistically induced VC.

For the example of the $\tilde{X}\ ^2\Pi$ state of GeCH, the LRVC parameter d as well as the other parameters of the RT vibronic model have been obtained with accurate *ab initio* electronic-structure methods. These parameters were independently determined by a least-squares fitting of the experimentally observed RT vibronic energy levels. The excellent agreement of the *ab initio* and empirically determined values provides convincing evidence that the strong perturbations of vibronic spectrum of the $\tilde{X}\ ^2\Pi$ state of GeCH, which previously have been termed "Sears resonances" [39], are effects of the LRVC

mechanism. The effects of the relativistically induced VC are comparatively pronounced in GeCH, since the SO splitting ζ and the bending frequency ω_2 are nearly equal and the nonrelativistic RT coupling is comparatively small ($c/\omega_2 \ll 1$), while the ratio d/ζ is relatively large.

The vibronic structure of the photoelectron spectra of the $\tilde{X}\ ^2\Pi$ states of XCN^+, X= F, Cl, and Br has been calculated including linear (relativistic) and quadratic (nonrelativistic) RT coupling. The two stretching modes have been taken into account in the linear-VC approximation. The parameters of the model have been determined from accurate *ab initio* calculations. The spectroscopic effects of SO and RT coupling and electron-vibrational coupling of the stretching modes have been analyzed in the photoelectron spectra. The calculated $\tilde{X}\ ^2\Pi$ photoelectron spectrum of FCN reproduces the experimental spectrum satisfactorily. ClCN is the most interesting case, since the resonance condition $\zeta \sim \omega_2$ is satisfied, resulting in nonnegligible effects of the LRVC. The calculated spectrum is shown to exhibit odd quanta of the bending mode with significant intensity, an unusual result for linear molecules. It is hoped that this computational prediction stimulates the recording of the $\tilde{X}\ ^2\Pi$ photoelectron spectrum of ClCN with higher resolution than the presently available spectra. For $BrCN^+$, the large SO coupling quenches RT coupling. It is expected that Σ-Π coupling is important for this case, that is, the approximation of an isolated $\tilde{X}\ ^2\Pi$ may be inappropriate for $BrCN^+$.

The analysis of RT effect with SO coupling has been extended to vibronically coupled $^2\Pi$ and $^2\Sigma$ electronic states of a linear molecule to study the combined effects of strong $\Sigma - \Pi$ and SO VC by employing the Breit-Pauli SO operator. The 6×6 vibronic Hamiltonian has been derived in the diabatic representation up to second order in the bending displacement. It has been found that there exists, in addition to the well-known nonrelativistic (quadratic) RT coupling term and nonrelativistic (linear) $\Sigma - \Pi$ coupling term, three coupling terms of relativistic origin. While the two components of the $^2\Pi$ state are coupled by a relativistic linear term, the $^2\Sigma$ and $^2\Pi$ states are relativistically coupled in zeroth and second order of the bending displacement. The quadratic coupling term of SO origin has been ignored in the present study, while the effects of the zeroth-order term have been studied explicitly.

The combined effects of nonrelativistic $\Sigma - \Pi$ coupling and strong SO splitting of the $^2\Pi$ state have been investigated by variational calculations of the vibronic energy levels. It has been shown that this problem is very rich and that very complex vibronic spectra can arise. For example, the $^2\Pi_{1/2}$ and $^2\Pi_{3/2}$ states can exhibit completely different vibronic structures when both the SO splitting and the nonrelativistic $\Sigma - \Pi$ coupling are strong. The effect

of zeroth-order relativistic $\Sigma - \Pi$ coupling has been shown to be important when $^2\Sigma_{1/2}$-$^2\Pi_{1/2}$ near degeneracies occur. In this case, for a sufficiently large SO coupling, the $^2\Pi_{3/2}$ state gets approximately decoupled, and the $^2\Pi_{1/2}$ and $^2\Sigma_{1/2}$ states exhibit a linear JT type interaction.

The $\Sigma - \Pi$ and SO VC model has been used to calculate the vibronic structure of the coupled $\tilde{X}\ ^2\Sigma^+$ and $\tilde{A}\ ^2\Pi$ states in the photodetachment spectra of $CCCl^-$ and $CCBr^-$. The stretching modes have been included in the linear-VC approximation. The parameters of the model have been determined from accurate *ab initio* calculations. The CCCl and CCBr radicals, like the CCH radical, exhibit closely spaced $^2\Sigma$ and $^2\Pi$ states with strong $\Sigma - \Pi$ VC. The $^2\Sigma$ state has been found to be the ground state at the equilibrium geometry of the corresponding anion. The $\Sigma - \Pi$ splitting is calculated as 156 cm^{-1} and 131 cm^{-1} for CCCl and CCBr, respectively. The separation of the two states is strongly modulated by the stretching coordinates. While the nonrelativistic VC parameters are of approximately equal strength in both cases, the relativistic VC is stronger in CCBr than in CCCl. The calculated photodetachment spectra of $CCCl^-$ and $CCBr^-$ have similar vibronic structure. While the low-energy part is dominated by peaks from bending excitations, the high-energy region exhibits a high density of vibronic levels involving excitations of bending and stretching modes. The spectral envelopes exhibit a double-hump reminiscent of strongly coupled E×E JT systems. It is hoped that the theoretical predictions stimulate the recording of the $\tilde{X}\ ^2\Sigma^+$-$\tilde{A}\ ^2\Pi$ photodetachment spectra of $CCCl^-$ and $CCBr^-$.

The present work is restricted to the SO VC of $^2\Pi$ and $^2\Sigma$ electronic states of linear molecules. The extension of the present formalism to other electronic states is straightforward. Furthermore, a systematic SO VC analysis for electronic states with different spin multiplicities (e.g., $^3\Pi$-$^3\Sigma$ SO VC) is highly desirable. Another possible extension of this work is the inclusion of rotational degrees of freedom in the present SO VC model to obtain information on spin-rovibronic levels of isolated molecules.

List of Figures

List of Tables

Appendix A

Lanczos Algorithm

For multi-mode VC problems, the solution of the eigenvalue problem of the Hamiltonian matrix (H) in the harmonic-oscillator basis functions is a formidable numerical task. The large dimension of the sparse-Hamiltonian matrix causes problem related to storing the matrix elements. Lanczos algorithm is used to circumvent this problem. In this method the structured sparsity of the Hamiltonian is exploited. The following is a brief description of the algorithm.

For some initial state $|p_0\rangle$, the state vector $|p_1\rangle$ is obtained by the relation

$$\begin{aligned} |q_1\rangle &= H|p_0\rangle - \langle p_0|H|p_0\rangle|p_0\rangle \\ |p_1\rangle &= q_1/\sqrt{\langle q_1|q_1\rangle}. \end{aligned} \tag{A.1}$$

Starting with the above states, the following three-term recurrence relations are performed [107].

$$\begin{aligned} |q_{i+1}\rangle &= H|p_i\rangle - \langle p_i|H|p_i\rangle|p_i\rangle \\ |p_{i+1}\rangle &= |q_{i+1}\rangle/\sqrt{\langle q_{i+1}|q_{i+1}\rangle} \end{aligned} \tag{A.2}$$

The above Lanczos iterations generate a sequence of orthonormal states $|p_0\rangle$, $|p_1\rangle$, $|p_2\rangle\ldots$ spanning the so-called Krylov subspace of H. The Hamiltonian matrix takes a tridiagonal form in this new basis, i.e.,

$$\begin{aligned} T_{ii} &= \langle p_i|H|p_i\rangle \\ T_{i,i+1} &= \sqrt{\langle q_{i+1}|q_{i+1}\rangle} = T_{i+1,i} \\ T_{i,j} &= 0 \qquad \text{for } |i-j| > 1. \end{aligned} \tag{A.3}$$

For our purposes we identify

$$|p_0\rangle = \mathcal{T}|\Psi_i\rangle \tag{A.4}$$

and use the basis-set expansion (2.38) to represent the Krylov subspace as the sequence of column vectors $\mathbf{p}_0, \mathbf{p}_1, \mathbf{p}_2 \ldots$. Similarly the coefficients C_m^ν are combined into a column vector $\mathbf{C}^\nu$. Using Eq. (A.3) we have

$$\mathbf{P}_m^\dagger \mathbf{H} \mathbf{P}_m = \mathbf{T}^m, \tag{A.5}$$

where $\mathbf{T}^m$ is the $m \times m$ tridiagonal matrix with elements resulting from m Lanczos iterations. Let $\mathbf{x}^m$ be the eigenvector of $\mathbf{T}^m$ with eigenvalue E_ν^m. Then $\mathbf{P}_m \mathbf{x}_\nu^m$ represents the corresponding eigenstates of the original Hamiltonian and its spectral intensity becomes

$$\begin{aligned} \mathbf{I}_\nu^m &= |\mathbf{p}_0^\dagger \mathbf{P}_m \mathbf{x}^m|^2 \\ &= |\mathbf{p}_0^\dagger \left(\mathbf{p}_0, \mathbf{p}_1, \ldots \mathbf{p}_m\right) \mathbf{x}_\nu^m|^2 \\ &= |(1, 0, \ldots 0) \mathbf{x}_\nu^m|^2 \\ &= |\mathbf{x}_\nu^m(1)|^2. \end{aligned} \tag{A.6}$$

Owing to the orthogonality of $\mathbf{p}_i$ and by the virtue of the choice of $|p_0\rangle$, it is only the first component $\mathbf{x}_\nu^m(1)$ of the eigenvectors of the tridiagonal matrix that determines the spectral intensity.

Bibliography

[1] M. Born, R. Oppenheimer, Ann. Physik 84 (1927) 457.

[2] M. Born, Nachrichten Akad. Wiss. Göttingen, Math.-Physik Kl. II, Berlin, 1951.

[3] M. Born, K. Huang, Dynamical Theory of Crystal Lattices, Oxford University Press, London, 1954.

[4] H. A. Jahn, E. Teller, Proc. R. Soc. London, Ser. A 161 (1937) 220.

[5] H. A. Jahn, Proc. R. Soc. London, Ser. A 164 (1938) 117.

[6] U. Öpik, M. H. L. Pryce, Proc. R. Soc. London, Ser. A 238 (1957) 425.

[7] Y. E. Perlin, M. Wagner (Eds.), The Dynamical Jahn-Teller Effect in Localized Systems, North-Holland, Amsterdam, 1984.

[8] G. Fischer, Vibronic Coupling, Academic Press, London, 1984.

[9] I. B. Bersuker, The Jahn-Teller Effect and Vibronic Interactions in Modern Chemistry, Plenum Press, New York, 1984.

[10] I. B. Bersuker, V. Z. Polinger, Vibronic Interactions in Molecules and Crystals, Springer-Verlag, Berlin, 1989.

[11] T. A. Barckholtz, T. A. Miller, Int. Rev. Phys. Chem. 17 (1998) 435.

[12] I. B. Bersuker, Chem. Rev. 101 (2001) 1067.

[13] W. Domcke, D. R. Yarkony, H. Köppel (Eds.), Conical Intersections: Electronic Structure, Dynamics and Spectroscopy, World Scientific, Singapore, 2004.

[14] I. B. Bersuker, The Jahn-Teller Effect, Cambridge University Press, 2006.

[15] J. G. Bednorz, K. A. Müller, Perovskite type oxides: The new approach to high-Tc superconductivity, in: Nobel Lectures, Physics 1981-1990, World Scientific, Singapore, 1993.

[16] J. M. Brown, F. Jørgensen, Adv. Chem. Phys. 52 (1983) 117.

[17] R. Renner, Z. Phys. 92 (1934) 172.

[18] K. Dressler, D. A. Ramsay, J. Chem. Phys. 27 (1957) 971.

[19] K. Dressler, D. A. Ramsay, Philos. Trans. R. Soc. London, Ser. A 251 (1959) 69.

[20] H. C. Longuet-Higgins, in: H. W. Thompson (Ed.), Advances in Spectroscopy, Vol. II, Interscience, New York, 1961, p. 429.

[21] J. A. Pople, H. C. Longuet-Higgins, Mol. Phys. 1 (1958) 372.

[22] J. T. Hougen, J. Chem. Phys. 36 (1962) 519.

[23] G. Duxbury, The electronic spectra of triatomic molecules and the Renner-Teller effect, in: Molecular Spectroscopy : Specialist Periodical Report, Vol. III, Chemical Society, London, 1975, p. 497.

[24] A. J. Merer, C. Jungen, in: K. N. Rao (Ed.), Molecular Spectroscopy : Modern Research, Vol. II, Academic Press, New York, 1976, Ch. 3, p. 127.

[25] A. N. Petelin, A. A. Kieslev, Int. J. Quantum Chem. 6 (1972) 701.

[26] A. J. Merer, D. N. Travis, Can. J. Phys. 43 (1965) 1795.

[27] C. F. Chang, Y. N. Chiu, J. Chem. Phys. 53 (1970) 2186.

[28] J. T. Hougen, J. P. Jesson, J. Chem. Phys. 38 (1963) 1524.

[29] P. Rosmus, G. Chambaud, The Renner-Teller effect and the role of electronically degenerate states in molecular ions, in: C. Y. Ng (Ed.), Photoionization and Photodetachment, Vol. 10A, World Scientific, Singapore, 2000, Ch. 5.

[30] J. A. Pople, Mol. Phys. 3 (1960) 16.

[31] T. Barrow, R. N. Dixon, G. Duxbury, Mol. Phys. 27 (1974) 1217.

[32] M. Perić, C. M. Marian, S. D. Peyerimhoff, J. Mol. Spectrosc. 166 (1994) 406.

[33] M. Perić, C. M. Marian, S. D. Peyerimhoff, J. Chem. Phys. 114 (2001) 6086.

[34] M. Perić, M. Mladenović, K. Tomić, C. M. Marian, J. Chem. Phys. 118 (2003) 4444.

[35] H. A. Bethe, E. E. Salpeter, Quantum Mechanics for One- and Two-Electron Atoms, Springer, Berlin, 1957.

[36] W. Pauli, Z. Phys. 43 (1927) 601.

[37] F. J. Northrup, T. J. Sears, Mol. Phys. 71 (1990) 45.

[38] F. J. Northrup, T. J. Sears, J. Chem. Phys. 91 (1989) 762.

[39] S. G. He, H. Li, T. C. Smith, D. J. Clouthier, A. J. Merer, J. Chem. Phys. 119 (2003) 10115.

[40] L. S. Cederbaum, W. Domcke, Adv. Chem. Phys. 36 (1977) 205.

[41] H. Köppel, W. Domcke, L. S. Cederbaum, Adv. Chem. Phys. 57 (1984) 59.

[42] S. Leutwyler, J. P. Maier, U. Spittel, J. Chem. Phys. 83 (1985) 506.

[43] M. Allan, J. P. Maier, Chem. Phys. Lett. 41 (1976) 231.

[44] J. Fulara, D. Klapstein, R. Kuhn, J. P. Maier, J. Phys. Chem. 89 (1985) 4213.

[45] F. J. Grieman, A. Mcllroy, J. Perkins, J. Chem. Phys. 84 (1986) 2481.

[46] F. G. Celii, J. Fulara, J. P. Maier, M. Rösslein, Chem. Phys. Lett. 131 (1986) 325.

[47] W. J. Lafferty, D. R. Lide, R. A. Toth, J. Chem. Phys. 43 (1965) 2063.

[48] E. Heilbronner, V. Hornung, K. A. Muszkat, Helv. Chim. Acta 53 (1970) 347.

[49] J. M. Hollas, T. A. Sutherley, Mol. Phys. 22 (1971) 213.

[50] G. Bieri, Chem. Phys. Lett. 46 (1977) 107.

[51] B. Kovac, J. Phys. Chem. 91 (1987) 4231.

[52] J. H. D. Eland, P. Baltzer, M. Lundqvist, B. Wannberg, L. Karlsson, Chem. Phys. 212 (1996) 457.

[53] J. H. D. Eland, P. Baltzer, L. Karlsson, B. Wannberg, Chem. Phys. 222 (1997) 229.

[54] T. J. Lee, S. C. Racine, Mol. Phys. 84 (1995) 717.

[55] T. J. Lee, J. M. L. Martin, C. E. Dateo, P. R. Taylor, J. Phys. Chem. 99 (1995) 15858.

[56] D. C. Wang, F. T. Chau, E. P. F. Lee, A. K. Leung, J. M. Dyke, Mol. Phys. 93 (1998) 995.

[57] H. Köppel, W. Domcke, L. S. Cederbaum, J. Chem. Phys. 74 (1981) 2945.

[58] P. S. H. Bolman, J. M. Brown, A. Carrington, I. Kopp, D. A. Ramsay, Proc. R. Soc. London, Ser. A 343 (1975) 17.

[59] R. N. Dixon, D. A. Ramsay, Can. J. Phys. 46 (1968) 2619.

[60] C. Fridh, L. Asbrink, J. Electron Spectrosc. Relat. Phenom. 7 (1975) 119.

[61] D. C. Frost, S. T. Lee, C. A. McDowell, Chem. Phys. Lett. 23 (1973) 472.

[62] H. Köppel, L. S. Cederbaum, W. Domcke, W. von Niessen, Chem. Phys. 37 (1979) 303.

[63] R. T. Wiedmann, M. G. White, J. Chem. Phys. 102 (1995) 5141.

[64] R. Tarroni, A. Mitrushenkov, P. Palmieri, S. Carter, J. Chem. Phys. 115 (2001) 11200.

[65] P. M. Dehmer, J. L. Dehmer, W. A. Chupka, J. Chem. Phys. 73 (1980) 126.

[66] L. S. Cederbaum, W. Domcke, J. Schirmer, H. Köppel, J. Chem. Phys. 72 (1980) 1348.

[67] M. Perić, S. D. Peyerimhoff, R. J. Bunker, Mol. Phys. 71 (1990) 693.

[68] A. Mebel, M. Baer, S. H. Lin, J. Chem. Phys. 112 (2000) 10703.

[69] R. Tarroni, S. Carter, J. Chem. Phys. 119 (2003) 12878.

[70] W. Chen, S. E. Novick, M. C. McCarthy, C. A. Gottlieb, P. Thaddeus, J. Chem. Phys. 103 (1995) 7828.

[71] R. Tarroni, Chem. Phys. Lett. 380 (2003) 624.

[72] R. Tarroni, S. Carter, J. Chem. Phys. 123 (2005) 014320.

[73] Y. Sumiyoshi, T. Ueno, Y. Endo, J. Chem. Phys. 119 (2003) 1426.

[74] R. F. Curl, P. G. Carrick, A. J. Merer, J. Chem. Phys. 82 (1985) 3479.

[75] W. B. Yan, J. L. Hall, J. W. Stephens, M. L. Richnow, R. F. Curl, J. Chem. Phys. 86 (1987) 1657.

[76] H. Kanamori, K. Seki, E. Hirota, J. Chem. Phys. 87 (1987) 73.

[77] H. Kanamori, E. Hirota, J. Chem. Phys. 88 (1988) 6699.

[78] W. B. Yan, H. E. Warner, T. Amano, J. Chem. Phys. 94 (1991) 1712.

[79] W. B. Yan, T. Amano, J. Chem. Phys. 99 (1993) 4312.

[80] C. A. Gottlieb, E. W. Gottlieb, P. Thaddeus, H. Kawamura, Astrophys. J. 275 (1983) 916.

[81] J. Wang, Y. Hsu, K. Liu, J. Phys. Chem. A 101 (1997) 6593.

[82] P. Löffler, E. Wrede, L. Shneider, J. B. Halpern, W. M. Jackson, K. H. Welge, J. Chem. Phys. 109 (1998) 5231.

[83] P. S. H. Bolman, J. M. Brown, Chem. Phys. Lett. 21 (1973) 213.

[84] J. M. Brown, J. Mol. Spectrosc. 68 (1977) 412.

[85] J. F. M. Aarts, Mol. Phys. 35 (1978) 1785.

[86] A. Largo, C. Barrientos, Chem. Phys. 138 (1989) 291.

[87] P. Bischof, G. Friedrich, J. Comput. Chem. 3 (1982) 486.

[88] G. L. Gutsev, T. S. Zyubina, Chem. Phys. 83 (1984) 89.

[89] A. Largo, C. Barrientos, Chem. Phys. Lett. 155 (1989) 550.

[90] V. M. Raýon, C. Barrientos, A. Largo, J. Mol. Struct.: THEOCHEM 432 (1998) 75.

[91] A. Largo, A. Cimas, P. Redondo, C. Barrientos, Int. J. Quantum Chem. 84 (2001) 127.

[92] L. Zhu, J. Bozzelli, Chem. Phys. Lett. 362 (2002) 445.

[93] G. Li, Z. Tang, J. Phys. Chem. A 107 (2003) 5317.

[94] J. Zhang, W. Wu, L. Wang, Z. Cao, J. Chem. Phys. 124 (2006) 124319.

[95] W. Lichten, Phys. Rev. 164 (1967) 131.

[96] F. T. Smith, Phys. Rev. 179 (1969) 111.

[97] T. Pacher, L. S. Cederbaum, H. Köppel, Adv. Chem. Phys. 84 (1993) 293.

[98] M. Baer, Chem. Phys. Lett. 35 (1975) 112.

[99] C. A. Mead, D. G. Truhlar, J. Chem. Phys. 77 (1982) 6090.

[100] M. Baer, Mol. Phys. 40 (1980) 1011.

[101] R. K. Preston, J. C. Tully, J. Chem. Phys. 54 (1971) 4297.

[102] G. Hirsch, P. J. Bruna, R. J. Buenker, S. D. Peyerimhoff, Chem. Phys. 45 (1980) 335.

[103] H. J. Werner, W. Meyer, J. Chem. Phys. 74 (1981) 5802.

[104] M. D. Sturge, Solid State Phys. 20 (1967) 91.

[105] R. Englman, The Jahn-Teller Effect, Wiley, New York, 1972.

[106] P. Bunker, P. Jensen, Molecular Symmetry and Spectroscopy, NRC Research Press, Ottawa, 1998.

[107] J. Cullum, R. Willoughby, Lanczos Algorithms for Large Symmetric Eigenvalue Problems, Birkhäuser, Boston, 1985.

[108] H. Köppel, W. Domcke, in: P. v. R. Schleyer, et al. (Eds.), Encyclopedia of Computational Chemistry, Wiley, New York, 1998.

[109] R. E. Moss, Advanced Molecular Quantum Mechanics, Chapman & Hall, London, 1973.

[110] P. Strange, Relativistic Quantum Mechanics, Cambridge University Press, Cambridge, 1998.

[111] K. Balasubramanian, K. S. Pitzer, Relativistic quantum chemistry, in: K. P. Lawley (Ed.), *Ab initio* Methods in Quantum Chemistry-I, John Wiley & Sons Ltd., 1987.

[112] P. A. M. Dirac, Proc. R. Soc. London, Ser. A 117 (1928) 610.

[113] G. Breit, Phys. Rev. 34 (1929) 553.

[114] F. Jensen, Introduction to Computational Chemistry, John Wiley & Sons Ltd., 1999.

[115] F. Gross, Relativistic Quantum Mechanics and Field Theory, Wiley, New York, 1993.

[116] C. M. Marian, Spin-orbit coupling in molecules, in: K. Lipkowitz, D. Boyd (Eds.), Reviews in Computational Chemistry, Wiley-VCH, 2001.

[117] A. Szabo, N. S. Ostlund, Modern Quantum Chemistry, Dover, New York, 1996.

[118] P. Schwerdtfeger (Ed.), Relativistic Electronic Structure Theory, Elsevier, Amsterdam, 2004.

[119] L. Visscher, T. J. Lee, K. G. Dyall, J. Chem. Phys. 105 (1996) 8769.

[120] L. Visscher, J. Comput. Chem. 23 (2002) 759.

[121] L. L. Foldy, S. A. Wouthuysen, Phys. Rev. 78 (1950) 29.

[122] M. Douglas, N. M. Kroll, Ann. Phys. 82 (1974) 89.

[123] B. A. Hess, Phys. Rev. A 33 (1986) 3742.

[124] M. Reiher, A. Wolf, J. Chem. Phys. 121 (2004) 2037.

[125] M. Reiher, A. Wolf, J. Chem. Phys. 121 (2004) 10945.

[126] P. A. Christiansen, W. C. Ermler, K. S. Pitzer, Annu. Rev. Phys. Chem. 36 (1985) 407.

[127] M. Dolg, Effective core potentials, in: Modern Methods and Algorithms of Quantum Chemistry, Vol. 1, John von Neumann Institute for Computing, Jülich, 2000.

[128] L. V. Poluyanov, W. Domcke, Chem. Phys. 301 (2004) 111.

[129] L. D. Landau, E. M. Lifshitz, Quantum Mechanics, Akademie-Verlag, Berlin, 1967.

[130] C. A. Mead, J. Chem. Phys. 70 (1979) 2276.

[131] H. Kramer, Acad. Sci. Amsterdam 33 (1930) 959.

[132] G. Herzberg, Molecular spectra and molecular structure, in: Electronic Spectra and Electronic Structure of Polyatomic Molecules, Vol. III, Van Nostrand, New York, 1966.

[133] M. Perić, S. D. Peyerimhoff, Adv. Chem. Phys. 124 (2002) 583.

[134] Molpro 2002.6, a package of *ab initio* programs, see http://www.molpro.net (2003).

[135] K. Raghavachari, G. W. Trucks, J. A. Pople, M. Head-Gordon, Chem. Phys. Lett. 157 (1989) 479.

[136] A. K. Wilson, D. E. Woon, K. A. Peterson, T. H. Dunning, Jr., J. Chem. Phys. 110 (1999) 7667.

[137] T. H. Dunning, Jr., J. Chem. Phys. 90 (1989) 1007.

[138] A. Bergner, M. Dolg, W. Kuechle, H. Stoll, H. Preuss, Mol. Phys. 80 (1993) 1431.

[139] A. D. Becke, J. Chem. Phys. 98 (1993) 5648.

[140] Gaussian 98, Gaussian, Inc., Pittsburgh, PA, see http://www.gaussian.com (2001).

[141] J. D. Watts, J. Gauss, R. J. Bartlett, J. Chem. Phys. 98 (1993) 8718.

[142] A. Berning, M. Schweizer, H. J. Werner, P. J. Knowles, P. Palmieri, Mol. Phys. 98 (2000) 1823.

[143] H. J. Werner, P. J. Knowles, J. Chem. Phys. 82 (1985) 5053.

[144] P. J. Knowles, H. J. Werner, Chem. Phys. Lett. 115 (1985) 259.

[145] M. Dolg, Ph.D. thesis, University of Stuttgart (1989).

[146] E. B. Wilson, J. C. Decius, P. C. Cross, Molecular Vibrations - The Theory of Infrared and Raman Vibrational Spectra, Dover Publications, New York, 1980.

[147] L. S. Cederbaum, J. Phys. B 8 (1975) 290.

[148] W. von Niessen, J. Schirmer, L. S. Cederbaum, Comput. Phys. Rep. 1 (1984) 57.

[149] H. J. Werner, P. J. Knowles, J. Chem. Phys. 89 (1988) 5803.

[150] P. J. Knowles, H. J. Werner, Chem. Phys. Lett. 145 (1988) 514.

[151] T. C. Smith, H. Li, D. J. Clouthier, C. T. Kingston, A. J. Merer, J. Chem. Phys. 112 (2000) 8417.

[152] L. Sari, Y. Yamaguchi, H. F. Schaefer III, J. Chem. Phys. 115 (2001) 5932.

[153] C. D. Esposti, P. G. Favero, S. Serenellini, G. G. Cazzoli, J. Mol. Struct. 82 (1982) 221.

[154] M. D. Harmony, V. W. Laurie, R. L. Kuczkowiski, R. H. Schwendeman, D. A. Ramsay, F. J. Lovas, W. J. Lafferty, A. G. Maki, J. Phys. Chem. Ref. Data 8 (1979) 619.

[155] M. Rösslein, M. A. Hanratty, J. P. Maier, Mol. Phys. 68 (1989) 823.

[156] M. Biczysko, R. Tarroni, Chem. Phys. Lett. 415 (2005) 223.

[157] D. H. Whiffen, Spectrochim. Acta A23 (1978) 1165.

[158] V. K. Wang, J. Overend, Spectrochim. Acta A29 (1973) 1623.

[159] A. Maki, J. Chem. Phys. 38 (1963) 1261.

[160] Y. Nakashima, T. Ogawa, M. Matsuo, K. Tanaka, T. Tanaka, in: Proceedings of the 18th International Conference on High Resolution Molecular Spectroscopy, Prague, Czech Republic, 2004, abstract No. H45.

[161] M. Alexander, D. Manolopoulos, H. Werner, J. Chem. Phys. 113 (2000) 11084.

[162] S. Mishra, V. Vallet, W. Domcke, ChemPhysChem 7 (2006) 723.

[163] E. P. F. Lee, T. G. Wright, J. Chem. Phys. 123 (2005) 144309.

[164] W. Domcke, S. Mishra, L. V. Poluyanov, Chem. Phys. 322 (2006) 405.

[165] A. Largo, P. Redondo, C. Barrientos, J. Am. Chem. Soc. 126 (2004) 14611.

[166] S. Mahapatra, H. Köppel, Phys. Rev. Lett. 81 (1998) 3116.